Supporting Information

Simple and efficient rhodamine-derived VO^{2+}and Cu^{2+}-responsive colorimetric and reversible fluorescent chemosensors toward the design of multifunctional materials

Daoyong Jiang[a], Xingying Xue[a], Guoning Zhang[b], Yucheng Wang[b], Han Zhang[a], Chao Feng[c], Zhifei Wang[a] and Hong Zhao[a],[*]

[a] School of Chemistry and Chemical Engineering, Southeast University, Nanjing, 211189, China
[b]Institute of Medicinal Biotechnology, Chinese Academy of Medical Sciences and Peking Union Medical College, Beijing, 100050, China
[c]School of Materials and Chemical Engineering, Bengbu University, Bengbu 233030, PR China
[*]Corresponding author E-mail address: zhaohong@seu.edu.cn

Apparatus and Reagents

The ^{1}H NMR and ^{13}C NMR spectra were run on a Bruker spectrometer using TMS as the internal standard. Elemental analysis was carried out with a Vario EL CHNS elemental analyzer. The mass spectrum was recorded with a VG ZAB-HS double focusing mass spectrometer (Thermo Onix Ltd, UK) or measured on a LC/MSD-Trap-XCT instrument. The FT-IR spectrum was collected on a Nicolet 5700 spectrometer (Thermo Electron Scientific Instruments Corp., America). Fluorescence spectra, fluorescence lifetime and quantum efficiency were measured with a Fluorolog 3-TSCPC and integrating sphere accessory (Horiba Jobin Yvon Inc., France). The UV−vis absorption spectra were measured on a Helios Gamma spectrophotometer. All the chemicals used in the present study were of high purity analytical grade (Merck, Aladdin, Sinopharm) and used as received without further purification. The solutions of metal ions were prepared from their analytical grade nitratesalts or chloridesalts except that VO^{2+} was prepared from its sulfatesalt (VOSO$_4$·H$_2$O) and Hg^{2+}(Hg(ClO$_4$)$_2$ · 3H$_2$O). All biological reagents were purchased from Sangon Biotech. MCF-7 cells were obtained from the Chinese Academy of Sciences Cells Bank. Water used throughout the experiment was purified by distillation of deionized water.

## X-ray crystallographic data collection and refinement of RhDBS

Single-crystal X-ray diffraction data for **RhDBS**, **RhBS** and **RhHS** were conducted on a Rigaku SCXmini CCD diffractometer with graphite-monochromatized Mo Ka radiation (k = 0.71073 Å) at room temperature using the x-scan technique. Lorentz polarization and absorption corrections were

applied. The structures were solved by direct methods with SHELXS-97 [1] and refined with the full-matrix least-squares technique using the SHELXL-97 [2] program. All nonhydrogen atoms were refined anisotropically. All H atoms were added according to theoretical calculations and refined isotropically. Single crystal structures of **RhBS** and **RhHS** were depicted (Fig. S1, ESI) and crystallographic data were provided (Table S1, ESI). The CCDC number of **RhDBS** and **RhBS** is 1447673 and 1447674 respectively.

Table S1. Crystallographic information table for **RhDBS**, **RhBS**, **RhHS**

| Compound	RhDBS	RhBS	RhHS
Mol. Form.	$C_{35}H_{34}N_4O_3Br_2$	$C_{35}H_{35}N_4O_3Br$	$C_{35}H_{36}N_4O_4$
Form. weight	718.48	639.58	576.68
T / K	293(2)	293(2)	293(2)
Col. and form	Strip,popcorn	Strip, pale pink	Strip, pale pink
Crystal system	monoclinic	monoclinic	monoclinic
Space group	$P2_1/c$	$P2_1/c$	$P2_1/c$
a / Å	11.757 (2)	21.676 (4)	9.4461 (4)
b / Å	12.113 (2))	11.875 (2)	26.6905 (12)
c / Å	22.483 (5)	12.363 (3)	12.2453 (5)
α / °	90	90	90
β / °	90	90	104.423 (2)
γ / °	90	90	90
V / Å³	3202.1 (11)	3182.1 (11)	2990.0 (2))
Z	4	4	4
$F(000)$	1464	1328	1224
D_{calcd}./ g cm⁻³	1.490	1.335	1.281
μ / mm⁻¹	2.57	1.33	0.09
θ range / °	3 to 25	3 to 25	1.5. to 25.1
Ref.coll./unique	18350/ 5644	17362/5017	15630/ 5130
R_{int}	0.073	0.067	0.087
Completeness	99.9%	99.9%	99.8%
Parameters	402	393	393
GOOF	1.04	1.07	1.02
$R_1[I \geq 2\sigma(I)]^{a,b)}$	0.063	0.051	0.07
$wR_2(alldata)^{a,b)}$	0.141	0.112	0.215
Residues/eÅ⁻³	1.18 ,−0.5	0.28 ,−0.34	0.25 ,−0.22

$w = 1/[\sigma^2(F_o^2) + (0.0482P)^2 + 3.7273P]$; $w = 1/[\sigma^2(F_o^2) + (0.0381P)^2 + 0.4426P]$; $w = 1/[\sigma^2(F_o^2) + (0.0857P)^2]$, where $P = (F_o^2 + 2F_c^2)/3$.
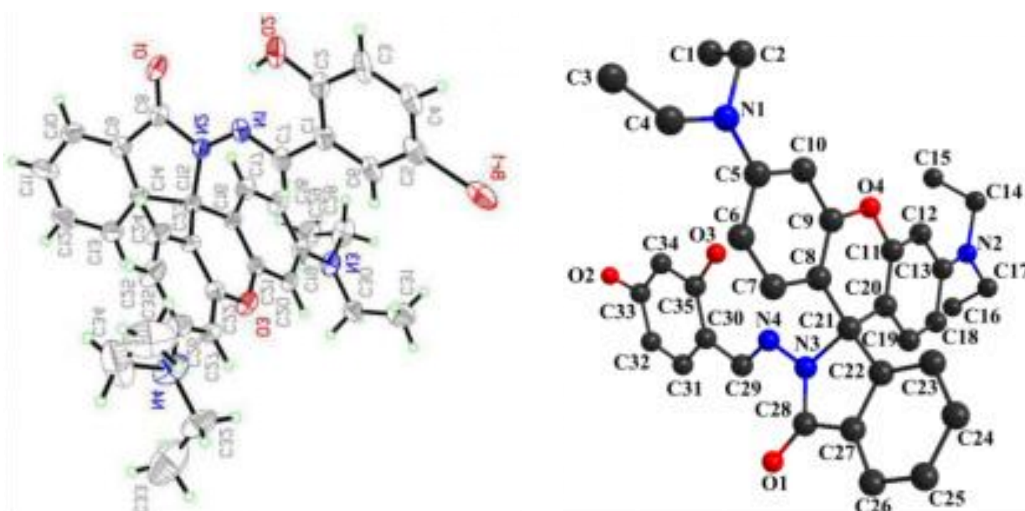
**Fig. S1.** Crystal structures of (a) **RhBS** and (b) **RhHS (**all hydrogen atoms were omitted for clarity).

The influence of media

The sensing medium was firstly studied to obtain the optimised spectral response by **RhDBS**. Sensor **RhDBS** exhibited good solubility in different polar organic solvents including dimethyl sulfoxide (DMSO), N,N-dimethylformamide (DMF), and acetonitrile (CH_3CN). First, we measured the Cu^{2+} ion (200 μM) with **RhDBS** (20 μM) in various solvents to select a solvent system. **RhDBS** exhibits good sensitivity for Cu^{2+} in DMSO–buffer mixed solution, pure DMSO, DMF, and MeCN solution (Fig. S2, ESI). However, due to the interference of Hg^{2+}, it shows poor selectivity in pure acetonitrile solution. Furthermore, taking into account higher toxicity of DMF than DMSO, the DMSO–buffer and DMSO solutions are favorable for the UV–vis and fluorescence spectral measurement. To control the emission intensity, the fluorescence behaviour of chemosensor **RhDBS** in different ratios of DMSO/Tris-HCl solutions was investigated (Fig. S3, ESI). It can be observed that upon adding of 10 equiv VO^{2+}, the dilute aqueous solution of **RhDBS** showed sharply enhanced fluorescence when the DMSO fraction was over 70%. For these reasons, in this work, DMSO/Tris-HCl buffer (pH 7.4, 7:3, v/v) was used throughout the experiment.
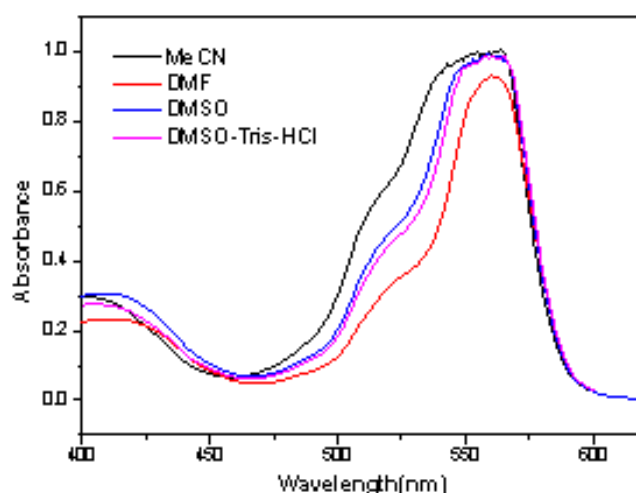
Fig. S2. The absorption spectra of **RhDBS**(10μM) in the presence of 10eqv. Cu^{2+} in different solvents (acetonitrile,

*N,N*-dimethylformamide, dimethyl sulfoxide, dimethyl sulfoxide-buffer mixture solution).
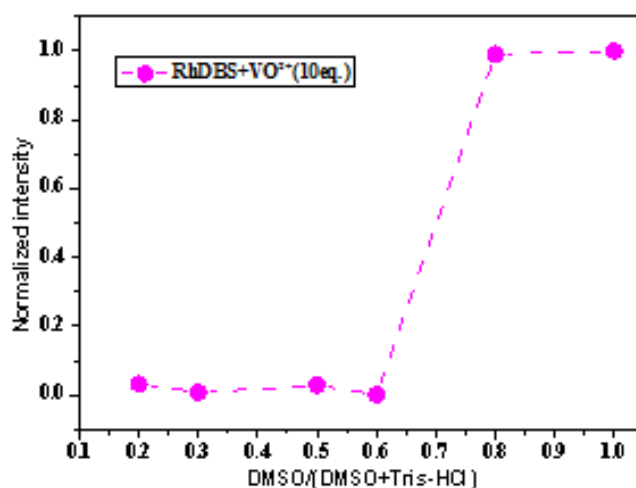
Fig. S3. Plot of fluorescence intensity of **RhDBS** (20 μM) and **RhDBS**-VO^{2+} at 586 nm versus solvent composition of DMSO/buffer mixture (λ_{ex} = 520 nm).

Effect of pH

The influence of pH changes on absorption and fluorescence intensity of **RhDBS** and its Cu^{2+} complex and VO^{2+} complex have been investigated respectively (Fig. S4, ESI). The pH-titration experiments showed that the absorbance and emission intensity of the free **RhDBS** are almost no changes in the pH range 3.0-11.0 and 3.0-9.0 respectively, whereas the absorbance of Cu^{2+} complex decreases sharply from pH 9.5 to 11.0 and emission intensity of VO^{2+} complex decreases dramatically in the pH range 7.0-9.0. The data suggested that a wide pH range of 3.0-10.0 is proper for the detection of Cu^{2+} ions and for the determination of VO^{2+} ions being pH range of 3.0-8.0, bacause VO^{2+} is not stable in higher pH value solution [3]. Thus, the sensor **RhDBS** can be an appropriate candidate for the potential use under physiological conditions.
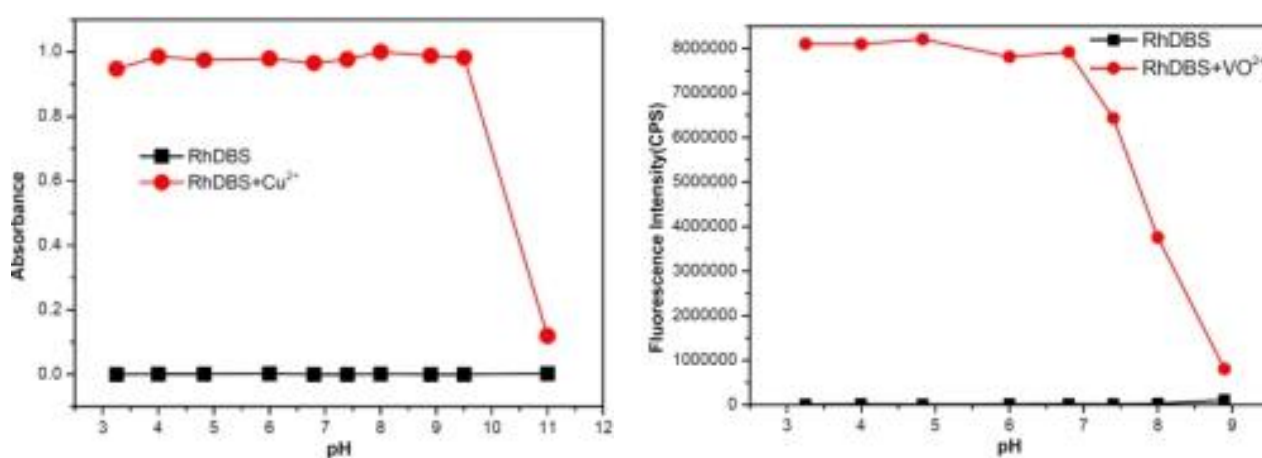
Fig. S4. pH dependence of (a) Absorbance responses of **RhDBS** and its [**RhDBS** +Cu^{2+}] complex and (b) Fluorescence responses of **RhDBS** and its [**RhDBS** +VO^{2+}] complex (l_{ex} = 520 nm, slit: 2.5/2.5).
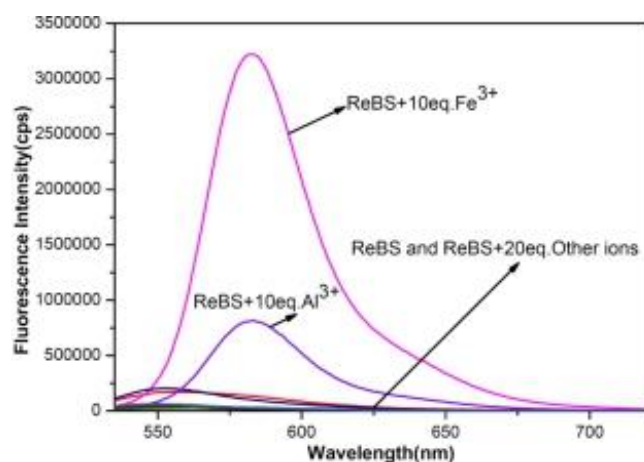
Fig. S5. Fluorescence spectra of **ReBS** (20 μM) in the presence of various metal ions (20 Eq. except Fe^{3+} that are 10 Eq.) in DMSO-Tris-HCl (7:3, v/v, pH 7.4) solution ($\lambda_{ex/em}$= 520/586 nm; slit: 5 nm/5 nm).
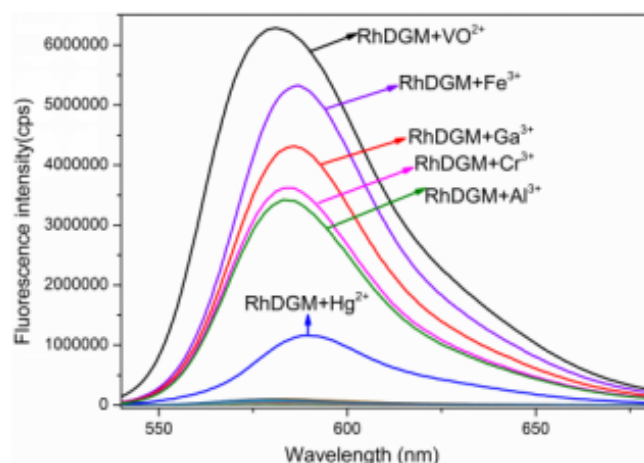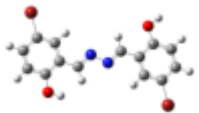
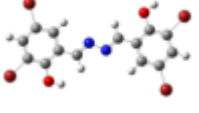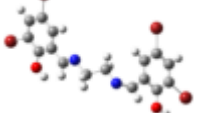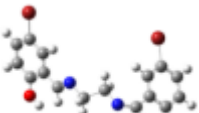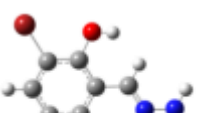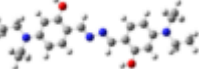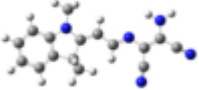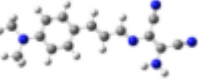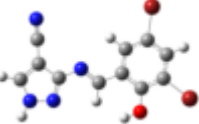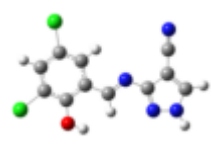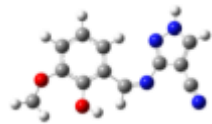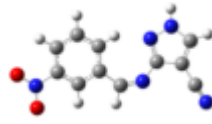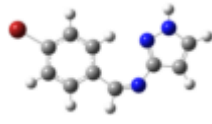**Fig. S6.** Fluorescence spectra of **RhDGM** (20 μM) in the presence of various metal ions in MeOH-H_2O (4:1, v/v) solution ($\lambda_{ex/em}$= 520/586 nm; slit: 5 nm/5 nm).
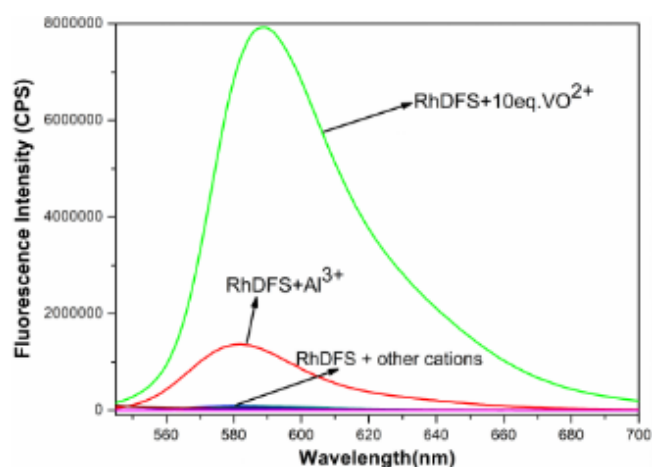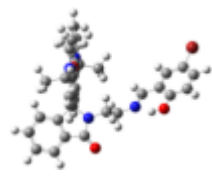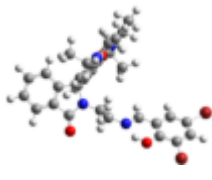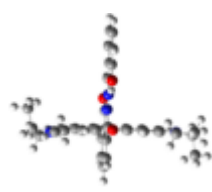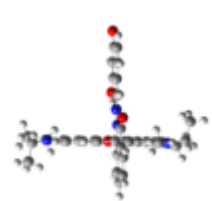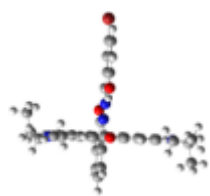

Fig. S7. Fluorescence spectra of **RhDFS** (20 μM) in the presence of various metal ions (10 Eq.) in DMSO-Tris-HCl (7:3, v/v, pH 7.4) solution ($\lambda_{ex/em}$= 520/589 nm; slit: 2.5 nm/5 nm).

Table S2. DFT calculation data of all ligands and the sensing performance for VO^{2+} and other cations.

Compounds (optimized structure)	HOMO(eV)	LUMO(eV)	$\triangle E$(eV)	VO^{2+} et al. cations sensing property
S₁	-6.0928	-2.3392	3.7536	NO
S₂	-6.3920	-2.6656	3.7264	NO
S₃	-6.4192	-1.9040	4.5152	NO
S₄	-6.1744	-1.6048	4.5696	Cu²⁺
S₅	-5.9296	-1.4144	4.5152	NO
L₁	-4.5424	-1.1424	3.4	NO
L₂	-5.0592	-2.2576	2.8016	Cu²⁺
L₃	-5.032	-2.0128	3.0192	Cu²⁺
A1	-6.4736	-2.5568	3.9168	NO

	E_{HOMO}	E_{LUMO}	Gap	Ion
A2	-6.664	-2.6384	4.0256	Mg^{2+}、Ca^{2+}
A3	-6.12	-2.04	4.08	NO
A4	-5.848	-1.5776	4.2704	NO
A5	-7.0176	-3.0736	3.944	NO
A6	-6.1744	-1.7136	4.4608	NO
ReBS	-5.168	-1.4688	3.6992	Fe^{3+}
ReDBS	-5.1952	-1.7136	3.4816	Fe^{3+}
RhS	-5.0048	-1.4688	3.536	Cu^{2+}、VO^{2+}
RhHS	-5.0048	-1.4144	3.5904	Cu^{2+}

RhBS	-5.0864	-1.6592	3.4272	VO^{2+}、Cu^{2+}
RhDBS	-5.1136	-1.8224	3.2912	VO^{2+}、Cu^{2+}
RhFS	-5.1430	-1.4966	3.6463	Cu^{2+}、VO^{2+}
RhIS	-5.0613	-1.4694	3.5919	Cu^{2+}
RhDFS	-5.1702	-1.5783	3.5919	VO^{2+}、Cu^{2+}
RhDIS	-5.0341	-1.6327	3.4014	VO^{2+}、Cu^{2+}
	-5.1702	-2.4218	2.7484	VO^{2+}, Hg^{2+}, Fe^{3+}，Cr^{3+}，Ga^{3+}，Al^{3+}
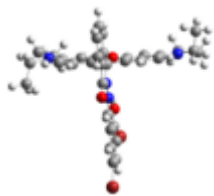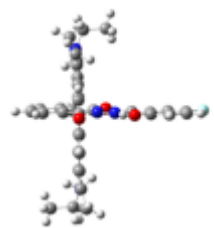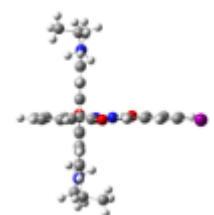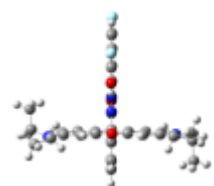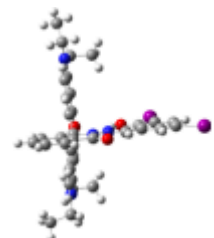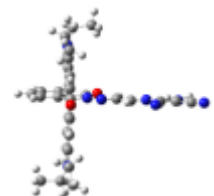
Photophysical property of control compounds
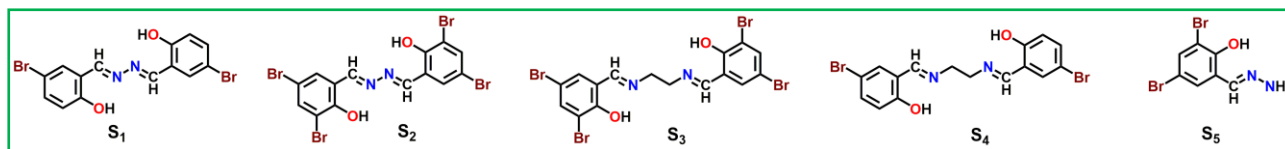
Scheme S1. The structures of the acceptors **S₁-S₅**.

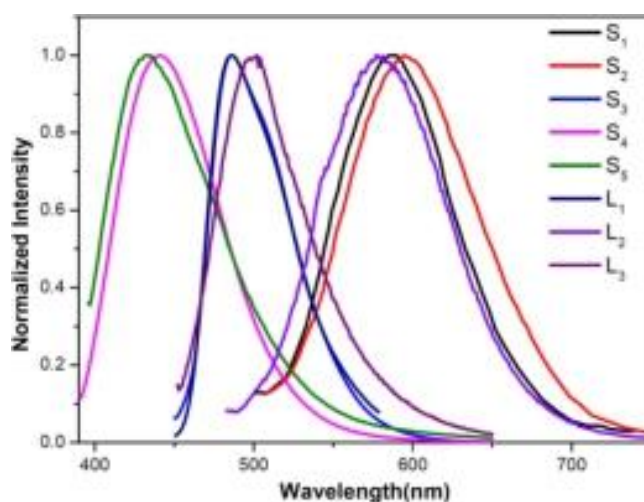10 ml 1.0 x 10⁻⁵ M solutions of the control compounds **S₁-S₅, L₁-L₃** and **A1-A6** were prepared separately by dissolving appropriate amount of the ligands in DMF-H₂O (1:9, v/v), and DMF for all the fluorescence studies.

Fig. S8. Emission spectra of compounds **S₁-S₅、 L₁-L₃** in DMF-H₂O (1:9, v/v) solution.

Table S3. Excitation and emission wavelength of **S₁-S₅、 L₁-L₃**

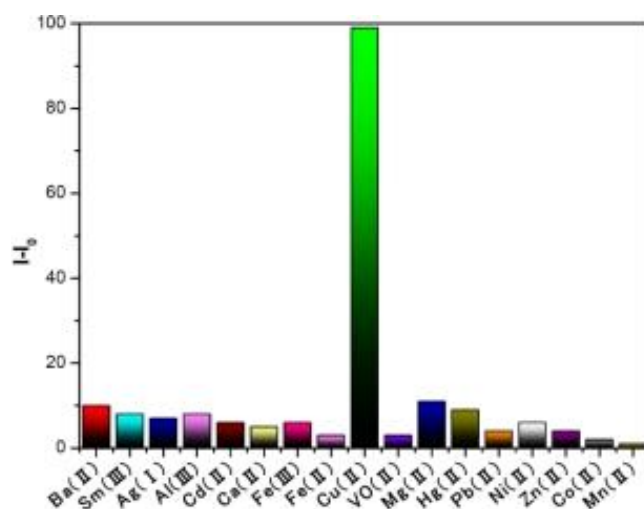| Compound	S₁	S₂	S₃	S₄	S₅	L₁	L₂	L₃
E_x (nm)	465	465	449	369	371	387	466	430
E_m (nm)	585	595	487	441	434	487	577	502
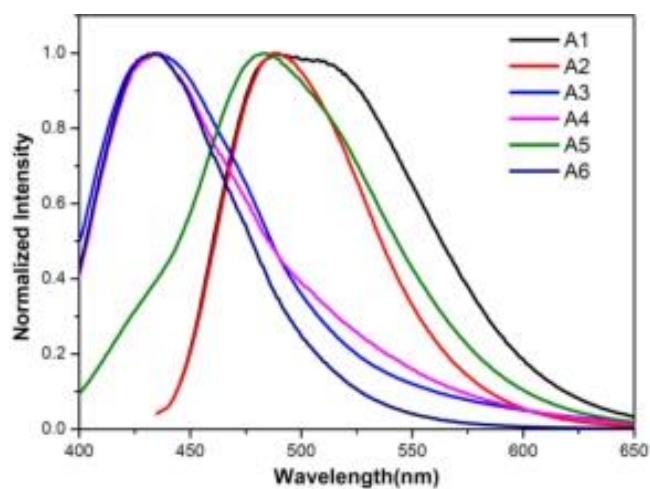
Fig. S9. Emission spectra of compounds **A1-A6** in DMF solution.

Table S4. Excitation and emission wavelength of **A1-A6**

Compound	A1	A2	A3	A4	A5	A6
E_x (nm)	420	420	375	375	375	375
E_m (nm)	488	489	435	435	483	434

Fig. S10. The relative fluorescence intensity of **L₁** (20 μM) in the presence of various metal ions (20 Eq. except Cu^{2+} that are 10 Eq.) in DMF-H_2O (9:1, v/v, pH = 7.4, 0.1 M Tris-HCl) solution ($\lambda_{ex/em}$= 400/513 nm; slit: 5 nm/5 nm).
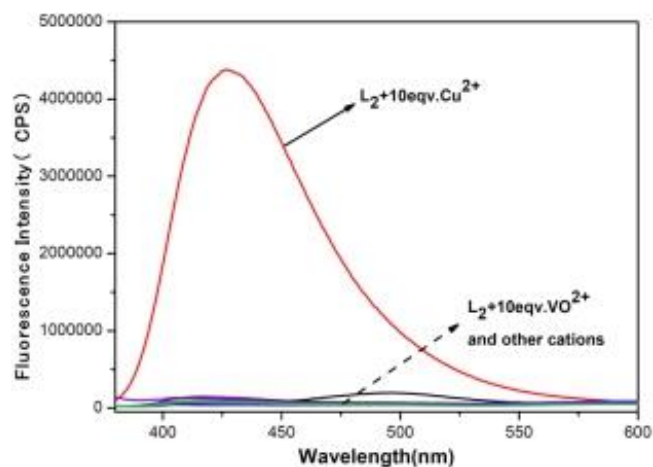
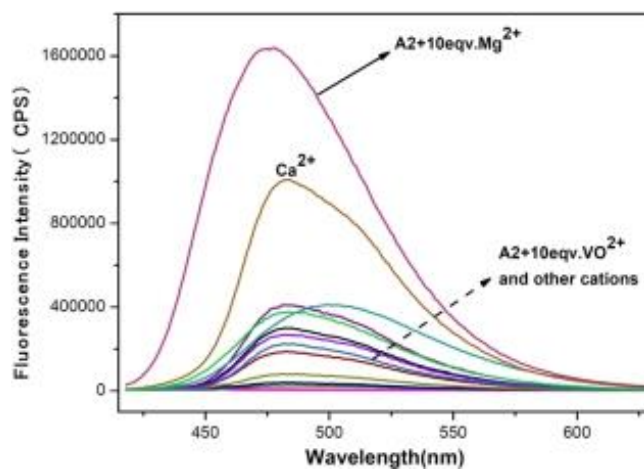**Fig. S11.** Fluorescence spectra of **L₂** (20 μM) in the presence of various metal ions (20 Eq. except Cu^{2+} that are 10 Eq.) in DMSO-H_2O (6:4, v/v) solution ($\lambda_{ex/em}$= 362/437 nm; slit: 5 nm/5 nm).
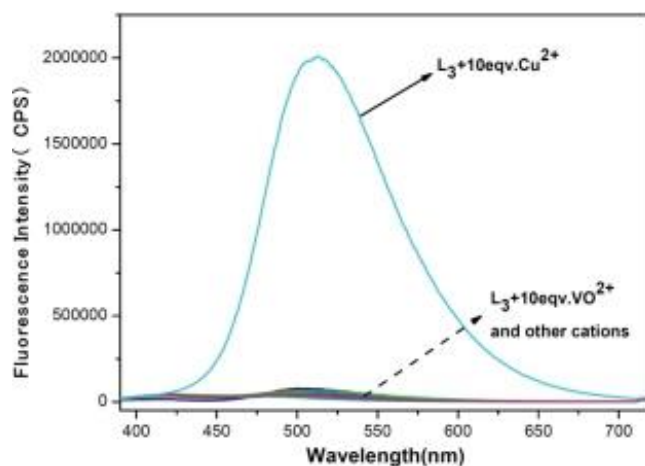
Fig. S12. Fluorescence spectra of **L₃** (20 μM) in the presence of various metal ions (20 Eq. except Cu^{2+} that are 10 Eq.) in DMSO-H_2O (7:3, v/v) solution ($\lambda_{ex/em}$= 364/500 nm; slit: 5 nm/5 nm).

Fig. S13. Fluorescence spectra of **A2** (20 μM) in the presence of various metal ions (20 Eq. except Mg^{2+} that are 10 Eq.) in DMSO-Tris-HCl (7:3, v/v, pH 7.4) solution ($\lambda_{ex/em}$= 403/475 nm; slit: 5 nm/5 nm).
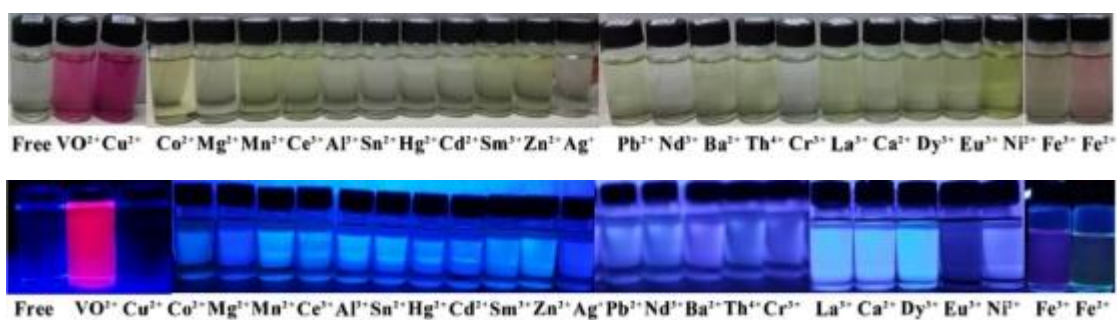
Fig. S14. Photograph of RhDBS (20 μM) showing the color (top) and the fluorescent (bottom) changes in the presence of various cations (20 Eq).
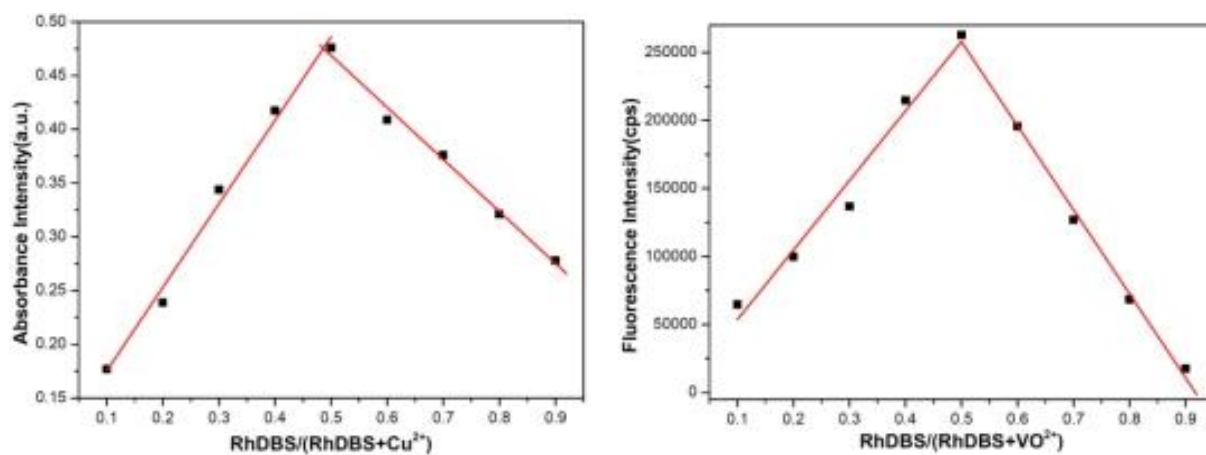

Fig. S15. Job's plots for (a) Cu^{2+} and (b) for VO^{2+}.
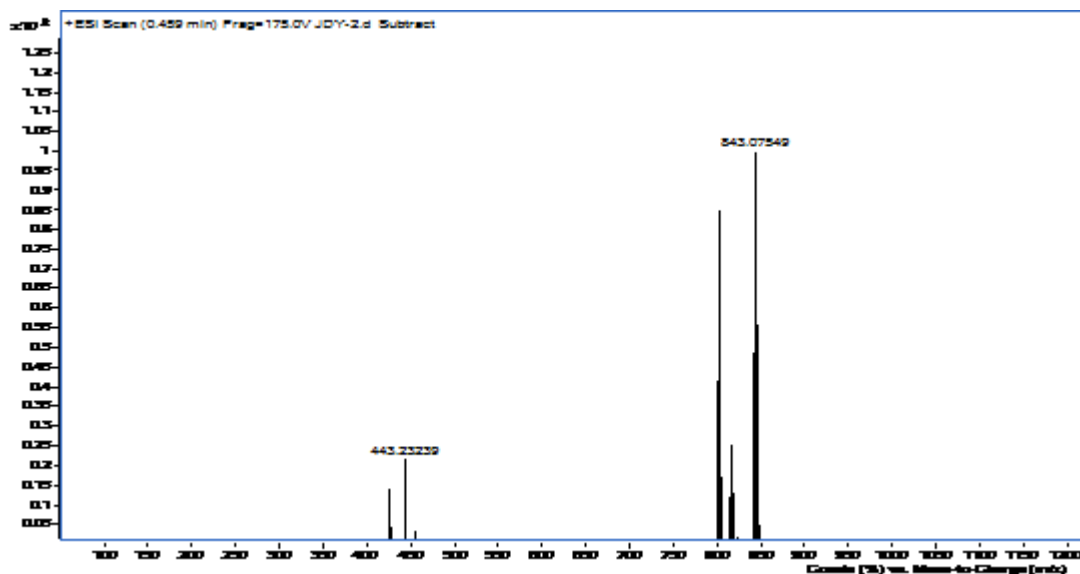
Fig. S16. MS of **RhDBS**+VO^{2+}.
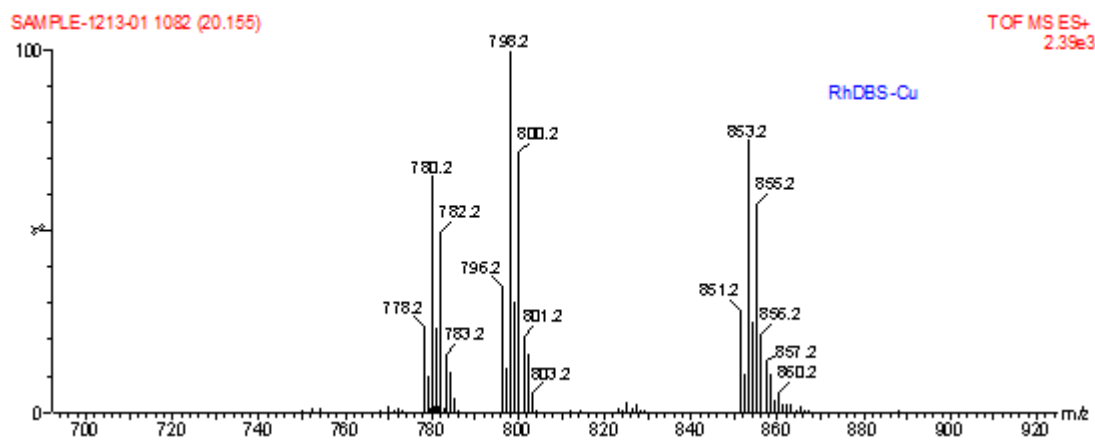
Fig. S17. MS of **RhDBS**+Cu^{2+}.
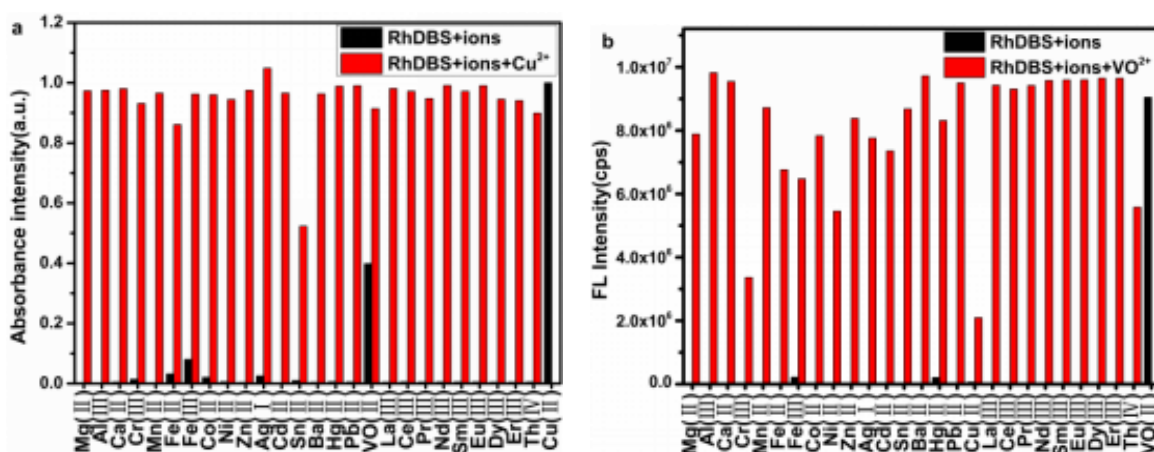
Fig. S18. (a) Absorption and (b) fluorescence spectra of **RhDBS** (20 μM) with various metal ions (20 Eq.) and Cu^{2+}/VO^{2+}(10 Eq.) in DMSO–Tris-HCl (7:3, v/v, pH 7.4) solution. The black and red bars represent the absorption or emission intensity of **RhDBS** in the presence of other metal ions (20 Eq.) and in the presence of the selected metal ions, followed by addition 10 Eq. of Cu^{2+}/VO^{2+} ion, respectively.

Fig. S19. calibration curve for (a) VO^{2+} and (b) for Cu^{2+}.

Fig. S20. QY of **RhDBS** in aqueous DMSO solution.
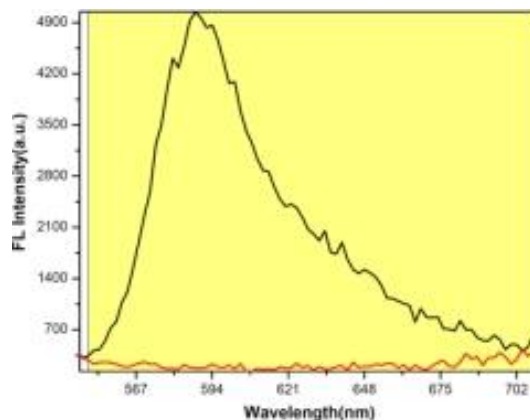
Fig. S21. QY of **RhBS**.
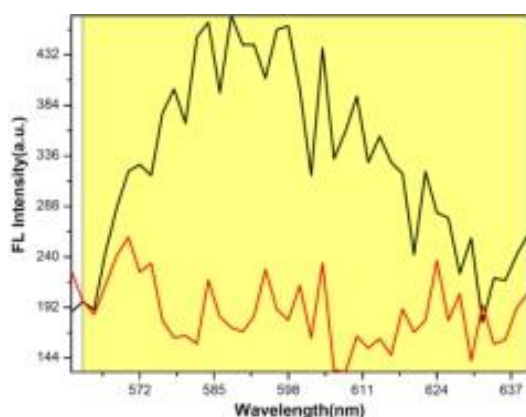
Fig. S22. QY of **RhHS**.
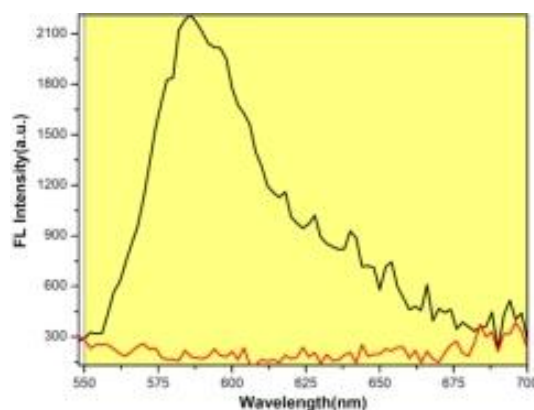
Fig. S23. QY of **RhS**.

Table S5. Quantum yield and lifetime value for the **RhDBS**(20 μM) in the presence and absence of VO^{2+} ion. Conditions: λ_{exc}= 520 nm; T= 298 K; DMSO:H_2O (7:3, v/v).

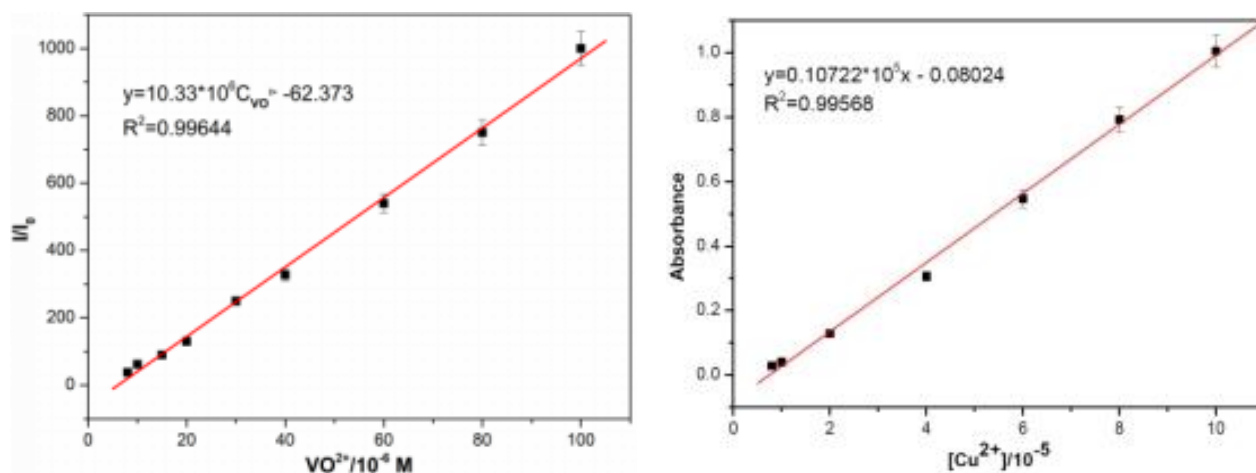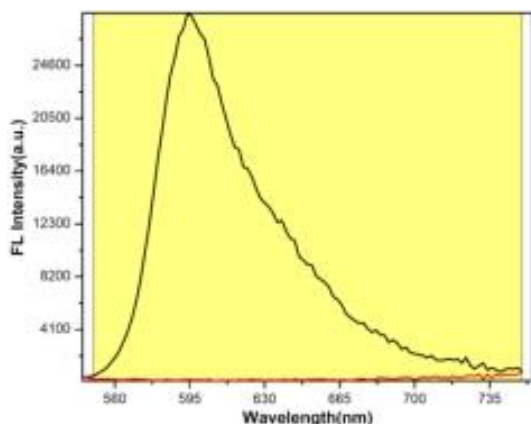| S.No	Ex (nm)	Em (nm)	$^a\tau_1$(ns)	$^a\tau_2$(ns)	T_{avg} (ns)	CHI-SQ	Quantum Yield (Φ_F%)	K_r	K_{nr}	K_r/K_{nr}
RhDBS	520	NA	0.95 (86.96)	2.44 (13.04)	1.03	1.35	0.028	0.0003	0.9706	0.0003
RhDBS+ VO^2	520	586	1.84 (100)	0	1.84	1.23	70.114	0.381	0.1624	2.346
RhBS	520	NA	0.41 (92.64)	3.6 (7.36)	0.44	0.905	0.058	0.0013	2.2714	0.0006
RhBS+ VO^{2+}	520	586	0.588 (89.31)	3.02 (10.69)	0.64 3	1.13	26.158	0.4068	1.1484	0.3542
RhHS+ VO^{2+}	520	586	-	-	-	-	0.902	-	-	-
RhS+ VO^{2+}	520	586	-	-	-	-	10.824	-	-	-

Absorption of **S.** λ_{max} = 560 nm; Fluorescence excitation λ_{exc} = 520 nm; Fluorescence emission λ_{max} = 586 nm. Concentration of VO^{2+} (10 eq.); ^{a} Abundances shown in brackets.
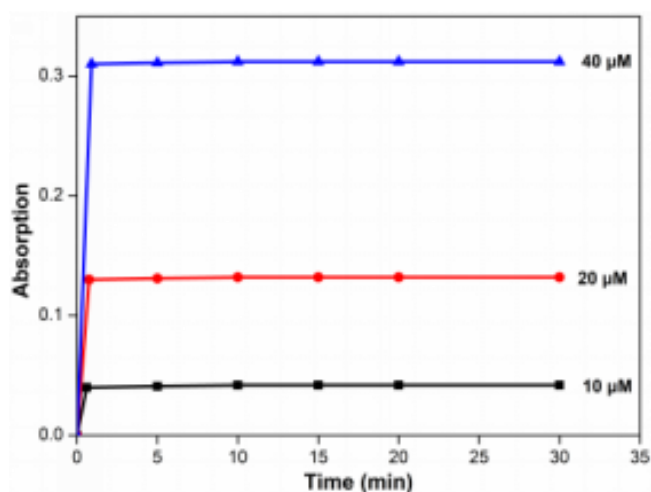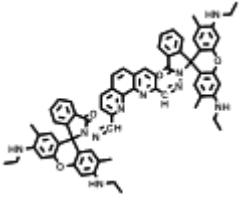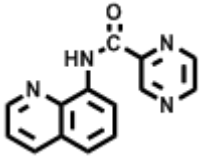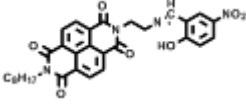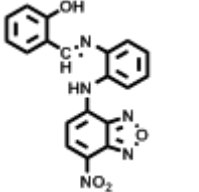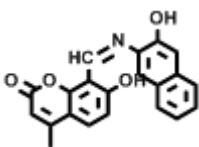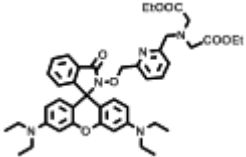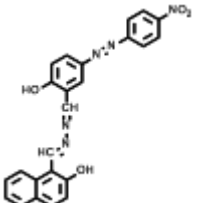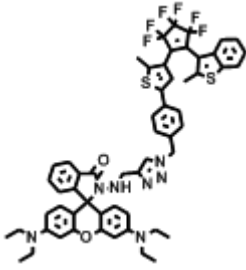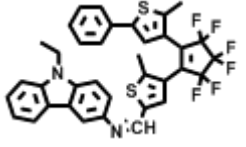
Fig. S24. Time course of the response of **RhDBS** (20 µmol/L, DMSO/Tris-HCl buffer, pH = 7.4) to 10.0 µmol/L, 20.0 µmol/L, 40 µmol/L of Cu^{2+} in aqueous solution. (For interpretation of the references to color in this figure legend, the reader is referred to the web version of this article.)
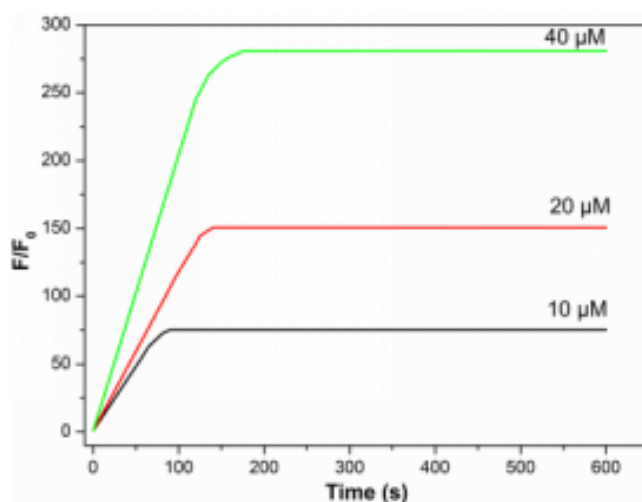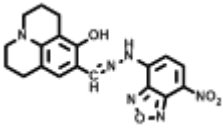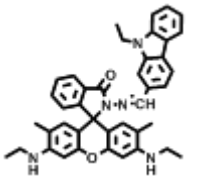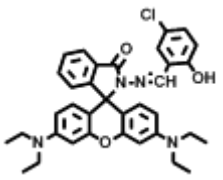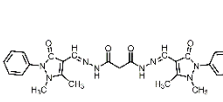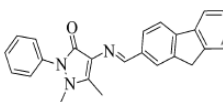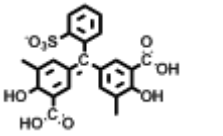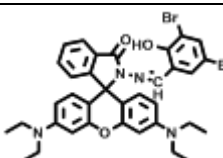
Fig. S25. Kinetics of the fluorescence enhancement of compound **RhDBS**(20 µM) in the presence of different concentrations of VO^{2+}. Fluorescence intensity is recorded at 586 nm. Excitation wavelength is 520 nm, slit: 2.5/5 nm.

Table S6. Comparison of analytical performances of our sensor with recently reported chemosensors.

SI. no.	Sensing probe	Ex. (nm)/ Em. (nm)	Medium	LOD	Theory study	Anion sensing property	Analytical applications	Advanced level logic gate study	Bio- imaging	Ref.
1.		505/554	ACN-HEPES (0.01 M, 4:1, v/v, pH 7.0)	NA(Cu^{2+}, Hg^{2+})	No	S^{2-}	No	Yes	HepG2 and HeLa cells	[4]

No.	Structure	λ	Solvent	LOD						Ref.
2.		360/476	ACN	14.8 µM Cu^{2+} 1.11 µM Zn^{2+}	Yes	SCN$^-$	No	Yes	No	[5]
3.		NA	DMSO-H$_2$O (9:1, v/v)(Cu^{2+}); THF-H$_2$O(9:1, v/v)(Fe^{3+})	0.26 µM Cu^{2+} 0.1 µM Fe^{3+}	Yes	No	No	No	No	[6]
4.		NA	CH$_3$OH-HEPES (1:1, v/v, pH 7.0)	0.18 µM Cu^{2+} 1.1 µM Ni^{2+}	Yes	No	Filter paper & silica gel	No	No	[7]
5.		NA	DMSO-H$_2$O(3:7, v/v)(Cu^{2+}); MeOH-H$_2$O(3:7, v/v)	7.99 µM Cu^{2+} 0.86 nM Ag$^+$	No	No	No	No	No	[8]
6.		483/576	ACN-HEPES (0.01 M, 1:99, v/v, pH 6.5)(Pb^{2+}); ACN-HEPES (0.01 M, 1:99, v/v, pH 7.2)(Cu^{2+})	0.58 µM Cu^{2+} 0.25 µM Pb^{2+}	Yes	No	No	No	HepG2 cells	[9]
7.		340/443	THF-Tris-HCl (9:1, v/v, pH 7.0)	1.26 µM Cu^{2+} 2.45 µM Co^{2+}	No	No	No	No	No	[10]
8.		520/595	ACN(Al^{3+}); ACN-H$_2$O(2:3, v/v)	NA(Cu^{2+}, Al^{3+})	No	No	No	Yes	No	[11]
9.		310/401	CH$_3$OH	1.2 µM Cu^{2+} 1.9 µM Sn^{2+}	No	No	Natural water samples	No	No	[12]

No.	Structure	λex/λem	Medium	LOD			Application			Ref.
10.		NA	DMSO-bis-Tris (0.01 M, 1:1, v/v, pH 7.0)	0.36 μM Cu^{2+} 0.59 μM Cr^{3+}	Yes	No	Water samples & filter papers	No	No	[13]
11.		531/552	CH$_3$CN-H$_2$O (5:5, v/v)	39 nM Cu^{2+} 1.49 mM Ce^{4+}	Yes	No	Filter paper	Yes	No	[14]
12.		530/583	MeOH-HEPES (10 mM, 1:1, v/v, pH 7.0)	μM (Cu^{2+}, VO^{2+})	No	P$_2$O$_7^{4-}$	No	No	No	[15]
13.		310/425, 310/375	DMF-H$_2$O (1:99, V/V, pH 7.4) for VO^{2+}; aqueous β-CD for Al^{3+}	50 nm VO^{2+} 0.5 μM Al^{3+}	Yes	No	No	No	No	[16]
14.		317/411	MeOH-H$_2$O (1:1, V/V)	μM VO^{2+}	Yes	EDTA	No	Yes	No	[17]
15.		colorimetric	Acetic acid-Ammonia(pH 6.0)	0.103 μM VO^{2+}	No	No	Real water samples	No	No	[18]
16.	DPCSV	NA	BRB (0.04 M, pH 4.0)	1.2 μM V(IV)	No	No	Benfield sample	No	No	[19]
17.		520/586	DMSO-Tris-HCl (0.01 M, 7:3, v/v, pH 7.4)	0.84 μM Cu^{2+} 3.65 nM VO^{2+}	Yes	P$_2$O$_7^{4-}$	Paper strip & TLC plate	Yes	MCF-7 cells	This work

TCSPC experiments

We have calculated the radiative rate constant (k_r) and the total non-radiative rate constant (k_{nr}) of the free **RhDBS**, and the **RhDBS-**VO^{2+} complex using the following equations [20]:

$$\tau^{-1} = k_r + k_{nr} \tag{1},$$
$$k_r = \Phi/\tau \tag{2}.$$

Where τ, k_r, k_{nr}, and Φ are the mean fluorescence lifetime, radiative rate constant, the total non-radiative rate constant and fluorescence quantum yield, respectively. The results were listed in Table S5.

Electrochemical measurements

Cyclic voltammetry (CV) of the samples were performed on a CHI760D electrochemical workstation using a three-electrode system at room temperature. Platinum plates were used as working and counter electrodes, and saturated calomel electrode as the reference electrode. The working electrode was centrally placed to keep a minimum distance between the counter and reference electrodes for minimizing the IR drop effect. The surface of working electrode was thorough rinsing with doubly distillated water before every experimental assay. All electrochemical experiments were carried out under nitrogen saturated solutions.
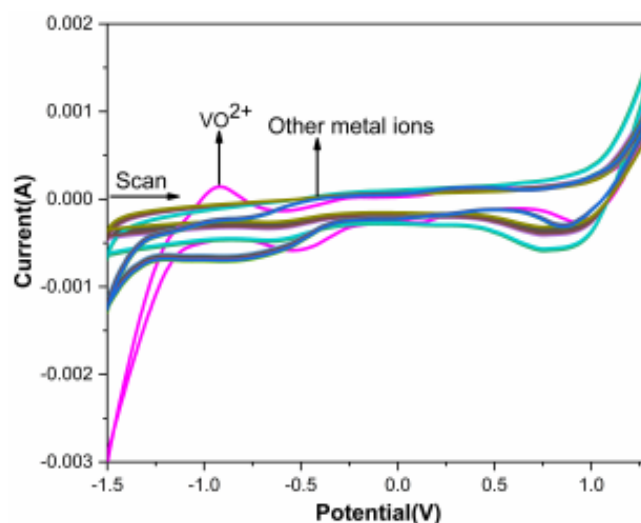
Fig. S26. Cyclic Voltammetry spectra of chemosensor **RhDBS** observed upon addition of 1 equiv. of various metal ions in DMSO/H_2O (7:3,v/v, 100 μM), KCl as supporting electrolyte and scanned at 50 mVs^{-1}.

Determination of quenching efficiency[21]

$$\text{Quenching efficiency} = (I_0 - I_f)/I_0 \times 100$$

In this equation I_0, I_f are the fluorescence intensities respectively, in the presence of 10 eqv. VO^{2+} and at the saturation of the interaction of PPi. Quenching efficiency of **RhDBS**-VO^{2+} for PPi ion = 95%.

(A) Truth table

INPUT		OUTPUT
IN1	IN2	OUT
VO²⁺	Cu²⁺	Emission at 586 nm
0	0	0
0	1	0
1	0	1
1	1	0

(B) Truth table

INPUT		OUTPUT
IN1	IN2	OUT
VO²⁺	PPi	Emission at 586 nm
0	0	0
0	1	0
1	0	1
1	1	0

INPUT		OUTPUT
IN1	IN2	OUT
Cu²⁺	PPi	Absorption at 560 nm
0	0	0
0	1	0
1	0	1
1	1	0
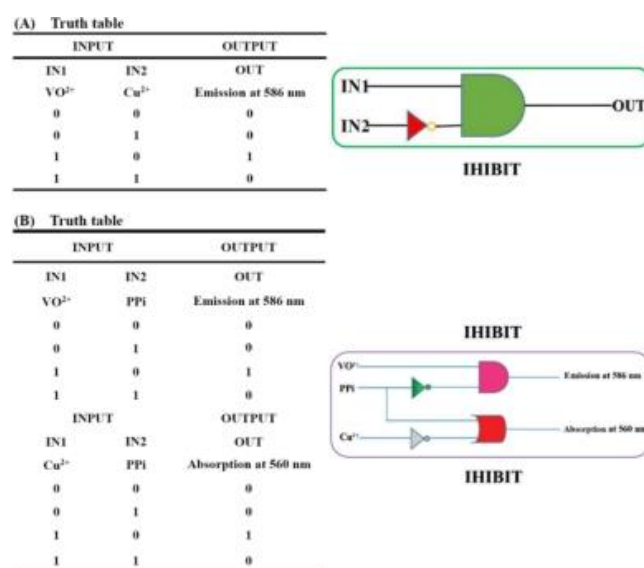
Fig. S27. Truth table and the monomolecular circuit based on (A) VO^{2+} and Cu^{2+} and (B) VO^{2+} with PPi and PPi with Cu^{2+}.

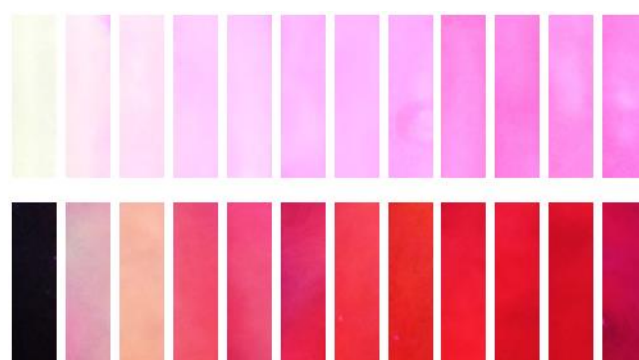**Fig. S28.** Fluorescent detection of VO^{2+} ions by paper film: after being sprayed with different concentration of aqueous VO^{2+} solutions (from left to right: 0 M, 10^{-7} M, 2×10^{-7} M, 5×10^{-7} M, 10^{-6} M, 2×10^{-6} M, 5×10^{-6} M, 10^{-5} M, 2×10^{-5} M, 5×10^{-5} M, 10^{-4} M, and 10^{-3} M). Top: day light; Bottom: UV light (365 nm).

Toxicity Evaluation

As a promising bio-probe, the cytotoxicity of the probe is also critical determinant for its long- and real-time and sensitively monitoring of the analytes. However, there are few reports on the investigation of the feature of the rhodamine-based sensor towards metal ions. To further evaluate the potential application of **RhDBS** as bio-probe for the detection of vanadyl in living cells, we studied their cytotoxicity in human breast carcinoma MCF-7 cells by determining cellular viability using an MTT assay. In the experiments, MCF-7 cells were incubated with different concentrations of **RhDBS** at dark for 24 h in advance. As shown in Fig. S28, **RhDBS** has no significant influence on cell viability even at high concentration of up to 100 μM (cell viability～80%), exhibiting very low and negligible cytotoxicity of **RhDBS**. Therefore, the probe can be further tested in vitro.
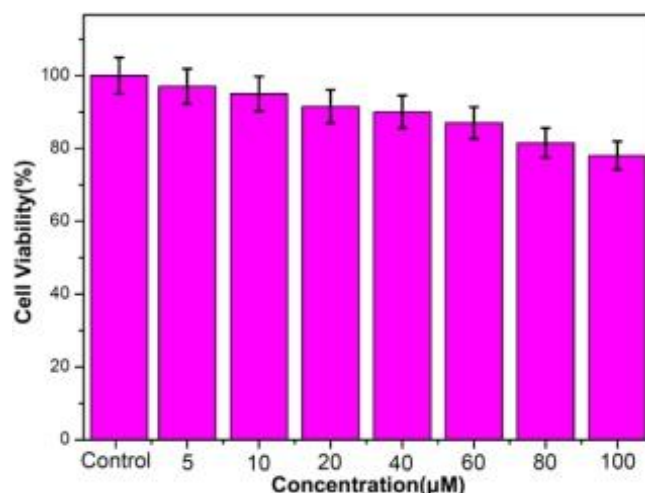
Fig. S29. MTT assay of MCF-7 cells viability after incubation with **RhDBS**(0−100 μM) for 24 h.

Cell imaging

The human breast cancer cells (MCF-7) were cultured in Roswell Park Memorial Institute (RPMI-1640) supplemented with 10% fetal bovine serum (FBS, Hyclone), 100 μg/mL penicillin and 100 μg/mL streptomycin at 37°C in a humidified atmosphere containing 5% CO_2. 24 h before imaging, cells were seeded in laser scanning confocal microscope (LSCM) culture dishes. The dishes were subsequently incubated at 37 °C in a humidified atmosphere containing 5% CO_2.
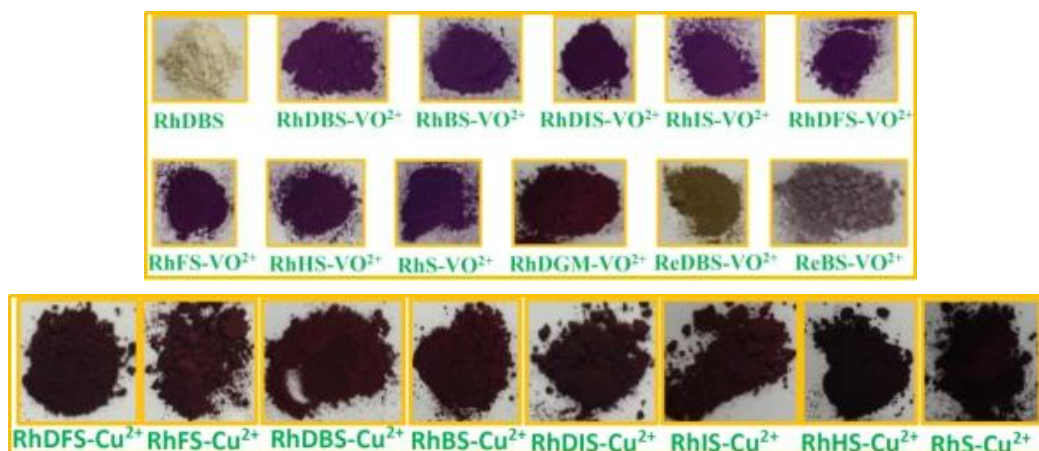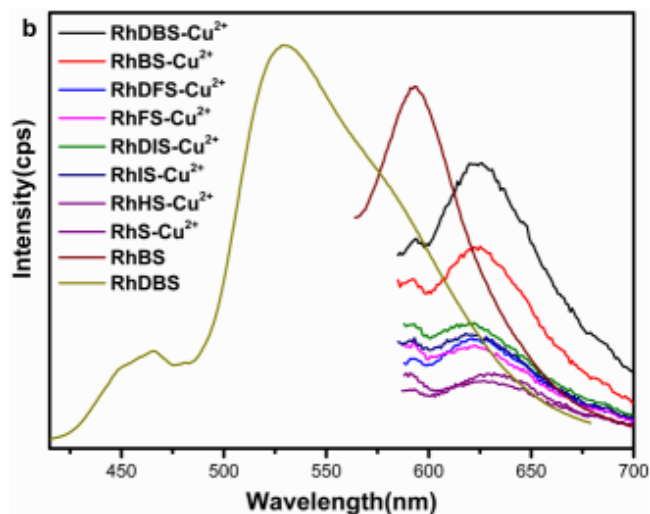
Fig. S30. Visual color change upon mechanical grinding receptors (RhDBS, RhBS, RhDFS, RhFS, RhDIS, RhIS, RhHS, RhS) with the nitratesalts of Cu^{2+} and VO^{2+} ions and their emission spectra in the solid state (λ_{ex}= 400 nm, slit: 2.5/5 nm).

Table S7. CIE coordinates table.

Sample composition	CIE 1931 indices	Em(nm)	Δλ(nm)
RhDBS-VO^{2+}	x = 0.6388; y = 0.3608	615	86
RhBS-VO^{2+}	x = 0.6388; y = 0.3608	615	
RhDFS-VO^{2+}	x = 0.6329; y = 0.3667	613	
RhFS-VO^{2+}	x = 0.6479; y = 0.3497	619	
RhDIS-VO^{2+}	x = 0.6479; y = 0.3518	614	
RhIS-VO^{2+}	x = 0.6381; y = 0.3616	614	
RhHS-VO^{2+}	x = 0.657; y = 0.3427	621	
RhS-VO^{2+}	x = 0.6584; y = 0.3413	616	
ReDBS-VO^{2+}	x = 0.572; y = 0.4273	591	
ReBS-VO^{2+}	x = 0.5721; y = 0.4272	592	
RhDGM-VO^{2+}	x = 0.6533; y = 0.3464	619	
RhDBS-Cu^{2+}	x = 0.6597; y = 0.34	626	97
RhDBS(Solid)	x = 0.3462; y = 0.5108	529	-
RhDBS-VO^{2+}(Solution)	x = 0.573; y = 0.4262	587	58
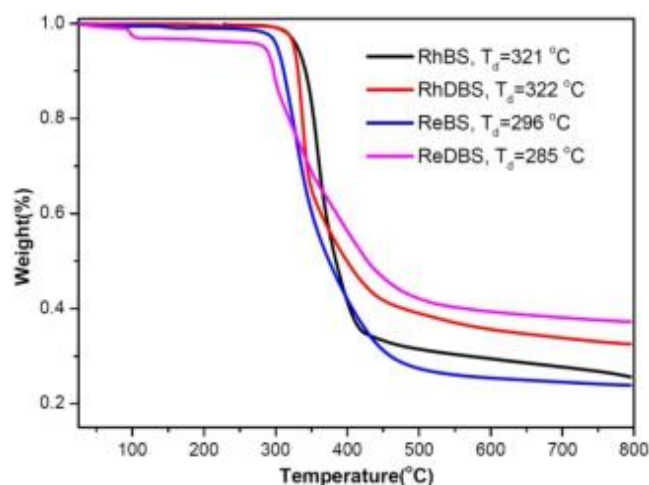
Fig. S31. Thermogravimetric analysis (TGA) of **RhDBS, RhBS, ReDBS** and **ReBS** at heating rate 10 °C/ min under a N_2 atmosphere.

Synthesis of pyrazole derivatives:
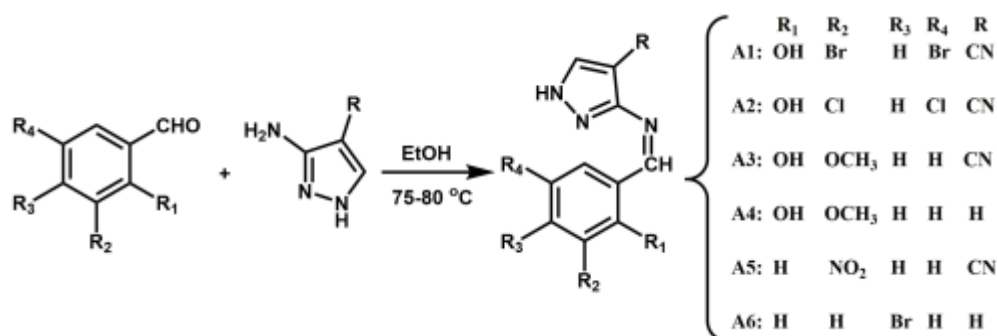
Scheme S2. Synthetic routes of pyrazole derivatives.

To a solution of pyrazole derivatives (10 mmol) and glacial acetic acid (catalyst, two or three drops) in absolute ethanol was added aryl aldehyde dropwise with a CP. dropping funnel (10 mmol). The resulting solution was refluxed for 3 h. The expected compound A precipitated and it was then hot-filtered and washed with cold ethanol-diethyl ether, and finally the crude product was recrystallized with ethanol and dried under vacuum.

3-[(3,5-dibromo-2-hydroxyl-phenyl)-imine]-4-carbonitrile-1*H*-pyrazole (**A1**): orange solid, yield 56%. Elemental analysis (Calc. %): C 35.61 (35.71), H 1.75 (1.63), N 15.03 (15.14). IR (KBr, ν, cm^{-1}): 3850 (m), 3420 (s), 2239 (s), 1600 (s), 1549 (w), 1491 (w), 1442 (w), 1378 (m), 1292 (m), 1222 (m), 1133 (w), 981 (w), 865 (w), 821 (w). ^{1}HNMR (300MHz，DMSO-d$_6$): δ = 13.699 (s, 1H, -C$_4$N$_3$H$_2$), δ = 13.000 (s, 1H, -OH), δ = 9.3000 (s, 1H, -CNH), δ = 8.5585 (s, 1H, -C$_4$N$_3$H$_2$), δ = 7.932 (s, 2H, -C$_6$H$_2$Br$_2$). ESI-MS m/z: calcd.for C$_6$H$_4$OBr$_2$: 251.892 found: 250.8 [M1-H]$^-$;calcd.for C$_7$H$_5$ONBr$_2$: 277.912 found: 276.8 [M2-H]$^-$;calcd.for C$_{11}$H$_6$ON$_4$Br$_2$: 369.95 found: 368.8 [M-H]$^-$.

3-[(3,5-dichloro-2-hydroxyl-phenyl)-imine]-4-carbonitrile-1*H*-pyrazole (**A2**): orange solid, yield 80%. Elemental analysis (Calc. %): C 44.01 (44.11), H 1.79 (1.68), N 18.60 (18.70). IR (KBr, ν, cm^{-1}

^{1}): 3448 (s), 3228 (s), 2241 (s), 1608 (s), 1550 (w), 1448 (s), 1382 (s), 1180 (m), 842 (m), 735 (s), 632 (s). ^{1}HNMR (300MHz，DMSO-d$_6$): δ = 13.90 (s, 1H, -C$_4$N$_3$H$_2$), δ = 13.40 (s, 1H, -OH), δ = 9.31 (s, 1H, -CNH), δ = 8.64 (s, 1H, -C$_4$N$_3$H$_2$), δ = 7.91 (s, 1H, -C$_6$H$_2$Cl$_2$), δ = 7.81 (s, 1H, -C$_6$H$_2$Cl$_2$).ESI-MS m/z: calcd.for C$_6$H$_3$OCl$_2$: 161.984 found: 160.9 [M1-H]$^-$;calcd.for C$_7$H$_5$ONCl$_2$: 190.02 found: 188.9 [M2-H]$^-$;calcd.for C$_{11}$H$_6$ON$_4$Cl$_2$: 281.07 found: 278.9 [M-H]$^-$.

3-[(2-hydroxyl-3-methoxyl-phenyl)-imine]-4-carbonitrile-1*H*-pyrazole (**A3**): yellow solid, yield 70%. Elemental analysis (Calc. %): C 59.40 (59.50), H 4.27 (4.16), N 23.03 (23.13). IR (KBr, ν, cm^{-1}): 3448 (w), 3311 (w), 3275 (w), 2231 (s), 1613 (s), 1466 (s), 1381 (w), 1252 (s), 969 (s), 778 (s), 731 (s). ^{1}HNMR (300MHz，DMSO-d$_6$): δ = 13.74 (s, 1H, -C$_4$N$_3$H$_2$), δ = 12.02 (s, 1H, -OH), δ = 9.29 (s, 1H, -CNH), δ = 8.61 (s, 1H, -C$_4$N$_3$H$_2$), δ = 7.385 (d, 1H, - C$_6$H$_3$), δ = 7.195 (d, 1H, - C$_6$H$_3$), δ = 6.94 (t, 1H, -C$_6$H$_3$), δ = 3.85 (s, 3H, -OCH$_3$).ESI-MS m/z: calcd.for C$_{12}$H$_{10}$O$_2$N$_4$: 242.16 found: 265 [M+Na]$^+$.

3-[(2-hydroxyl-3-methoxyl-phenyl)-imine]-1*H*-pyrazole (**A4**): yellow solid, yield 46%. Elemental analysis (Calc. %): C 60.72 (60.82), H 5.22 (5.10), N 19.22 (19.34). IR (KBr, ν, cm^{-1}): 3448 (ms), 3150 (w), 1615 (s), 1477 (s), 1251 (s), 1070 (ms), 976 (s), 798 (ms), 784 (s), 736 (s). ^{1}HNMR (300MHz，DMSO-d$_6$): δ = 13.25 (s, 1H, -C$_3$N$_2$H$_3$), δ = 12.87 (s, 1H, -OH), δ = 9.09 (s, 1H, -CNH), δ = 7.78 (d, 1H, -C$_3$N$_2$H$_3$), δ = 7.21 (d, 1H, -C$_6$H$_3$), δ = 7.12 (d, 1H, -C$_6$H$_3$), δ = 6.91 (t, 1H, -C$_6$H$_3$), δ = 6.53 (d, 1H, -C$_3$N$_2$H$_3$), δ = 3.82 (s, 3H, -OCH$_3$). ESI-MS m/z: calcd.for C$_{11}$H$_{11}$O$_2$N$_3$: 217.14 found: 240 [M+Na]$^+$.

3-[(3-nitro-phenyl)-imine]-4-carbonitrile-1*H*-pyrazole (**A5**): off-white solid, yield 65%. Elemental analysis(Calc. %): C 54.65 (54.77), H 3.04 (2.93), N 28.93 (29.03),. IR (KBr, ν, cm^{-1}): 3567 (m), 2242 (s), 1524 (s), 1354 (s), 810 (s), 741 (s), 1292 (m), 699 (s). ^{1}HNMR (300MHz，DMSO-d$_6$): δ = 13.75 (s, 1H, -C$_4$N$_3$H$_2$), δ = 9.22 (s, 1H, -CNH), δ = 8.80 (s, 1H, -C$_4$N$_3$H$_2$), δ = 8.62 (t, 1H, -C$_6$NH$_4$O), δ = 8.43 (d, 2H, -C$_6$NH$_4$O), δ = 7.84 (s, 1H, -C$_6$NH$_4$O).ESI-MS m/z: calcd.for C$_{11}$H$_7$O$_2$N$_5$: 241.216 found: 241.0 [M-H]$^-$.

3-[(4-bromophenyl)-imine]-1*H*-pyrazole (**A6**): colourless solid, yield 40%. Elemental analysis (Calc. %) : C 48.02 (48.02), H 3.33 (3.22), N 16.70 (16.80). IR (KBr, ν, cm^{-1}): 3178 (m), 3127 (m), 1620 (s), 1586 (s), 1485 (ms), 1376 (s), 1187 (s), 1061 (s), 1009 (s), 991 (s), 820 (s), 779 (s). ^{1}HNMR (300MHz，DMSO-d$_6$): δ = 12.76 (s, 1H, -C$_3$N$_2$H$_3$), δ = 8.88 (s, 1H, -CNH), δ = 7.865 (d, 2H, -C$_6$H$_4$Br), δ = 7.725 (d, 2H, -C$_6$H$_4$Br), δ = 7.725 (d, 1H, -C$_3$N$_2$H$_3$), δ = 6.44 (d, 1H, -C$_3$N$_2$H$_3$).ESI-MS m/z: calcd.for C$_{10}$H$_{8Br}$N$_3$: 250.094 found: 247.9 [M-H]$^-$.

Table S8. Crystallographic information table for **A1**, **A4**, **A6**.

	A1	**A4**	**A6**
Empirical formular	C$_{11}$H$_6$ON$_4$Br$_2$	C$_{11}$H$_{11}$O$_2$N$_3$	C$_{10}$H$_8$N$_3$Br
Formula weight	370.00	217.23	250.10
Crystal size/mm^3	0.3×0.28×0.20	0.30×0.28×0.18	0.26×0.23×0.22
Temperature/K	293(2)	293(2)	293(2)

Crystal system	Monoclinic	Orthorhombic	Monoclinic
Space group	$P2_1/c$	$P2_12_12_1$	$P2_1$
a / Å	8.9518(8)	5.2596(5)	5.5766(5)
b / Å	14.1336(11)	11.9561(11)	5.1057(4)
c / Å	9.5923(10)	16.2307(15)	17.3046(14)
α/°	90.00	90.00	90.00
β /°	91.233(8)	90.00	94.285(9)
γ/°	90.00	90.00	90.00
V / Å^3	1213.35(19)	1020.66(16)	491.33(7)
Z	4	4	2
D_{calc} /g·cm^{-3}	2.026	1.414	1.691
μ/ mm^{-1}	6.673	0.101	4.143
θ range/°	3.4 to 25.0	3.0 to 25.0	3.5 to 26.0
Reflections collected	5028	2765	1777
Independent reflections	2130	1763	1422
Observed reflections	1665	1471	1131
$F(000)$	712	456	248
Data/restraints/parameters	2130/0/168	1763/0/148	1422/1/129
Goodness-of-fit on F^2	1.062	1.170	1.09
R(all data)	$R_1 = 0.0537$, $wR_2 = 0.0881$	$R_1 = 0.0615$, $wR_2 = 0.1200$	$R_1 = 0.1028$, $wR_2 = 0.2391$
R indexes [$I>2\sigma(I)$]	$R_1 = 0.0367$, $wR_2 = 0.0881$	$R_1 = 0.0489$, $wR_2 = 0.120$	$R_1 = 0.0795$, $wR_2 = 0.2321$
Largest diff. peak and and hole/e·Å^{-3}	1.05 and -0.79	0.13 and -0.18	0.88 and -1.12

a)$R=\Sigma\|F_o|-|F_c\|/\Sigma|F_o|$; $wR(F^2)=[\Sigma w(F_o^2-F_c^2)^2/\Sigma w(F_o^2)^2]^{1/2}$, $w=1/[\sigma^2(F_o^2)+(0.0351P)^2+1.1683P]$ where $P=(F_o^2+2F_c^2)/3$ for **A1**; $w=1/[\sigma^2(F_o^2)+(0.1347P)^2]$ where $P=(F_o^2+2F_c^2)/3$ for **A4**; $w=1/[\sigma^2(F_o^2)+(0.0425P)^2+0.1770P]$ where $P=(F_o^2+2F_c^2)/3$ for **A6**.
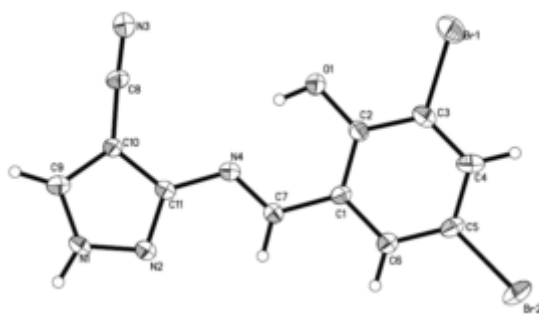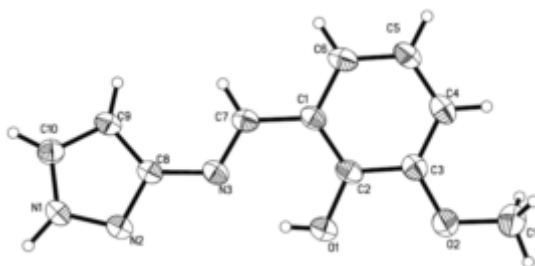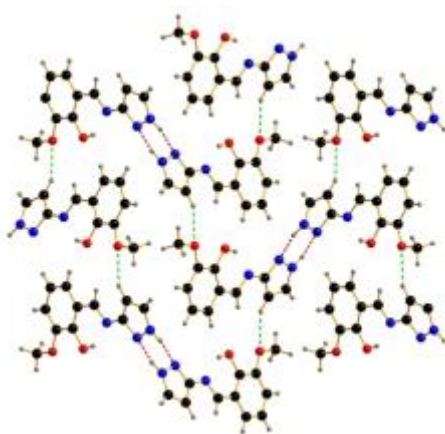
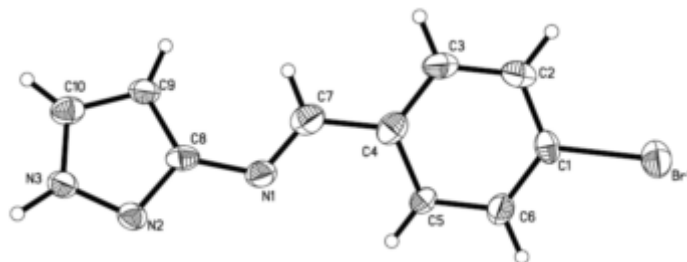**Fig. S32.** Crystal structure of **A1**, the ellipsoid contour percent probability level is 30%.
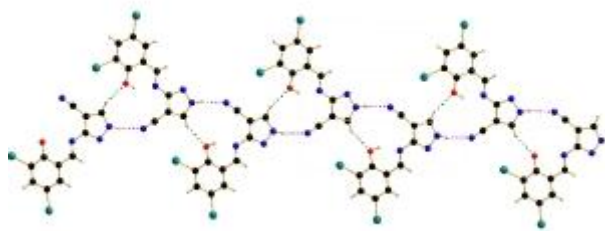
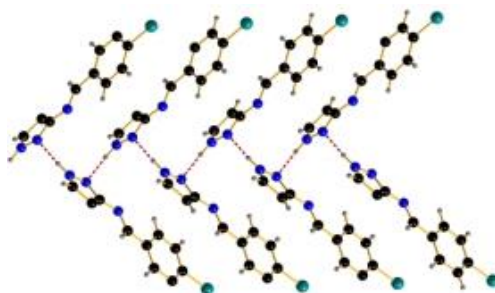**Fig. S33.** The hydrogen bonds (N1—H1···N3 and C9—H2···O) in crystals of **A1**.
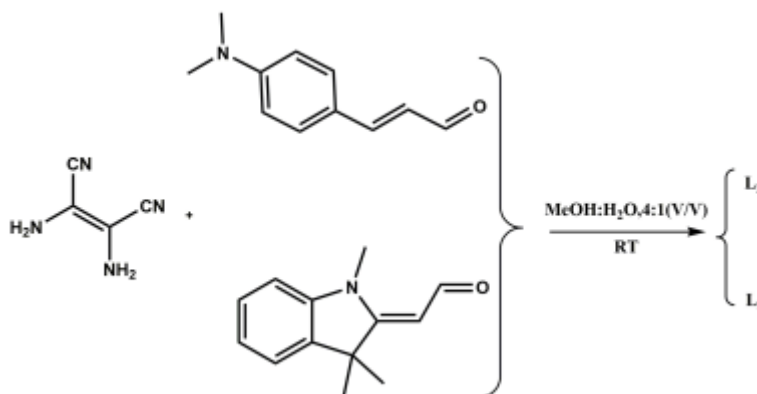

Fig. S34. Crystal structure of **A4**, the ellipsoid contour percent probability level is 30%.

Fig. S35. The hydrogen bonds (N1—H1···N2 and C9—H3···O2) in crystals of **A4**.

Fig. S36. Crystal structure of **A6**, the ellipsoid contour percent probability level is 30%.

Fig. S37. The hydrogen bonds (N1—H1···N2 and C9—H3···O2)in crystals of **A6**.

Preparation of L₂-L₃

Scheme S2. Synthetic routes of receptors **L₂**, **L₃**.

The receptors (**L₂-L₃**) were synthesised by the same procedure mentioned below:
To the stirring solution of 2-equivalents of diaminomalenonitrile (DAMN) in distilled water add 2-3 drops of conc. HCl, followed by dropwise addition of methanolic solution of 1 equivalents of substituted benzaldehydes. The resulted imine solidifies within a minute, was filtered, washed with water and recrystalized with ethanol, and finally dried under vacuum.

L₂: ESI-MS, m/z: calcd for $C_{15}H_{15}N_5$, 265.32; found, [M-H]⁻ 264.12561.FT-IR (KBr, v/cm⁻¹): 3297(N-H); 3178(NH₂); 2903(C-H); 2224, 2205(C≡N); 1597(C=N); 1582, 1550(C=C); 1368(C-N); 1150, 814(C–H). ¹H NMR (DMSO-d_6, 500 MHz) δ(ppm): 8.045 (d, J=9.00 Hz, 1H), 7.464 (bs, 2H), 7.458(d, J=8.50 Hz, 2H), 7.311 (d, J=15.50 Hz, 1H), 6.824(dd, J=9.00,16 Hz, 1H), 6.745 (d, J=9.00 Hz, 2H),

2.988 (s, 6H) ; ^{13}C NMR (DMSO-d_6, 300MHz) δ(ppm): 157.98, 151.27, 145.29, 129.15, 124.39, 122.93, 121.87, 114.61, 113.97, 113.65, 111.83.

L₃: ESI-MS, m/z: calcd for $C_{17}H_{17}N_5$, 291.356; found, [M-H]⁻ 290.14121.FT-IR (KBr, v/cm⁻¹): 3233(N-H); 3097(NH₂); 2986(C-H); 2233, 2208(C≡N); 1662, 1624(C=N); 1595, 1548(C=C); 1330(C-N); 1120, 846, 801, 750(C–H); ^{1}H NMR(300 MHz, DMSO-d_6) δ(ppm)：8.23 (d, J = 12.1 Hz, 1H), 7.59 (d, J = 7.3 Hz, 2H), 7.43 (d, J = 3.4 Hz, 2H), 7.29 (d, J = 3.1 Hz, 1H), 6.35 (d, J = 11.2 Hz, 1H), 3.71 (s, 1H), 3.55 (s, 3H), 1.62 (s, 6H); ^{13}C NMR (300 MHz, DMSO-d_6) δ(ppm): 154.05, 152.04, 142.33, 140.26, 128.28, 125.03, 122.12, 119.73, 114.10, 111.20, 91.54, 88.78, 48.80, 31.19, 27.46.

The other Schiff base receptors (**S₁-S₅, L₁**) were obtained according to the modified literature procedures[22].

Preparation of rhodamine derivatives

The rhodamine B hydrazide (**M1**) was prepared according to the literature method[23]. FT-IR(KBr, v/cm⁻¹): 3430(–NH₂); 2968(–C–H); 1718(C=O, carbonyl); 1615(–NH₂). ESI-MS: m/z , calcd for $C_{28}H_{32}N_4O_2$, 456.576; found, [M+H]⁺ 457.26.

Rhodamine B-ethylenediamine (**M2**) was prepared according to the literature method with minor modifications[24]. The residue was dissolved in 1 M HCl completely to generate a clear red solution. 1 M NaOH was added to the solution dropwise with stirring until the pH of the solution reached 9-10. The suspension was filtered and washed with water, dried in vacuo, affording a pink solid. FT-IR (v/cm⁻¹): 3433(–NH₂); 2970(–C–H); 1687(C=O, carbonyl); 1617(–NH₂). ESI-MS, m/z: calcd for $C_{30}H_{36}N_4O_2$, 484.628; found, [M+H]⁺ 485.292.

M3 was prepared according to the literature method [25].

RhBS: 85% yield. T_d = 321 ^{0}C; ^{1}H NMR (DMSO-d_6, 300 MHz) δ(ppm): 1.10 (t, 12H, NCH₂CH₃, J = 6.9 Hz), 3.34 (q, 8H, NCH₂CH₃, J = 6 Hz), 6.36 (dd, 2H, Xanthene-H, J_1= 3 Hz, J_2= 9 Hz), 6.43 (d, 4H, Xanthene-H, J = 9 Hz), 6.76 (d, 1H, Phen-H, J = 9 Hz), 7.13 (d, 1H, Phen-H, J = 9 Hz), 7.35 (dd, 1H, Phen-H, J_1= 3 Hz, J_2= 9 Hz), 7.51 (d, 1H, Phen-H, J = 3 Hz), 7.55-7.66 (m, 2H, Phen-H), 7.93 (d, 1H, Phen-H, J = 9 Hz), 9.03(s, 1H, NCH), 10.49(s, 1H, OH); ^{13}C NMR (300 MHz, DMSO-d_6) δ(ppm): 163.49, 156.04, 152.65, 150.76, 148.49, 146.43, 133.86, 133.57, 129.81, 128.73, 128.51, 127.40, 123.73, 122.92, 121.57, 118.50, 110.31, 108.09, 104.91, 97.36, 65.52, 43.50, 12.23; FT-IR (KBr, v/cm⁻¹): 3400 (–OH); 2969 (–C–H); 1717 (C=O, carbonyl); 1633 (C=N); 1614 (ArCH); 1545, 1517, 1467, 1428(C=C); 1402, 1373(C-N); 1357 (C=O, carbonyl); 1330, 1304, 1274(–C–H); 1234, 1220(C-O); 1120, 822, 787, 757(–C–H); ESI–MS, m/z: calcd for $C_{35}H_{35}BrN_4O_3$, 639.57; found, [M+H]⁺ 641.19157.

RhS: ESI–MS, m/z: calcd for $C_{35}H_{36}N_4O_3$, 560.3; found, [M+H]⁺ 561.4. FT-IR (KBr, v/cm⁻¹): 2972 (C–H); 1693 (C=O, carbonyl); 1617 (C=N); 1548, 1516, 1428(C=C); 1307, 1266(–C–H); 1223(C-O); 1121, 817, 785, 757(–C–H).^{1}H NMR (DMSO-d_6, 300 MHz) δ(ppm): 1.09 (t, 12H, NCH₂CH₃, J = 6 Hz), 3.34 (q, 8H, NCH₂CH₃, J = 6 Hz), 6.36 (d, 2H, Xanthene-H, J = 6 Hz), 6.44 (d, 4H, Xanthene-

H, J = 6 Hz), 6.83 (t, 2H, Phen-H, J = 9 Hz), 7.13 (d, 1H, Phen-H, J = 9 Hz), 7.24 (t, 1H, Phen-H, J = 9 Hz), 7.30 (d, 1H, Phen-H, J = 9 Hz), 7.56-7.65 (m, 2H, Phen-H), 7.93 (d, 1H, Phen-H, J = 6 Hz), 9.10 (s, 1H, NCH), 10.44 (s, 1H, OH);

RhHS: ESI–MS, m/z: calcd for $C_{35}H_{36}N_4O_4$, 576.3; found, $[M-H]^-$ 575.3. FT-IR (KBr, v/cm^{-1}): 3240 (–OH); 2972 (–C–H); 1659 (C=O, carbonyl); 1620 (C=N); 1547, 1516, (C=C); 1331, 1271(–C–H); 1220(C-O); 1121, 816, 784, 755(–C–H). ^{1}H NMR (DMSO-d$_6$, 300 MHz) δ(ppm): 1.09 (t, 12H, NCH$_2$CH$_3$, J = 5.7 Hz), 3.31 (d, 8H, NCH$_2$CH$_3$, J = 6 Hz), 6.18 (s, 1H, Phen-H), 6.29 (d, 1H, Phen-H, J = 9 Hz), 6.36 (d, 2H, Xanthene-H, J = 6 Hz), 6.42 (s, 4H, Xanthene-H), 7.10 (d, 2H, Phen-H, J = 9 Hz), 7.58 (s, 2H, Phen-H), 7.90 (d, 1H, Phen-H, J = 6 Hz), 9.02(s, 1H, NCH), 9.95(s, 1H, OH), 10.63(s, 1H, OH);

RhDFS: ^{1}H NMR (DMSO-d$_6$,500 MHz) δ(ppm): 1.08 (s, 12H, NCH$_2$CH$_3$), 3.31 (t, 8H, NCH$_2$CH$_3$, J$_1$= 5 Hz, J$_2$= 10 Hz), 6.36 (d, 2H, Xanthene-H, J= 10 Hz), 6.43 (t, 4H, Xanthene-H, J$_1$= 10 Hz, J$_2$= 5 Hz), 7.05 (d, 1H, Phen-H, J = 5 Hz), 7.14 (d, 1H, Phen-H, J = 5 Hz), 7.25 (t, 1H, Phen-H, J$_1$= 5 Hz, J$_2$= 10 Hz), 7.65 (q, 2H, Phen-H, J = 10 Hz), 7.94 (d, 1H, Phen-H, J = 5 Hz), 9.18(s, 1H, NCH), 10.37(s, 1H, OH); ^{13}C NMR (300 MHz, DMSO-d$_6$): 163.70, 152.73, 150.75, 149.77, 149.67, 148.54, 146.04, 141.47, 134.12, 128.90, 128.50, 127.53, 123.89, 123.08, 122.10, 108.70, 108.52, 108.13, 104.77, 97.33, 65.69, 43.57, 12.29; ESI–MS, m/z: calcd for $C_{35}H_{34}F_2N_4O_3$, 596.663; found, $[M+H]^+$ 597.60.

RhDIS: ^{1}H NMR (DMSO-d$_6$,500 MHz) δ(ppm): 1.11 (s, 12H, NCH$_2$CH$_3$), 3.33 (t, 8H, NCH$_2$CH$_3$, J$_1$= 10 Hz, J$_2$= 15 Hz), 6.39 (d, 2H, Xanthene-H, J= 10 Hz), 6.47 (t, 4H, Xanthene-H, J$_1$= 15 Hz, J$_2$= 5 Hz), 7.16 (d, 1H, Phen-H, J = 5 Hz), 7.67 (q, 3H, Phen-H, J = 10 Hz), 7.98 (s, 2H, Phen-H), 8.87(s, 1H, NCH), 11.69(s, 1H, OH); ^{13}C NMR (300 MHz, DMSO-d$_6$): 163.67, 156.09, 152.59, 151.06, 148.91, 148.65, 146.84, 138.90, 134.35, 128.97, 127.75, 127.47, 123.83, 123.21, 120.30, 108.29, 104.09, 97.50, 87.70, 82.07, 65.57, 43.60, 12.31; ESI–MS, m/z: calcd for $C_{35}H_{34}I_2N_4O_3$, 812.473; found, $[M+H]^+$ 813.20.

RhFS: ^{1}H NMR (DMSO-d$_6$, 300 MHz) δ(ppm): 1.06 (t, 12H, NCH$_2$CH$_3$, J$_1$= 9 Hz, J$_2$= 6 Hz), 3.32 (q, 8H, NCH$_2$CH$_3$, J = 6 Hz), 6.43 (dd, 4H, Xanthene-H, J$_1$= 9 Hz, J$_2$= 21 Hz), 6.80 (q, 2H, Xanthene-H, J = 3 Hz), 7.05 (td, 1H, Phen-H, J$_1$= 9 Hz, J$_2$= 3 Hz), 7.13 (t, 1H, Phen-H, J$_1$ =J$_2$= 3 Hz), 7.16 (d, 2H, Phen-H, J = 3 Hz), 7.56-7.65 (m, 2H, Phen-H), 7.93 (d, 1H, Phen-H, J = 9 Hz), 9.16(s, 1H, NCH), 10.20(s, 1H, OH); ^{13}C NMR (300 MHz, DMSO-d$_6$) δ(ppm): 163.59, 156.78, 153.67, 153.33, 152.80, 150.78, 148.53, 147.17, 133.97, 128.88, 127.60, 123.90, 123.03, 120.27, 118.33, 117.67, 113.24, 108.12, 105.02, 97.35, 65.67, 43.52, 12.34; ESI–MS, m/z: calcd for $C_{35}H_{35}FN_4O_3$, 578.67; found, $[M+H]^+$ 579.30.

RhIS: ^{1}H NMR (DMSO-d$_6$, 300 MHz) δ(ppm): 1.08 (t, 12H, NCH$_2$CH$_3$, J$_1$= 6 Hz, J$_2$= 9 Hz), 3.32 (d, 8H, NCH$_2$CH$_3$, J = 6 Hz), 6.43 (dd, 4H, Xanthene-H, J$_1$= 21 Hz, J$_2$= 9 Hz), 6.64 (d, 2H, Xanthene-H, J = 9 Hz), 7.13 (d, 1H, Phen-H, J= 9 Hz), 7.48 (d, 1H, Phen-H, J = 6 Hz), 7.63 (dd, 2H, Phen-H, J$_1$= 15 Hz, J$_2$= 9 Hz), 7.66 (d, 2H, Phen-H, J = 3 Hz), 7.93 (d, 1H, Phen-H, J = 9 Hz), 8.95(s, 1H, NCH), 10.49(s, 1H, OH); ^{13}C NMR (300 MHz, DMSO-d$_6$) δ(ppm): 163.59, 156.67, 152.70, 150.96, 148.55, 146.09, 139.46, 135.82, 134.02, 128.87, 12851, 127.52, 123.85, 123.06, 122.22, 118.98, 108.15, 104.88, 97.37, 81.27, 65.51, 43.63, 12.37; ESI–MS, m/z: calcd for $C_{35}H_{35}IN_4O_3$, 686.58; found,

[M+H]$^+$ 687.20.

ReBS: Yield: 0.286 g, 82%. T_d = 296 ^{0}C; ^{1}H NMR (DMSO-d$_6$, 300 MHz) δ(ppm): 1.10 (t, 12H, NCH$_2$CH$_3$, J = 6 Hz), 3.34 (q, 12H, CH$_2$, J = 9 Hz), 6.29 (s, 4H, Xanthene-H), 6.38 (s, 2H, Xanthene-H), 6.8 (d, 1H, Phen-H, J = 9 Hz), 7.02 (d, 1H, Phen-H, J = 6 Hz), 7.45 (t, 2H, Phen-H, J = 9 Hz), 7.51 (t, 2H, Phen-H, J = 3 Hz), 7.80 (d, 1H, Phen-H, J = 6 Hz), 8.03(s, 1H, NCH), 13.05(s, 1H, OH); ^{13}C NMR (300 MHz, DMSO-d$_6$) δ(ppm): 167.05, 164.70, 159.66, 153.16, 152.54, 148.31,134.36, 133.08, 132.55, 130.18, 128.16, 128.11, 123.46, 122.16, 120.15, 118.73, 108.77, 108.03, 104.93, 97.21, 63.88, 56.00, 43.49, 12.23; ESI-MS(m/z): calcd for C$_{37}$H$_{39}$BrN$_4$O$_3$, 667.622; found, [M+H]$^+$ 669.22347; FT-IR (KBr, v/cm^{-1}): 3436 (–OH); 2968, 2927 (–C–H); 1690 (C=O, carbonyl); 1634 (C=N); 1615 (ArCH); 1546, 1515, 1467, 1446, 1426(C=C); 1376(C-N); 1356 (C=O, carbonyl); 1329, 1305, 1266(–C–H); 1232, 1219(C-O); 1118, 819, 787, 759(–C–H).

ReDBS: Yield: 0.286 g, 82%. T_d = 285 ^{0}C; ^{1}H NMR (DMSO-d$_6$, 300 MHz) δ(ppm): 1.09 (t, 12H, NCH$_2$CH$_3$, J = 6 Hz), 3.37 (dd, 10H, CH$_2$, J$_1$ = 6 Hz, J$_2$ = 24 Hz), 3.44 (s, 2H, CH$_2$), 6.25-6.36 (m, 6H, Xanthene-H), 7.00 (d, 1H, Phen-H, J = 3 Hz), 7.41 (s, 1H, Phen-H), 7.49 (d, 2H, Phen-H, J = 3 Hz), 7.72 (s, 1H, Phen-H), 7.80 (t, 1H, Phen-H, J = 3 Hz), 8.05(s, 1H, NCH), 14.24(s, 1H, OH); ^{13}C NMR (300 MHz, DMSO-d$_6$) δ(ppm): 167.37, 165.13, 161.36, 153.28, 152.50, 148.29, 140.23, 137.26, 133.45, 132.64, 129.98, 128.08, 123.46, 122.22, 118.39, 113.60, 108.08, 105.64, 104.72, 97.23, 64.01, 55.88, 53.06, 43.49, 12.25; FT-IR (KBr, v/cm^{-1}): 3430 (–OH); 2968, 2927 (–C–H); 1690 (C=O, carbonyl); 1634 (C=N); 1615 (ArCH); 1546, 1515, 1467, 1446, 1426(C=C); 1376(C-N); 1356 (C=O, carbonyl); 1329, 1305, 1266(–C–H); 1232, 1219(C-O); 1118, 819, 787, 759(–C–H); ESI-MS(m/z): calcd. for C$_{37}$H$_{38}$Br$_2$N$_4$O$_3$, 746.514; found, [M+H]$^+$ 747.13309.
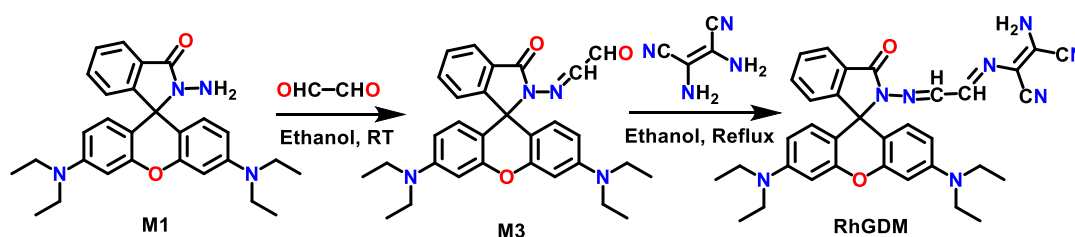
Scheme S3. Synthetic route of receptor **RhGDM**.

RhDGM: ^{1}H NMR (DMSO-d$_6$, 500 MHz) δ(ppm)：8.50 (d, J = 5.0 Hz, 1H), 8.30 (d, J = 10 Hz, 1H), 7.95 (d, J = 10 Hz, 1H), 7.67~7.53 (m, 3H), 7.07 (d, 2H, NH$_2$, J = 5 Hz,), 6.38 (t, 6H, J$_1$= 30 Hz, J$_2$= 10 Hz), 3.61 (d, J = 10 Hz, 8H), 1.09 (t, 12H, J$_1$= 10 Hz, J$_2$= 5 Hz). ^{13}C NMR (300 MHz, DMSO-d$_6$) δ: 165.03, 152.86, 152.25, 149.07, 145.89, 135.20, 130.12, 129.45, 127.98, 127.82, 127.72, 124.27, 123.91, 114.48, 113.76, 108.60, 105.22, 103.06, 97.96, 66.26, 44.11, 12.91. ESI-MS, m/z: calcd for C$_{34}$H$_{34}$N$_8$O$_2$, 586.334; found, [M+H]$^+$ 587.2.
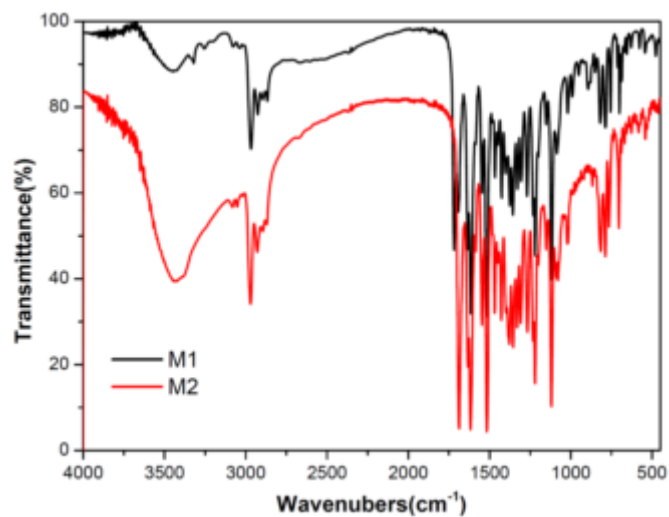
Fig. S38. IR of **M1**、**M2**.
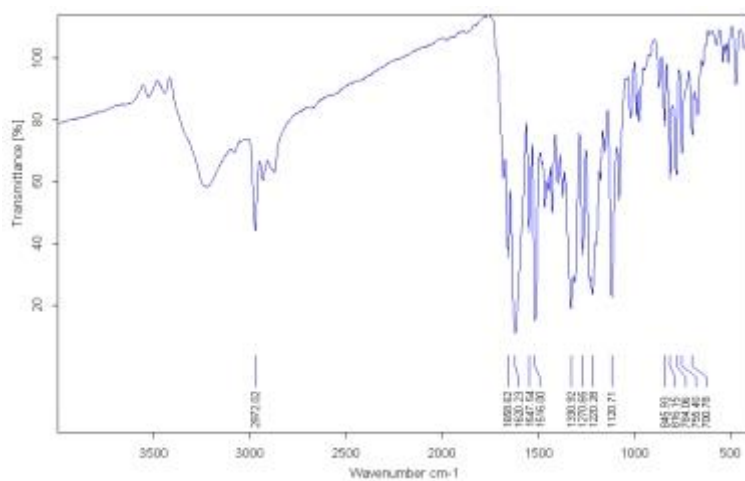
Fig. S39. IR of **RhHS**.
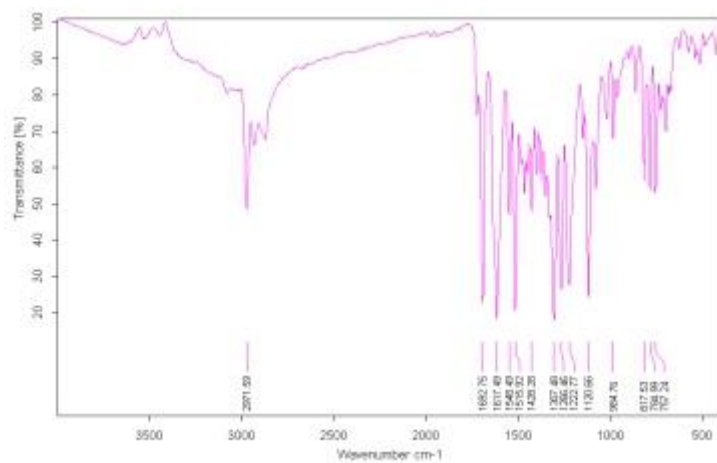
Fig. S40. IR of **RhS**.
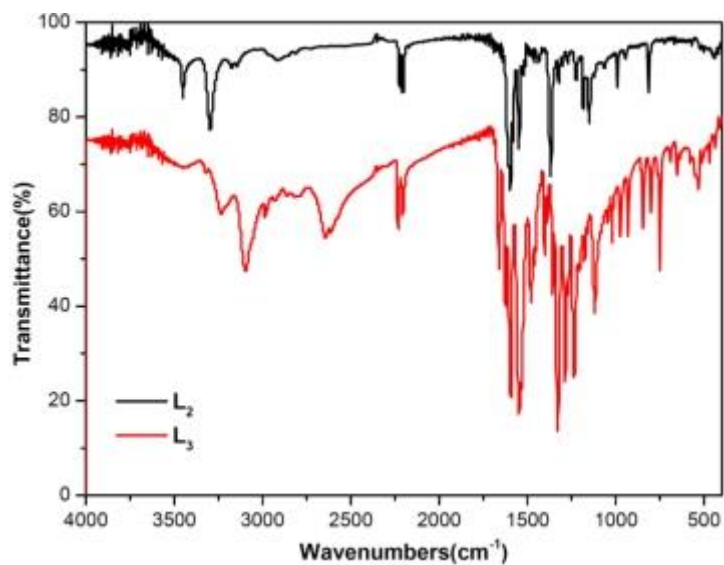
Fig. S41. IR of **L₂**、**L₃**.
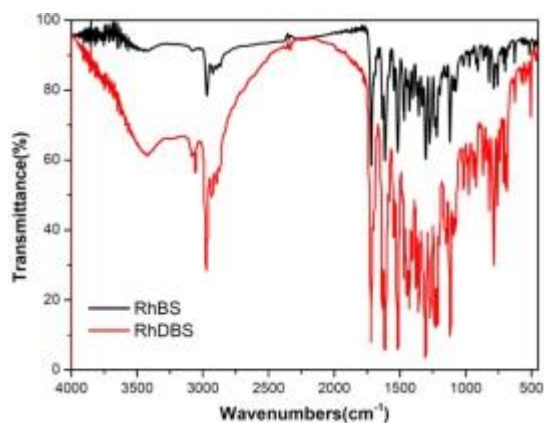
Fig. S42. IR of **RhDBS**、**RhBS**.
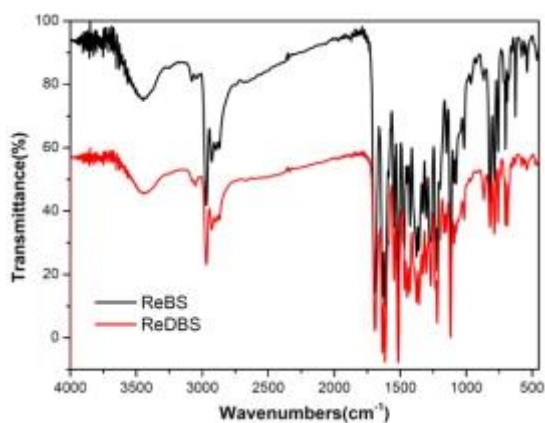
Fig. S43. IR of **ReDBS**、**ReBS**.
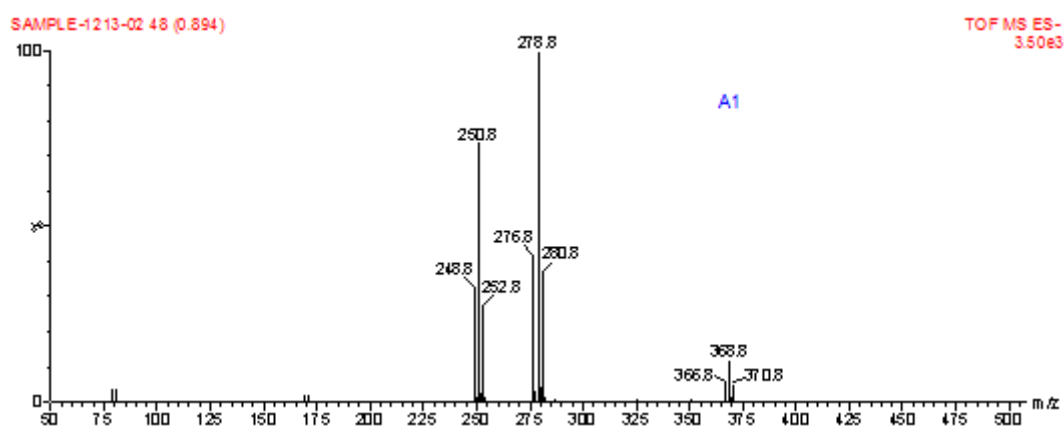
Fig. S44. Mass spectrum of **A1** in EtOH.

31
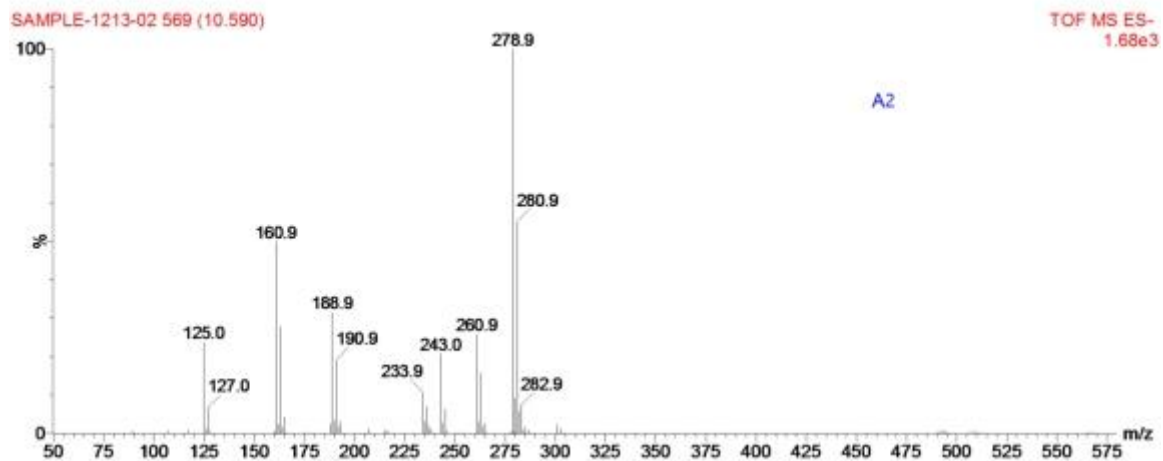
Fig. S45. Mass spectrum of **A2** in EtOH.
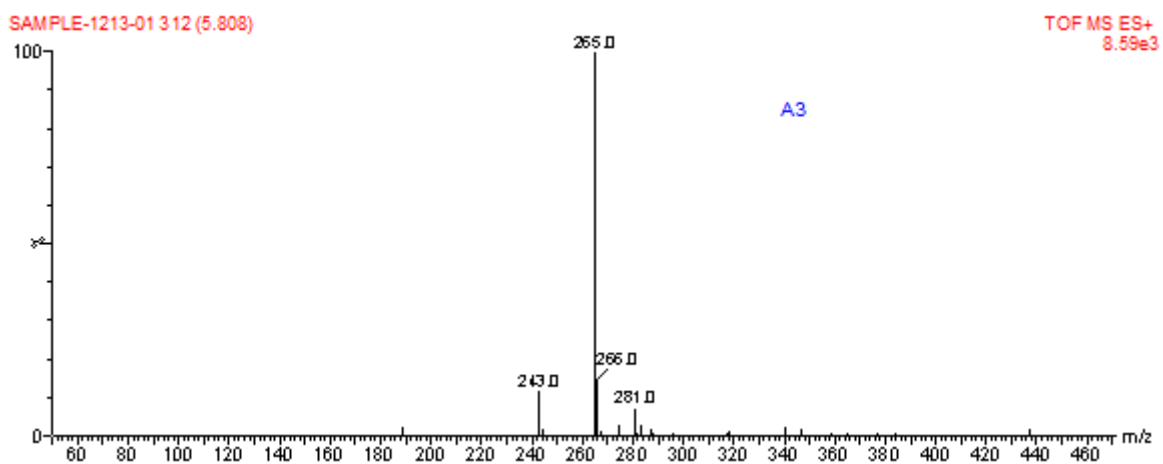
Fig. S46. Mass spectrum of **A3** in EtOH.
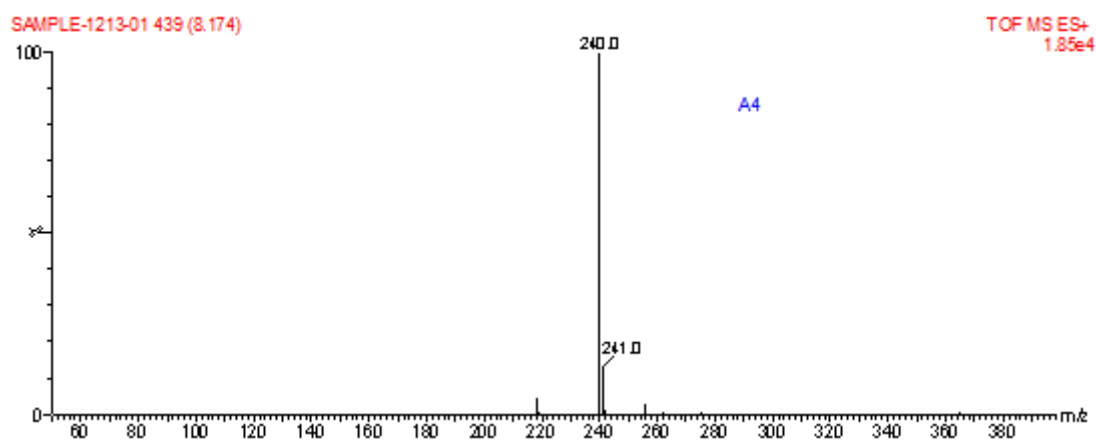
Fig. S47. Mass spectrum of **A4** in EtOH.
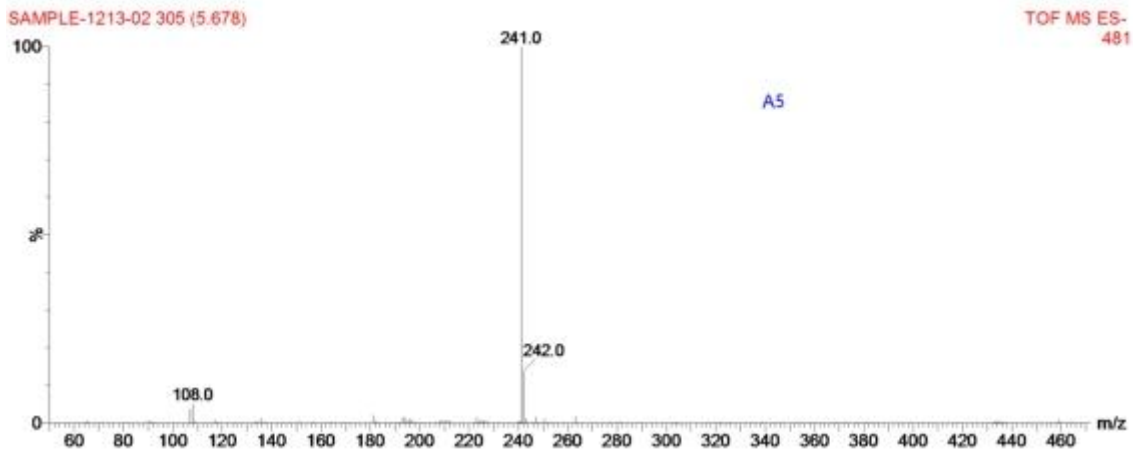
Fig. S48. Mass spectrum of **A5** in EtOH.
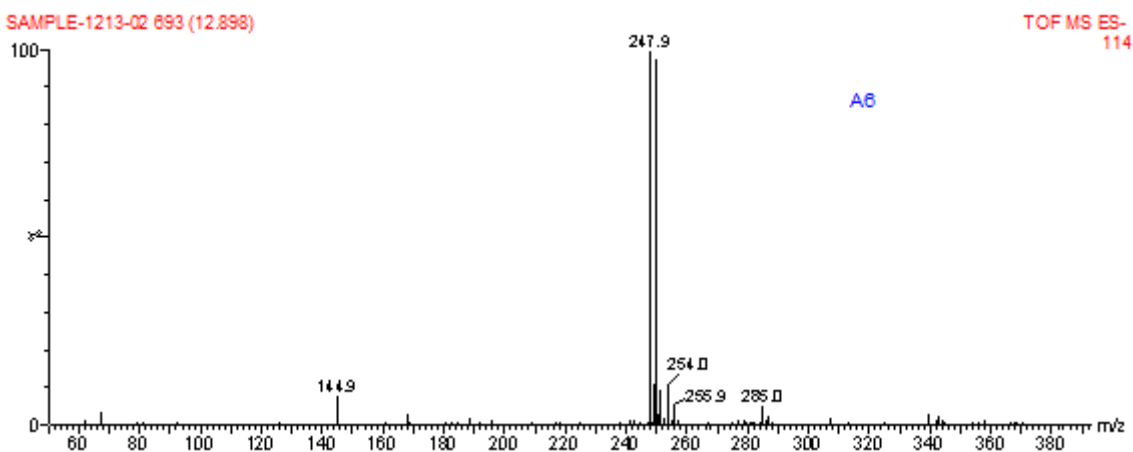
Fig. S49. Mass spectrum of **A6** in EtOH.
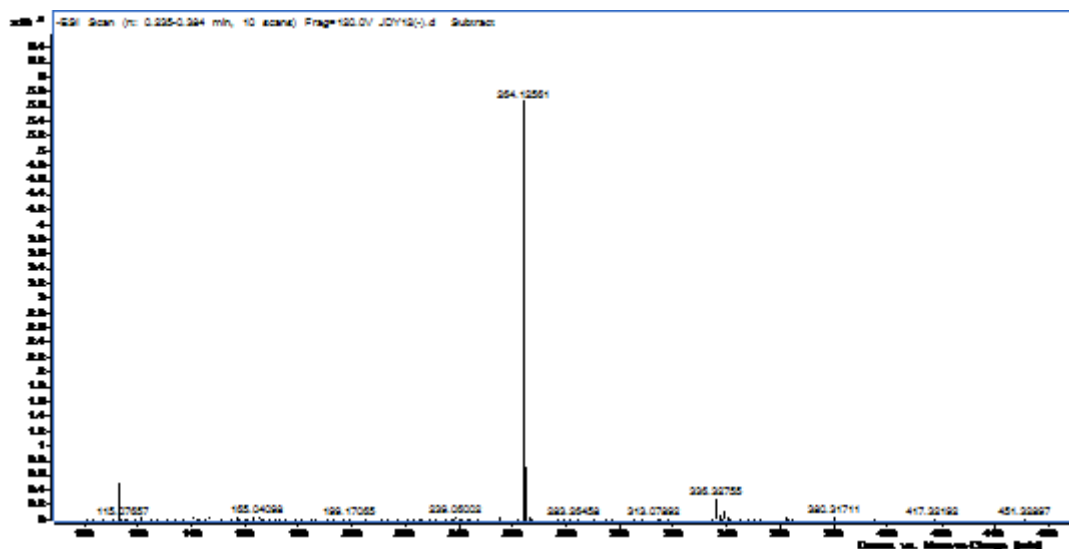
Fig. S50. MS of **L₂**.
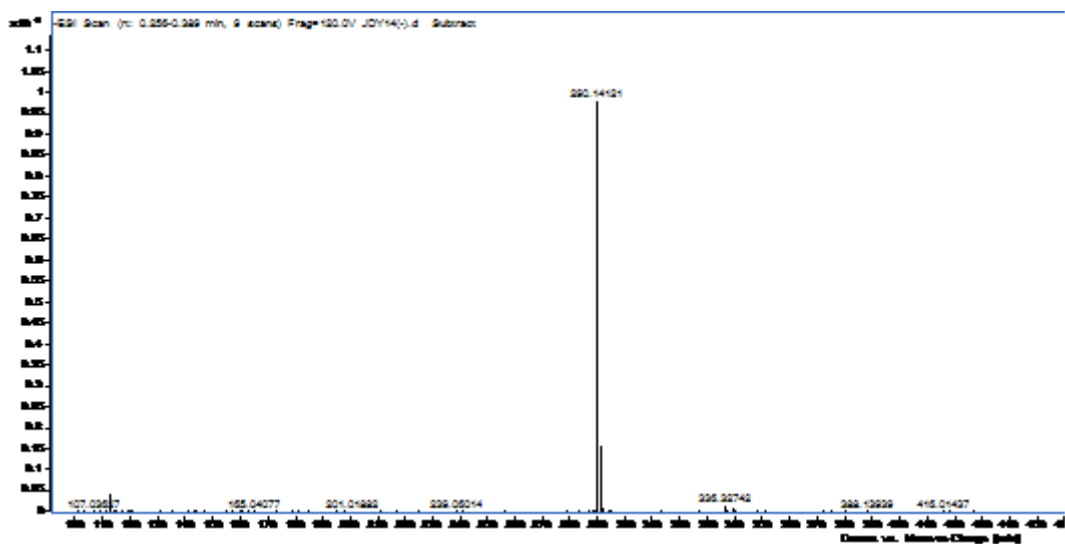
Fig. S51. MS of **L3**.
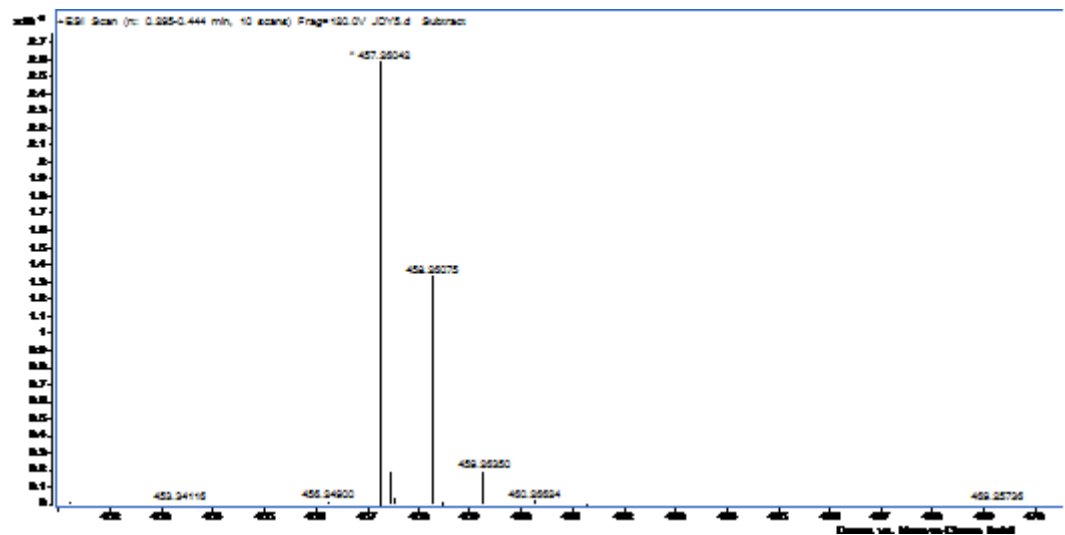
Fig. S52. MS of **M1**.
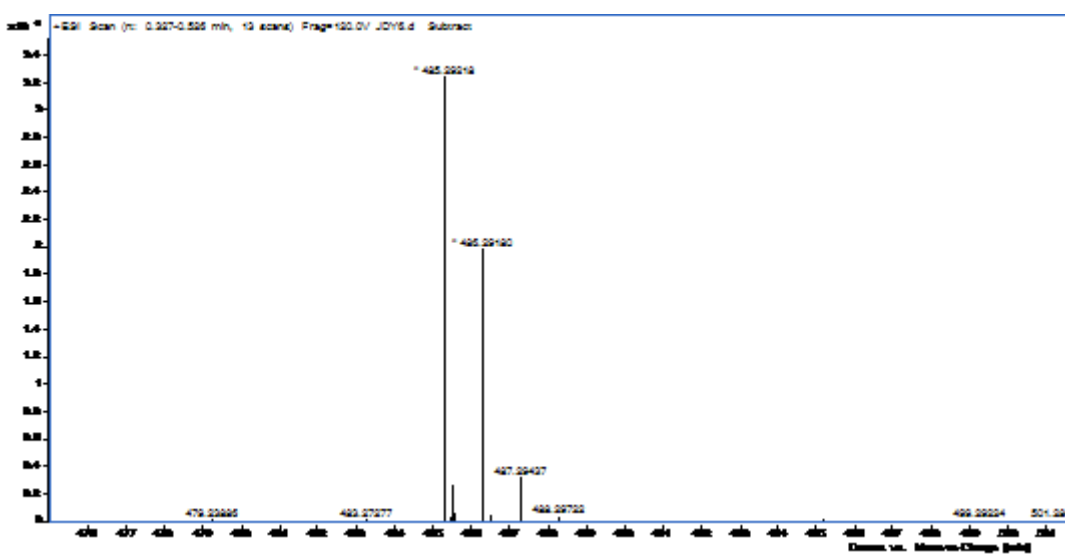
Fig. S53. MS of **M2**.
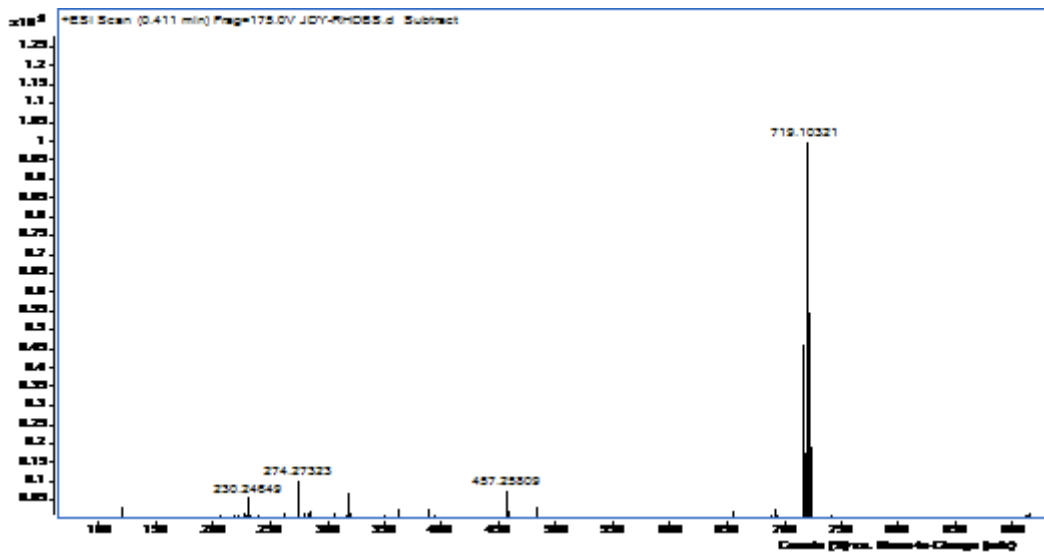
Fig. S54. MS of **RhDBS**.
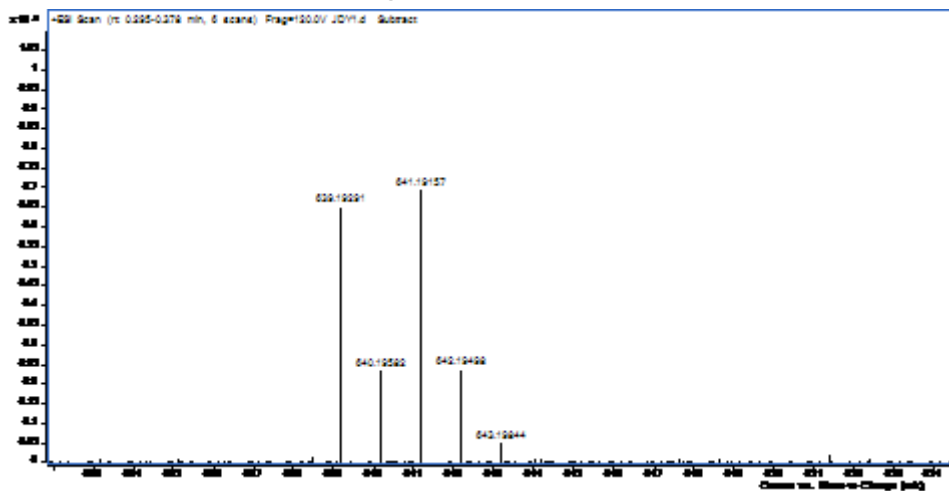
Fig. S55. MS of **RhBS**.
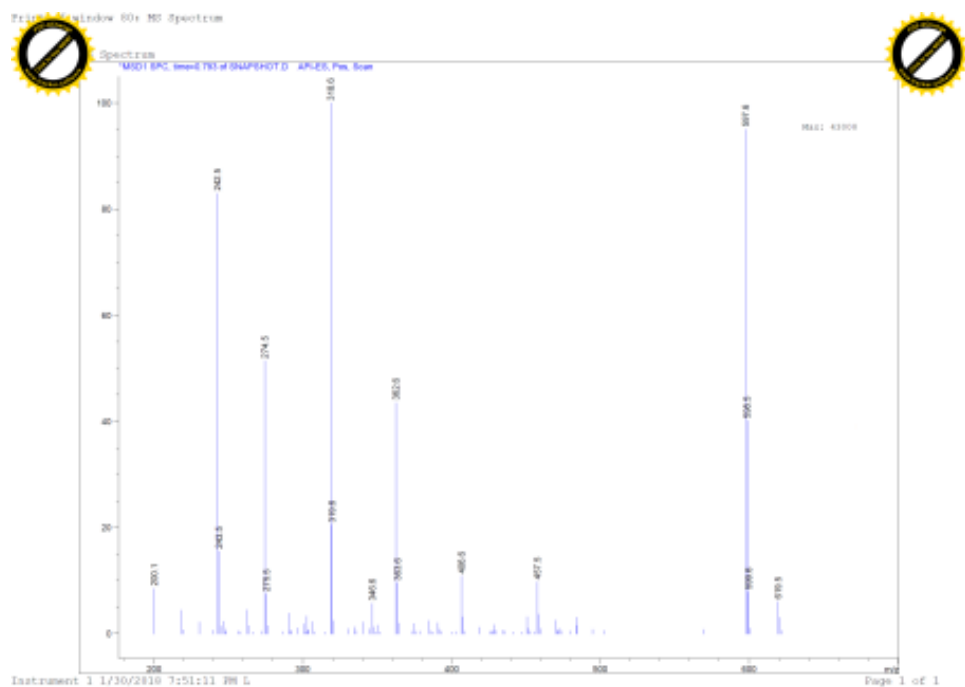
Fig. S56. MS of **RhDFS**.
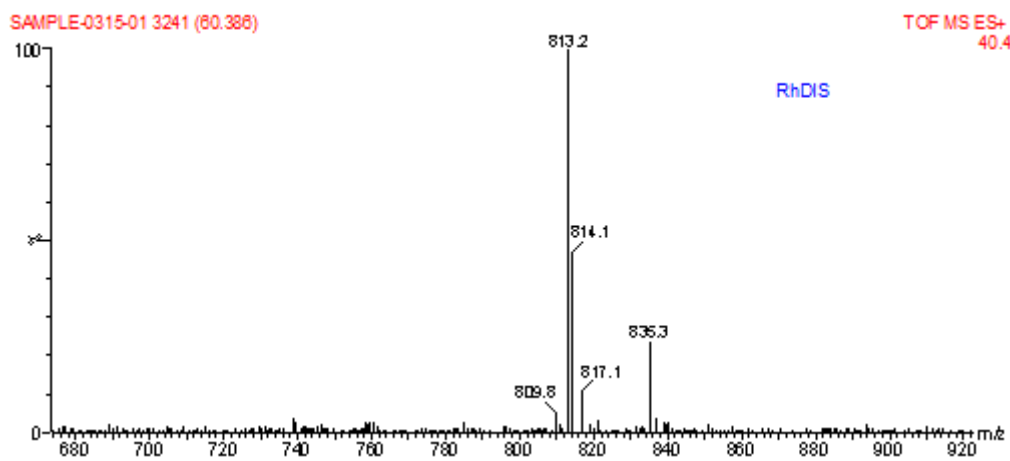
Fig. S57. MS of **RhDIS**.
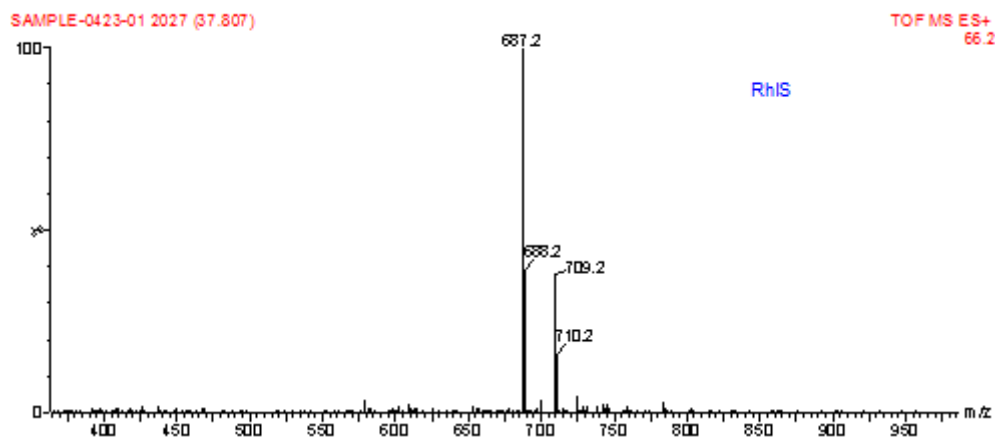
Fig. S58. MS of **RhIS**.
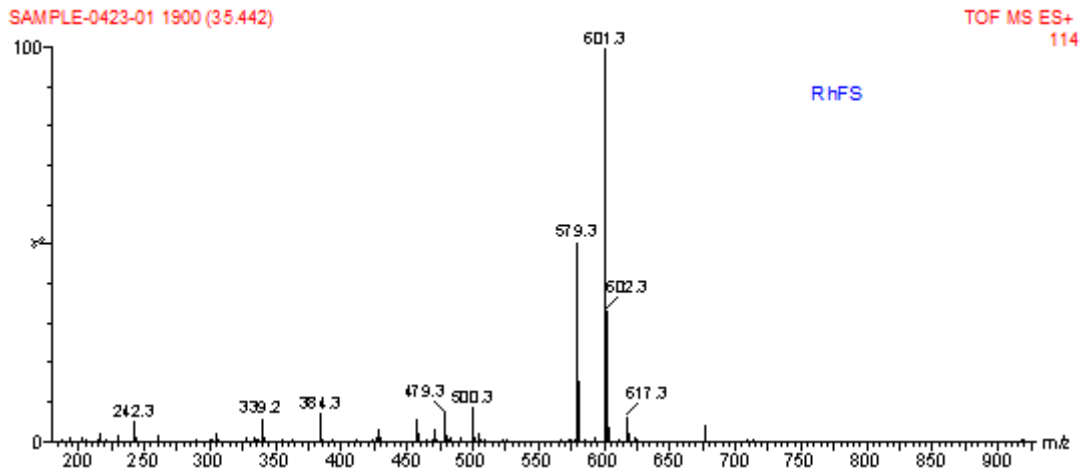
Fig. S59. MS of **RhFS**.
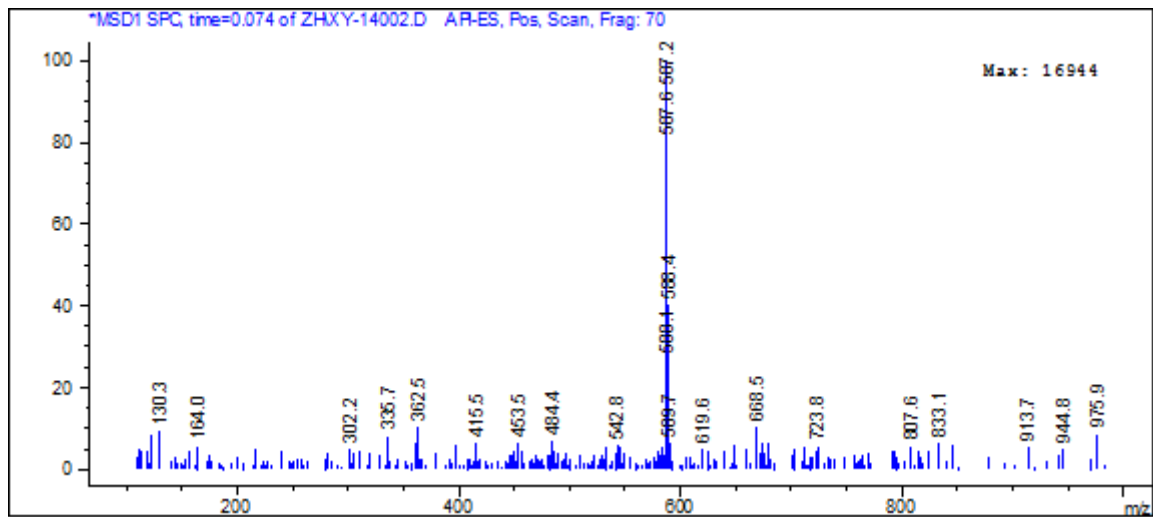
Fig. S60. MS of **RhGDM**.
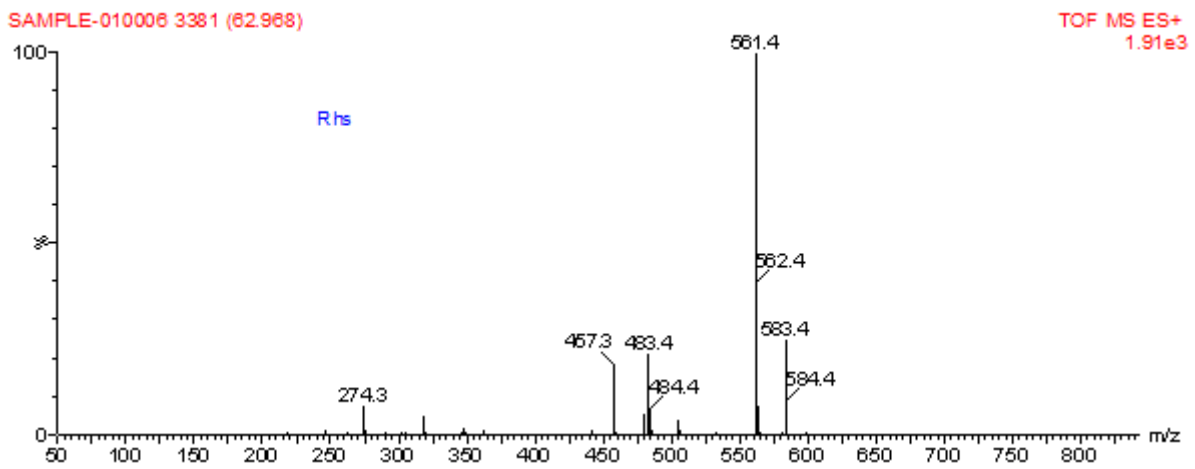
Fig. S61. MS of **RhS**.
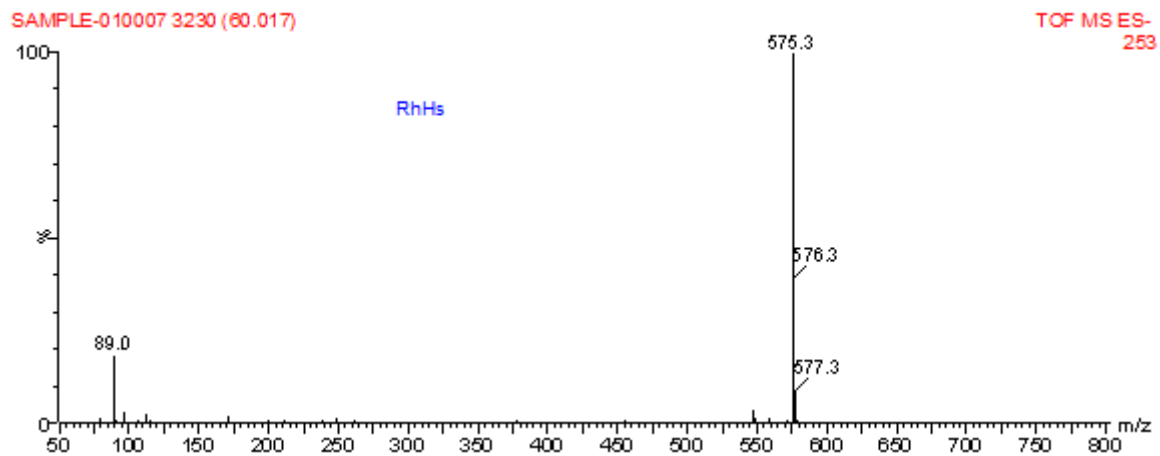
Fig. S62. MS of **RhHS**.
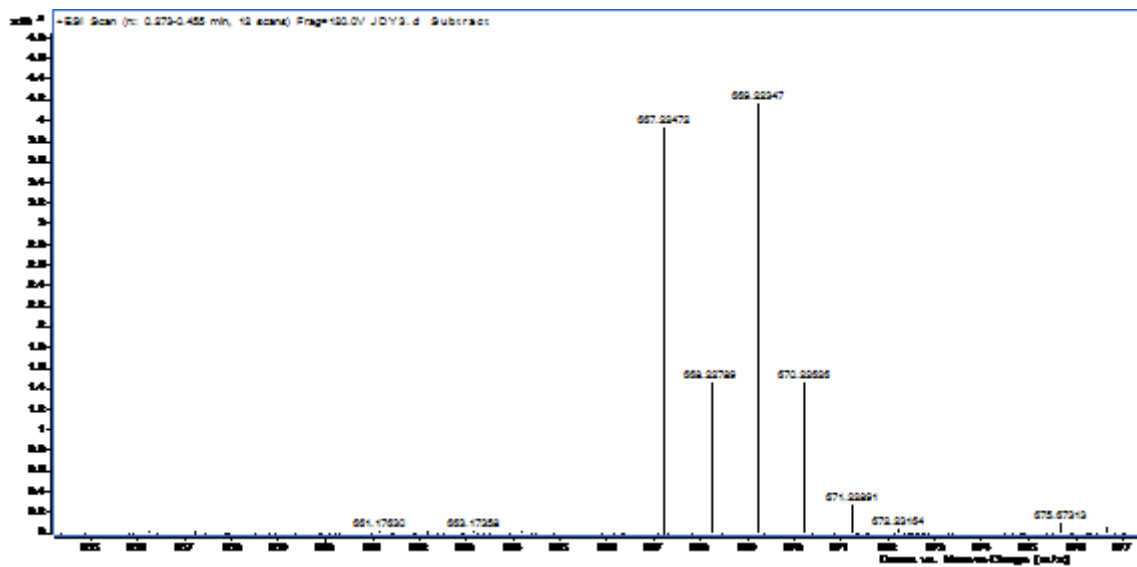
Fig. S63. MS of **ReBS**.
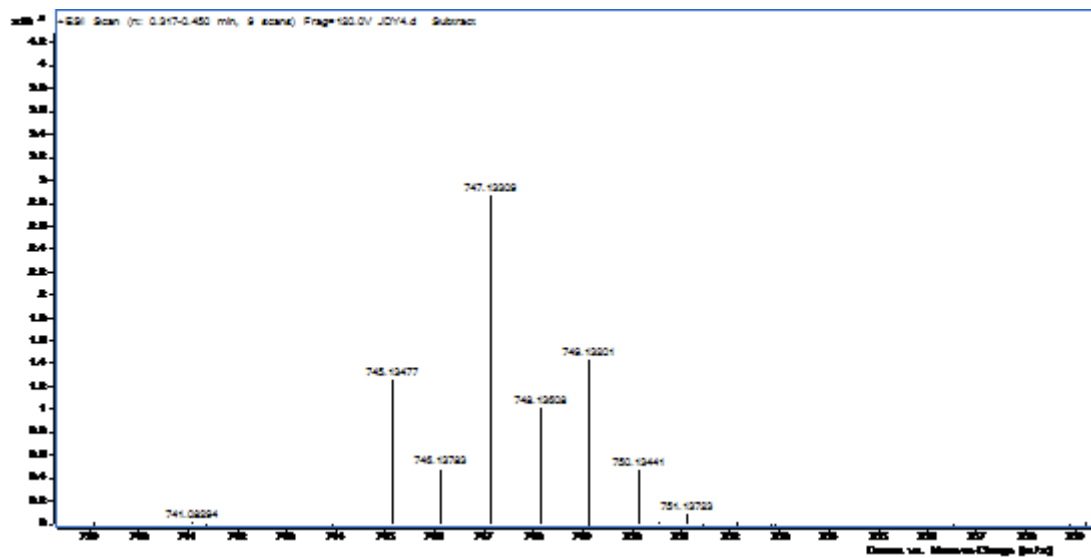
Fig. S64. MS of **ReDBS**.
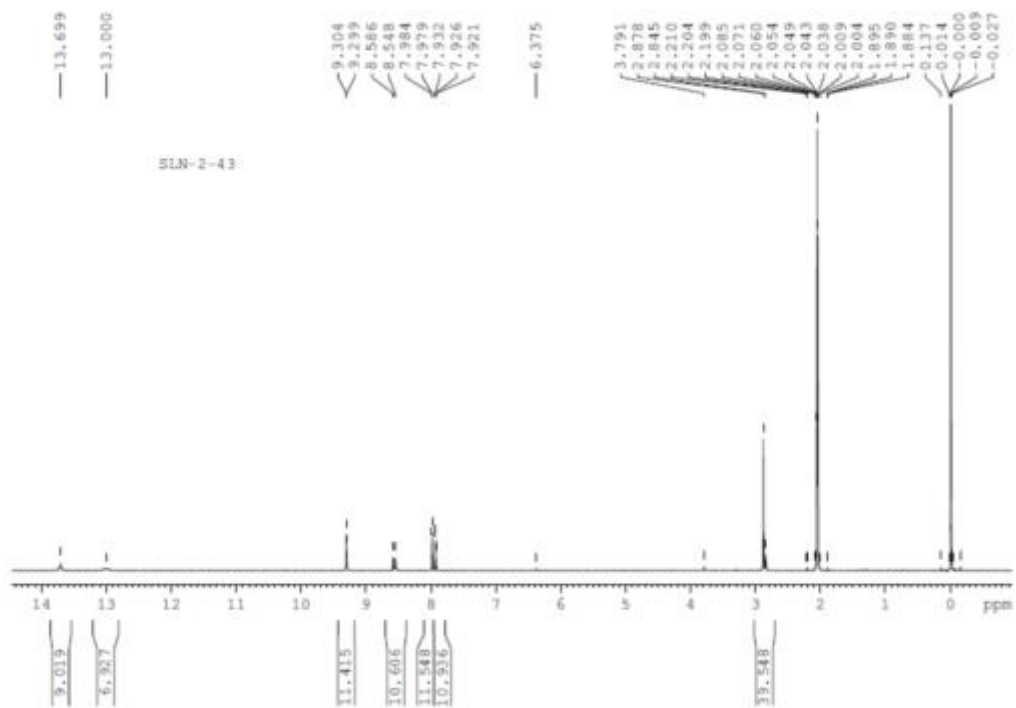
Fig. S65. ^{1}H NMR spectrum of **A1** in DMSO-d_6.
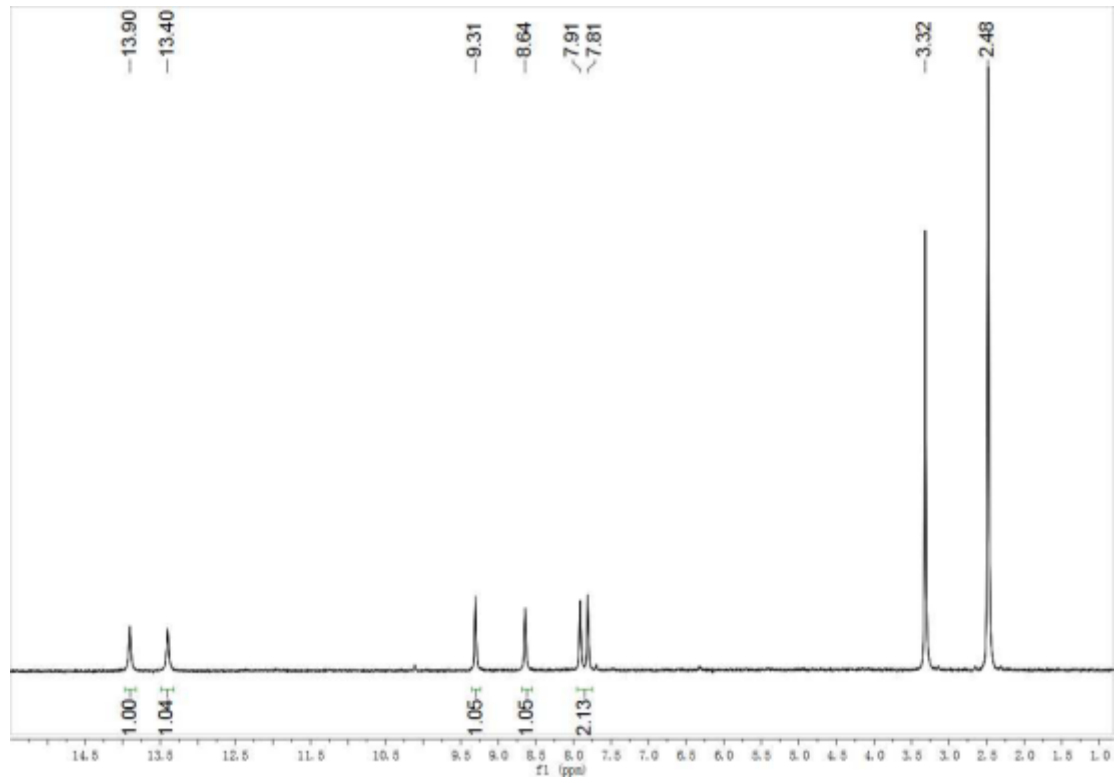
Fig. S66. ^{1}H NMR spectrum of **A2** in DMSO-d_6.
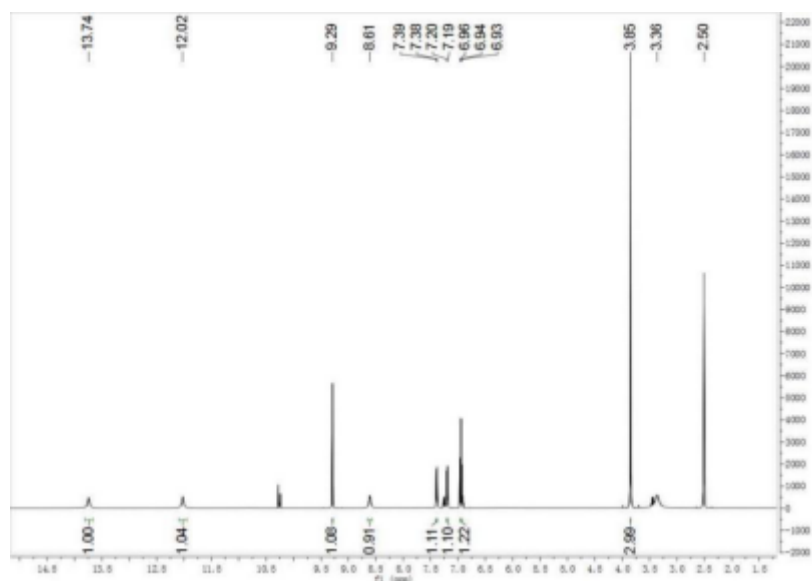
Fig. S67. ^{1}H NMR spectrum of **A3** in DMSO-d_6.
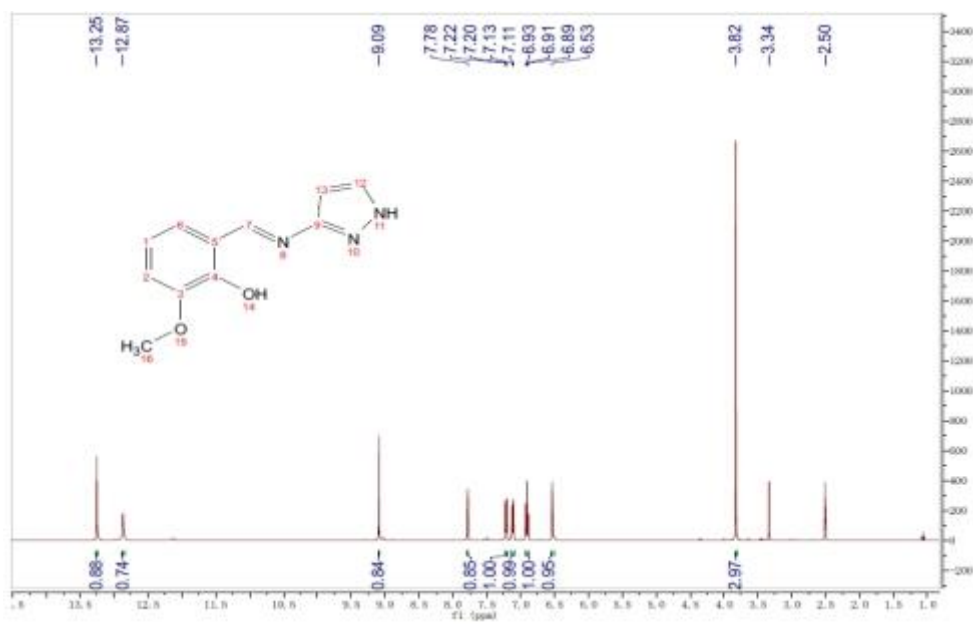
Fig. S68. ^{1}H NMR spectrum of **A4** in DMSO-d_6.
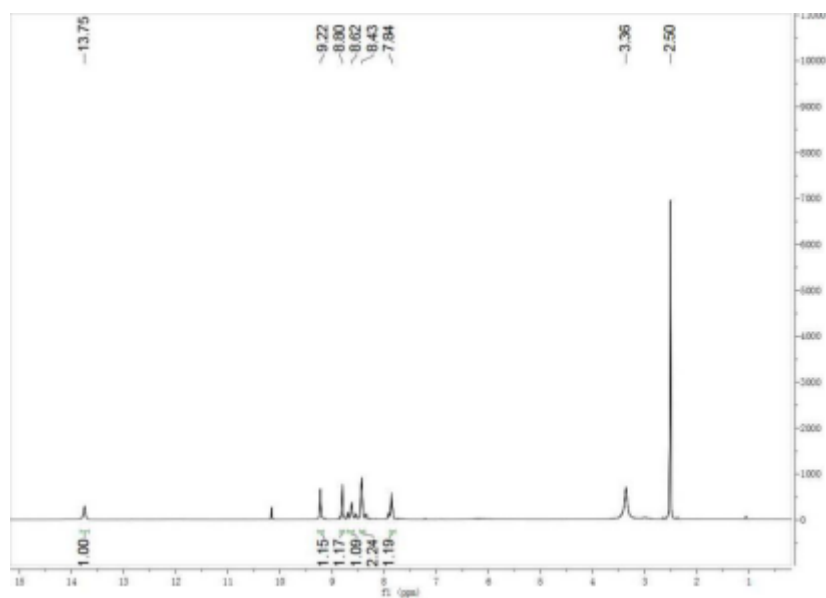
Fig. S69. ^{1}H NMR spectrum of **A5** in DMSO-d_6.
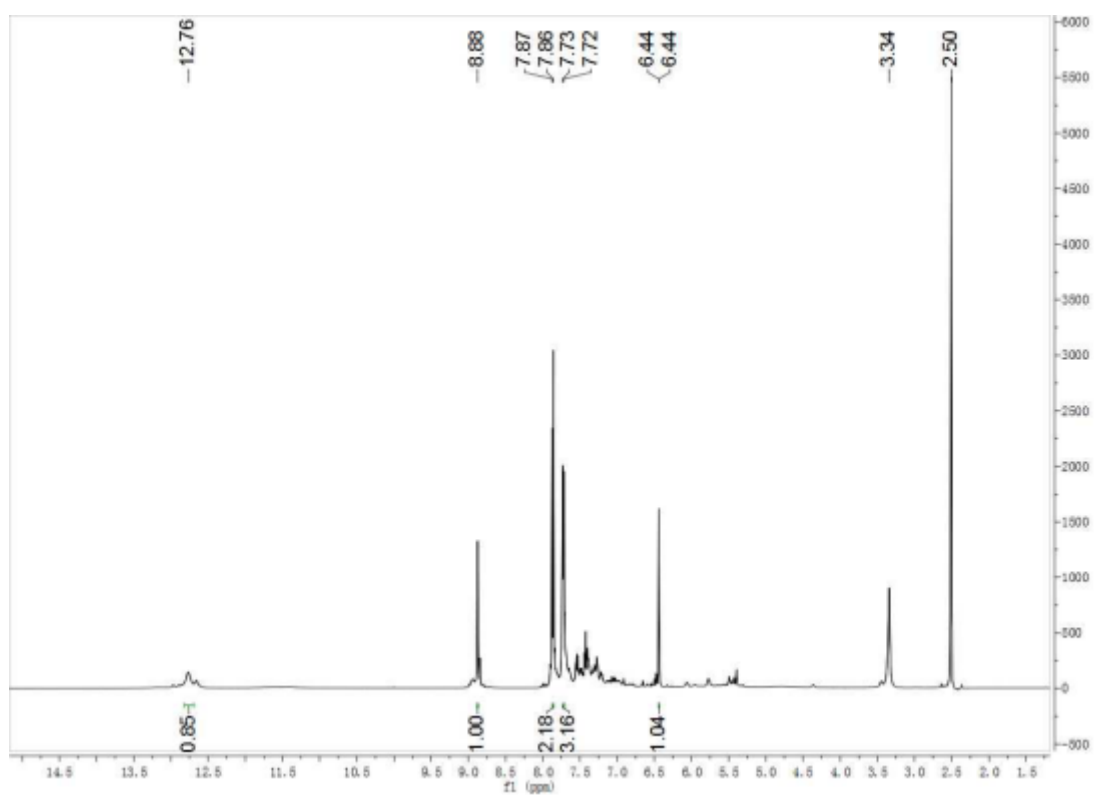
Fig. S70. ^{1}H NMR spectrum of **A6** in DMSO-d_6.
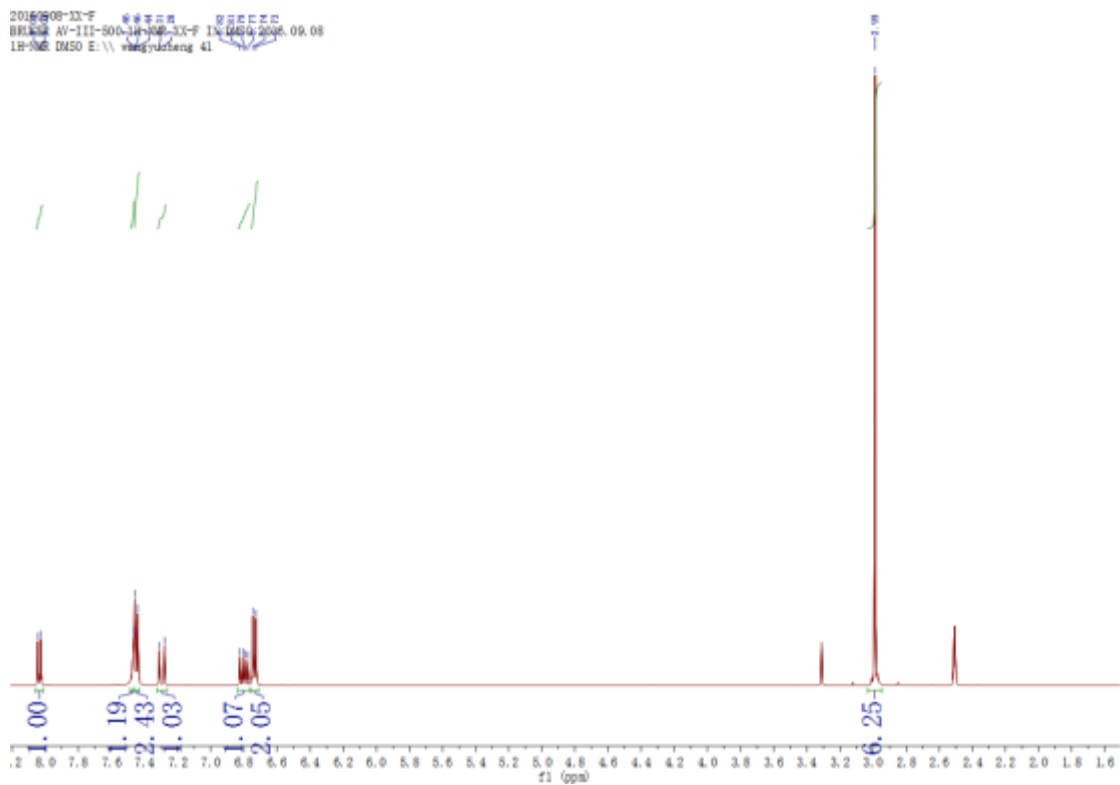
Fig. S71. ^{1}H NMR spectrum of **L$_2$** in DMSO-d_6.
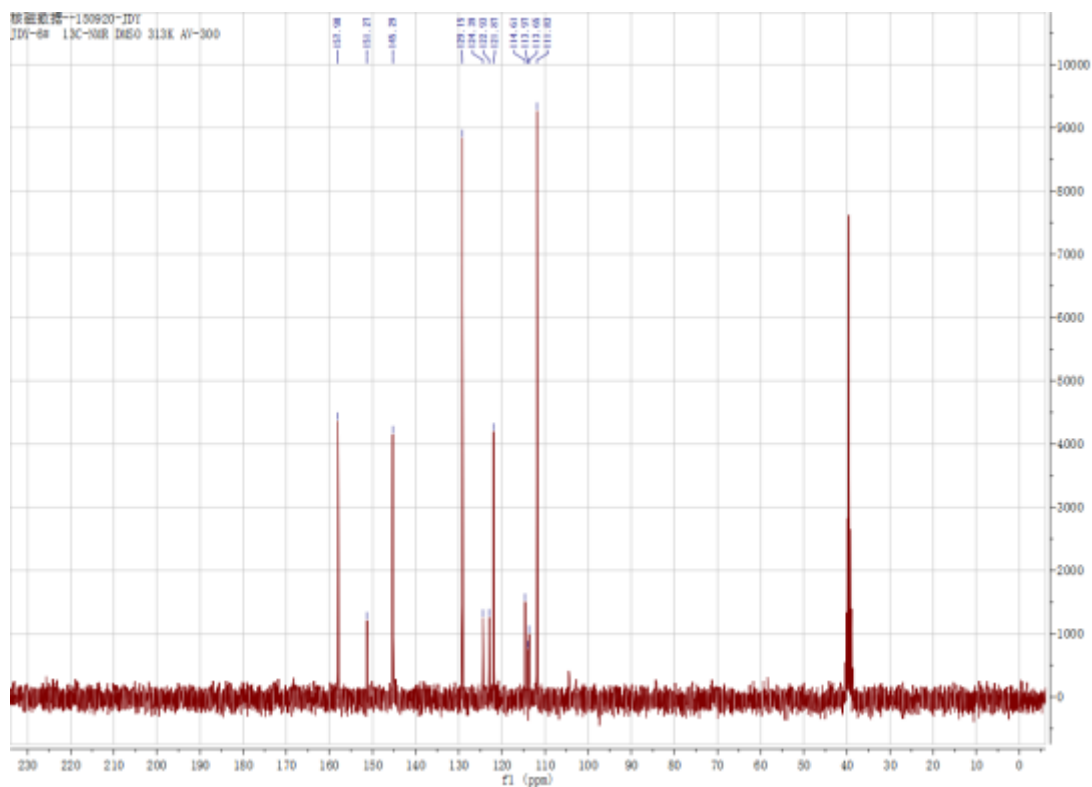
Fig. S72. ^{13}C NMR spectrum of **L$_2$** in DMSO-d_6.
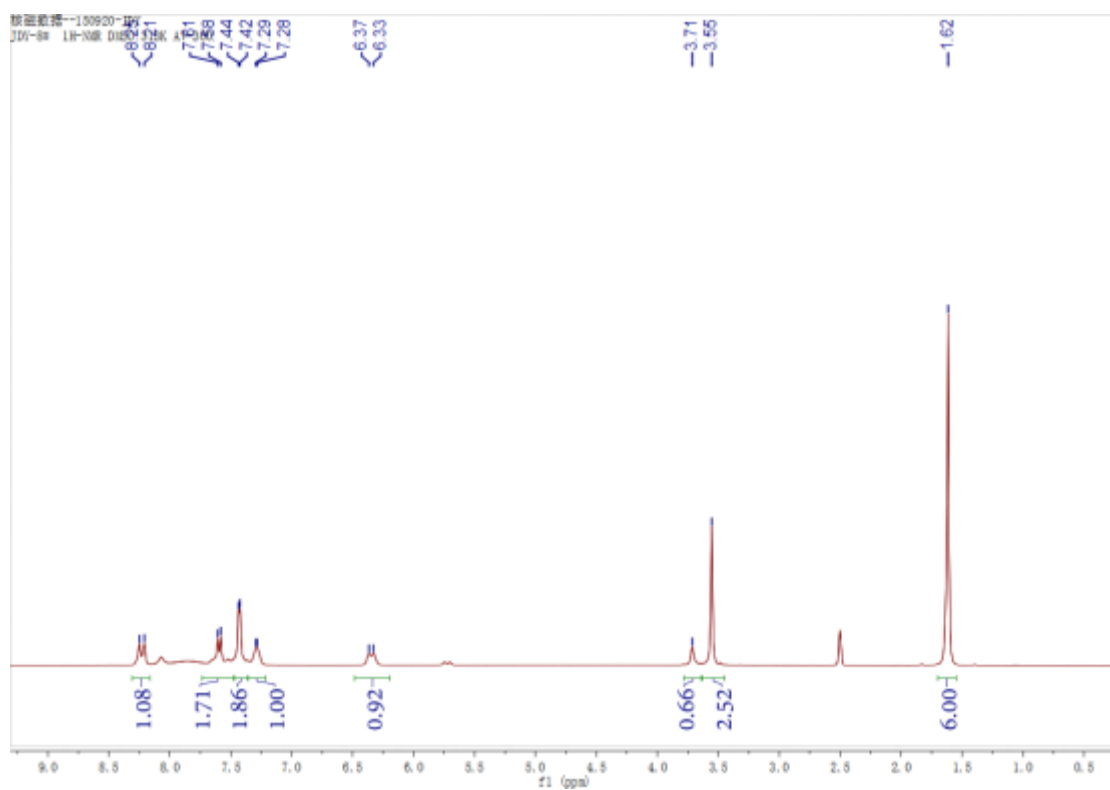
Fig. S73. ^1H NMR spectrum of **L₃** in DMSO-d_6.
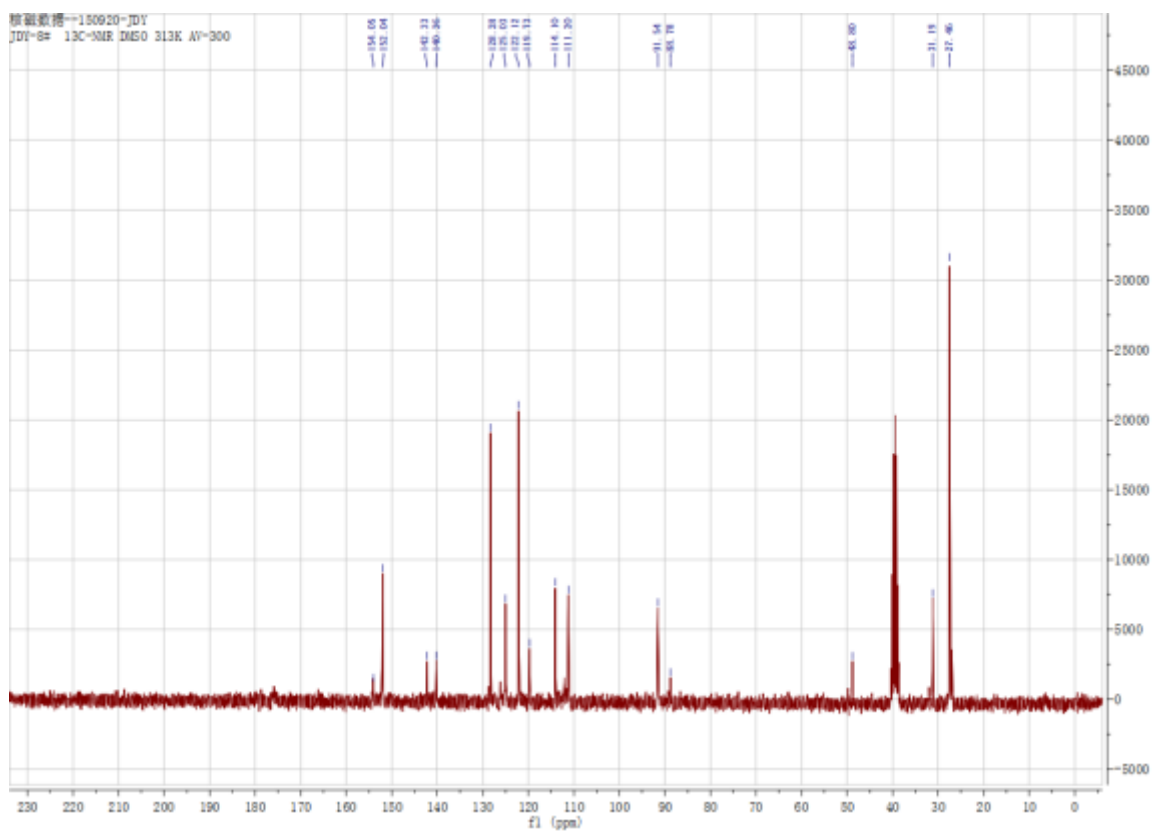
Fig. S74. ^{13}C NMR spectrum of **L₃** in DMSO-d_6.
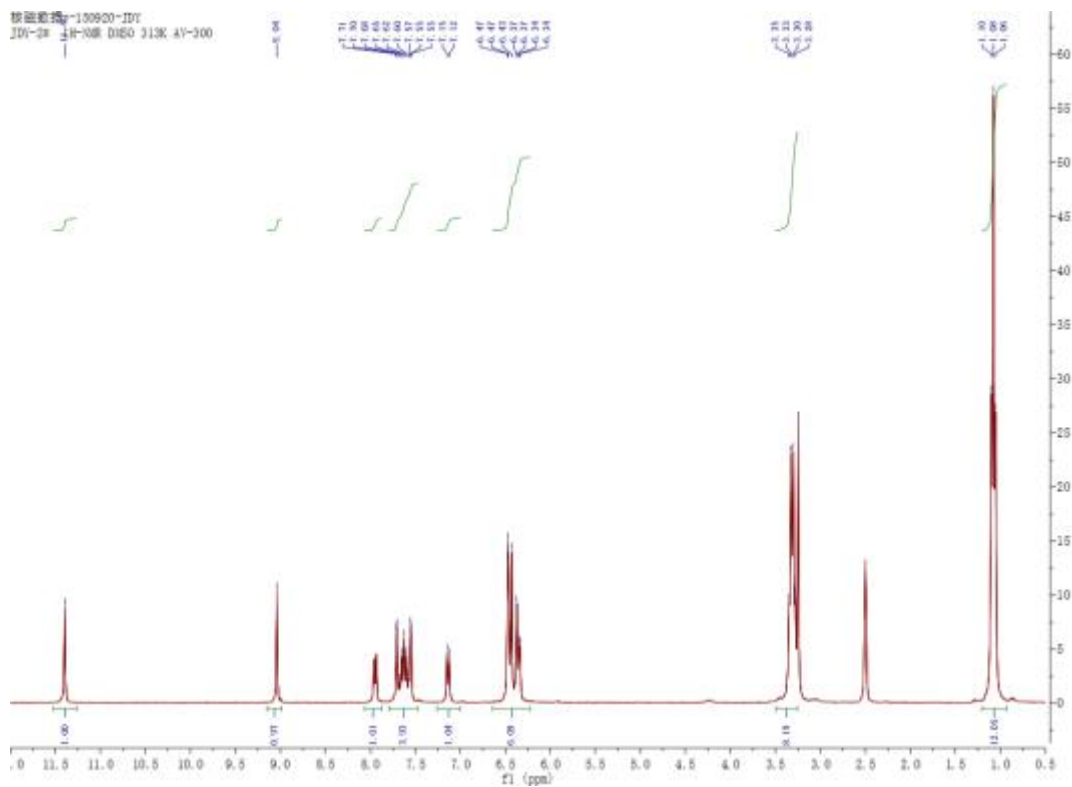
Fig. S75. ¹H NMR spectrum of **RhDBS** in DMSO-d_6.
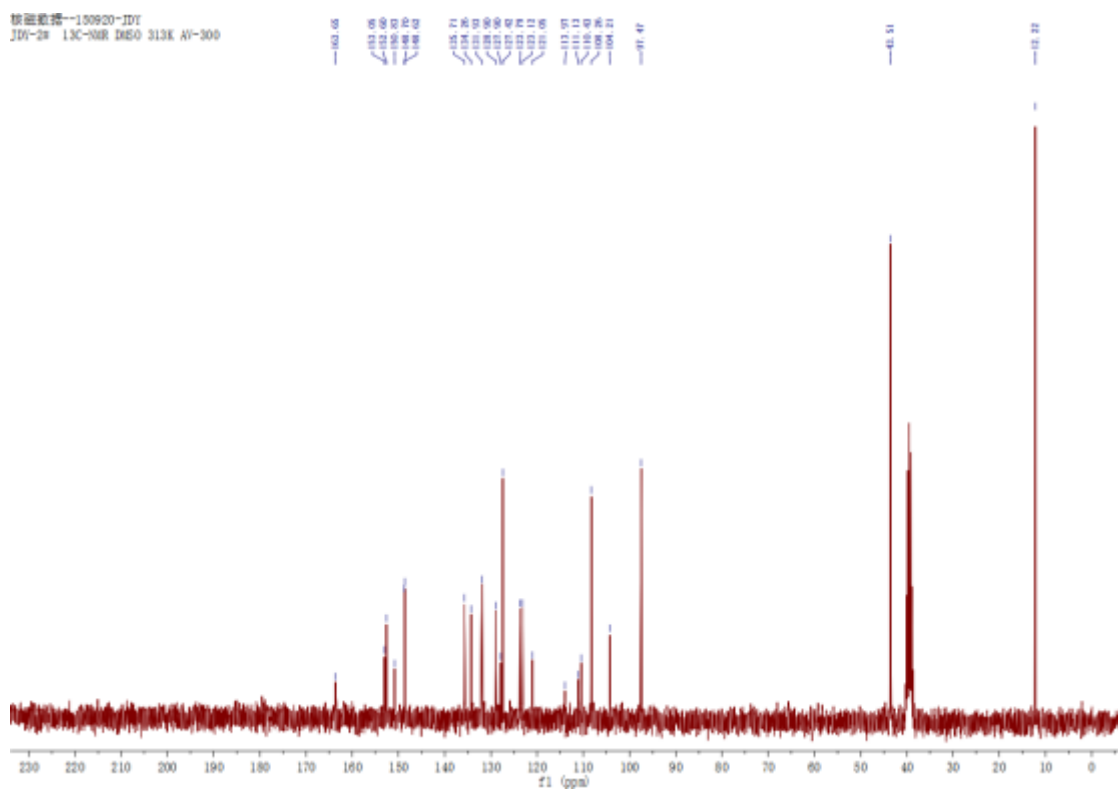
Fig. S76. ¹³C NMR spectrum of **RhDBS** in DMSO-d_6.
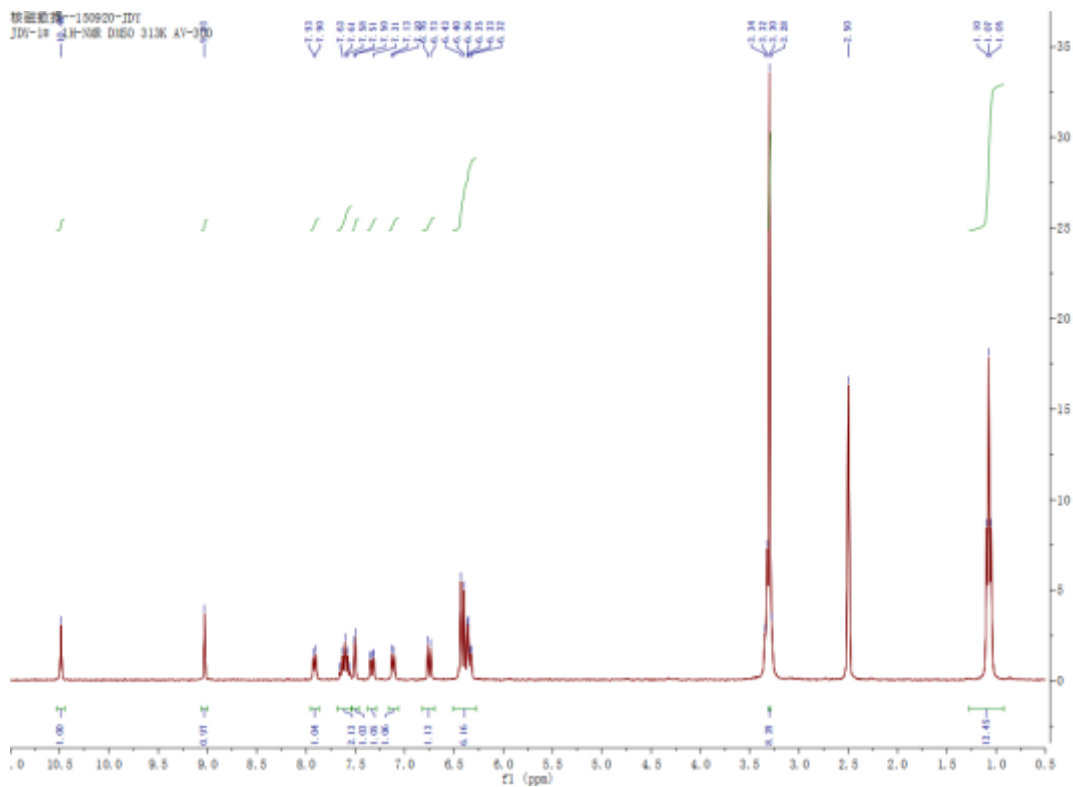
Fig. S77. ^{1}H NMR spectrum of **RhBS** in DMSO-d_6.
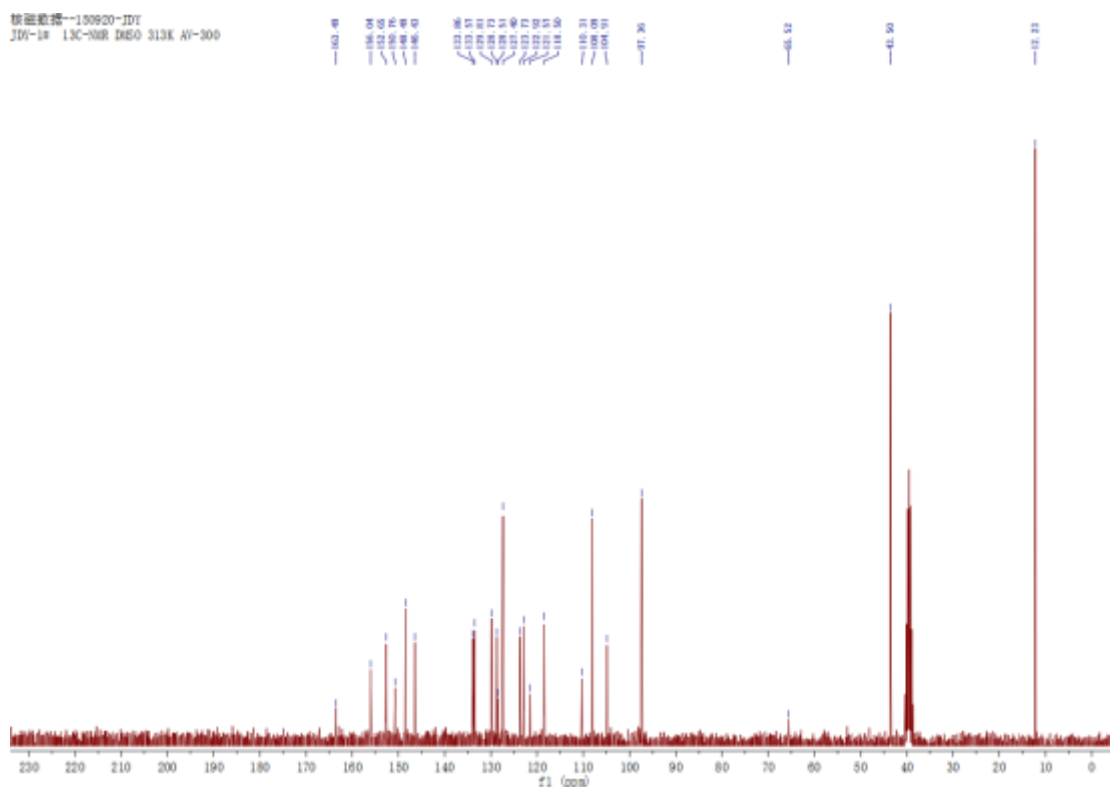
Fig. S78. ^{13}C NMR spectrum of **RhBS** in DMSO-d_6.
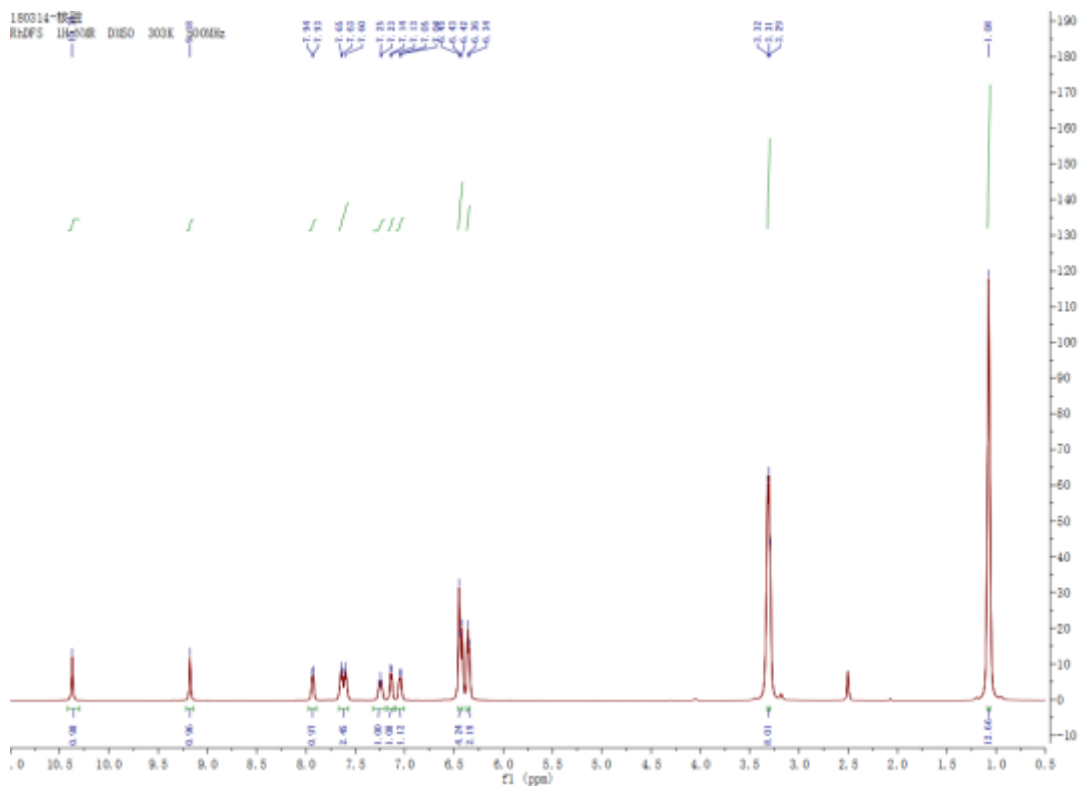
Fig. S79. ^{1}H NMR of **RhDFS** in DMSO-d_6.
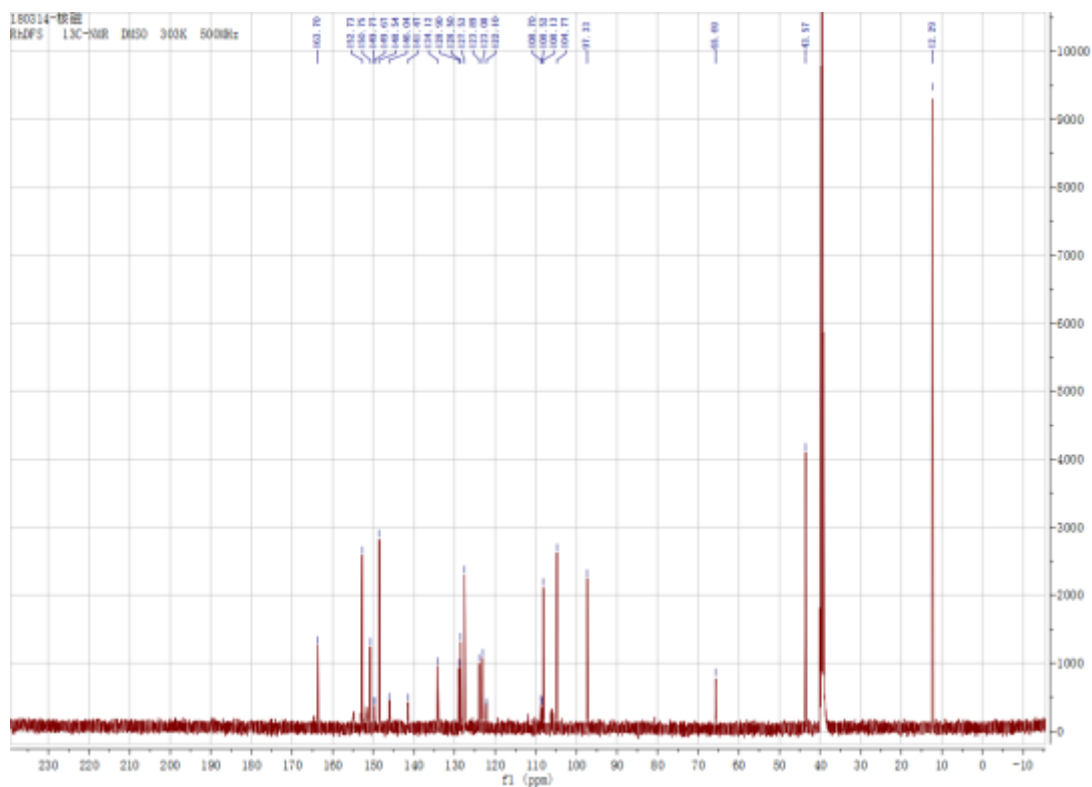
Fig. S80. ^{13}C NMR of **RhDFS** in DMSO-d_6.
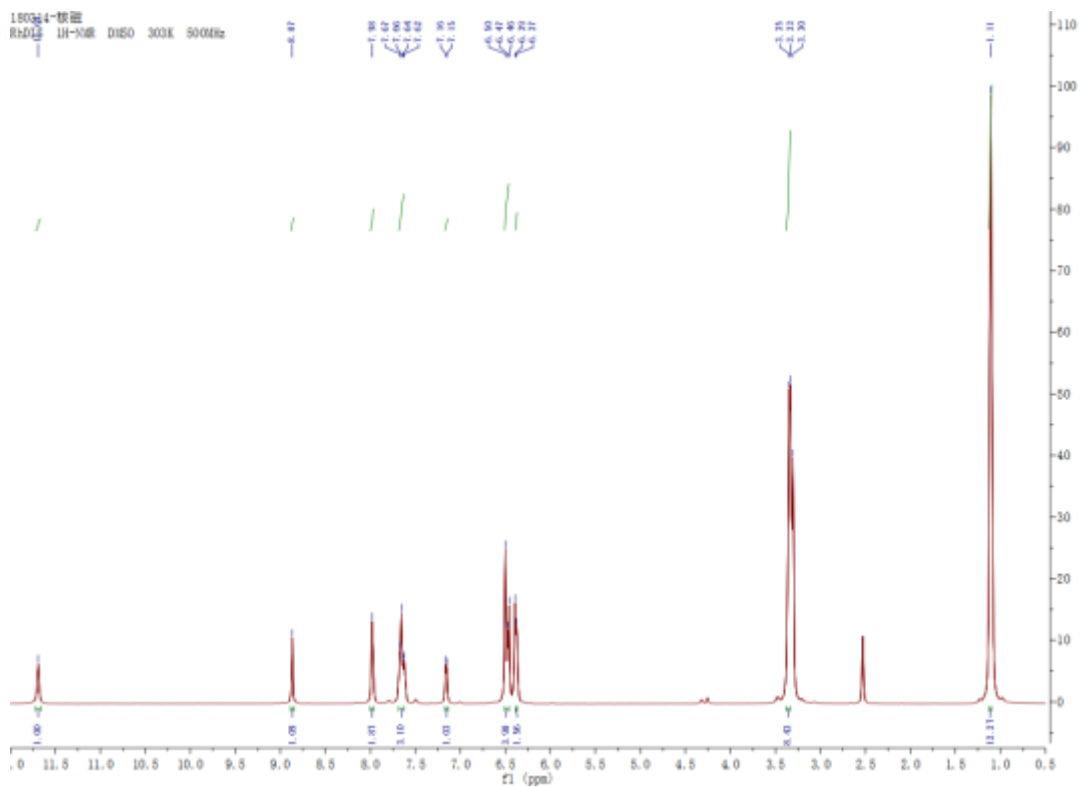
Fig. S81. ^{1}H NMR of **RhDIS** in DMSO-d_6.
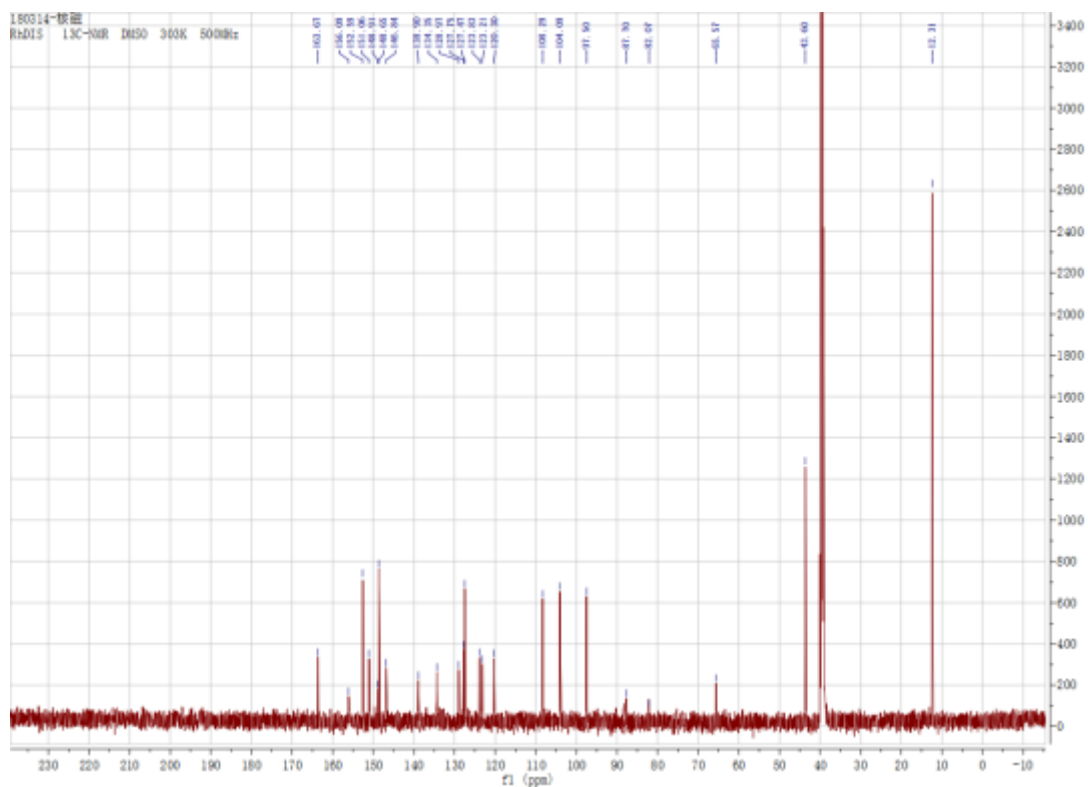
Fig. S82. ^{13}C NMR of **RhDIS** in DMSO-d_6.
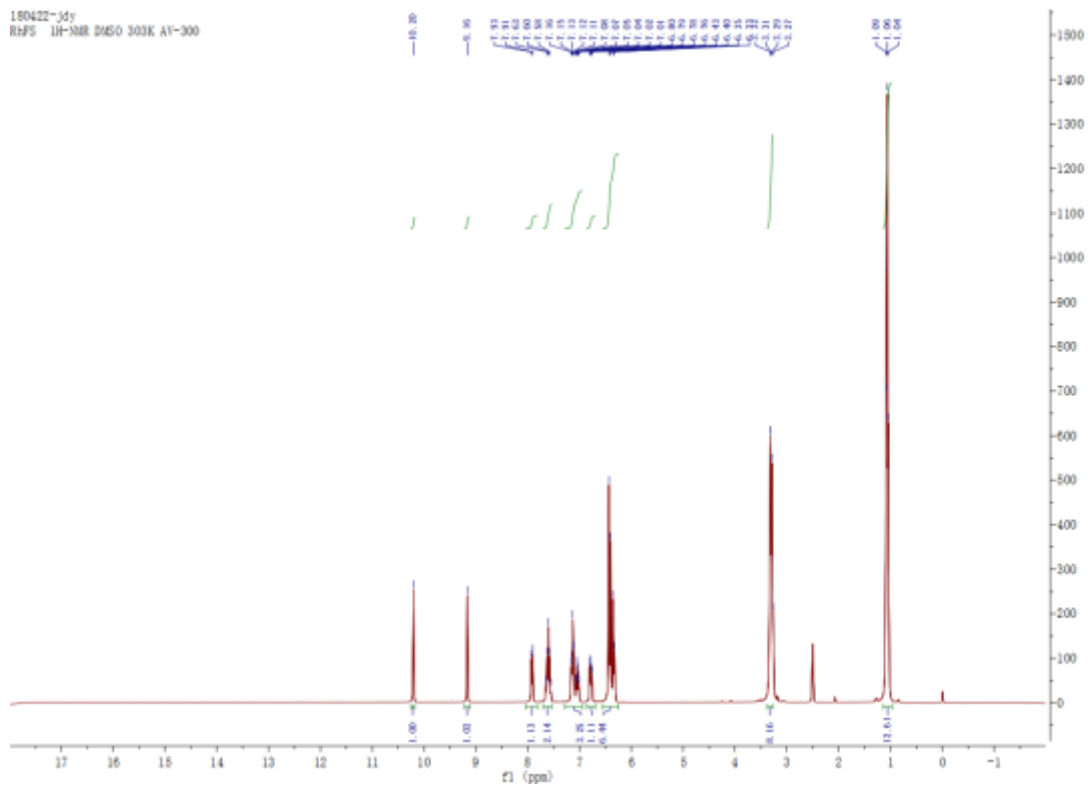
Fig. S83. ^{1}H NMR of **RhFS** in DMSO-d_6.
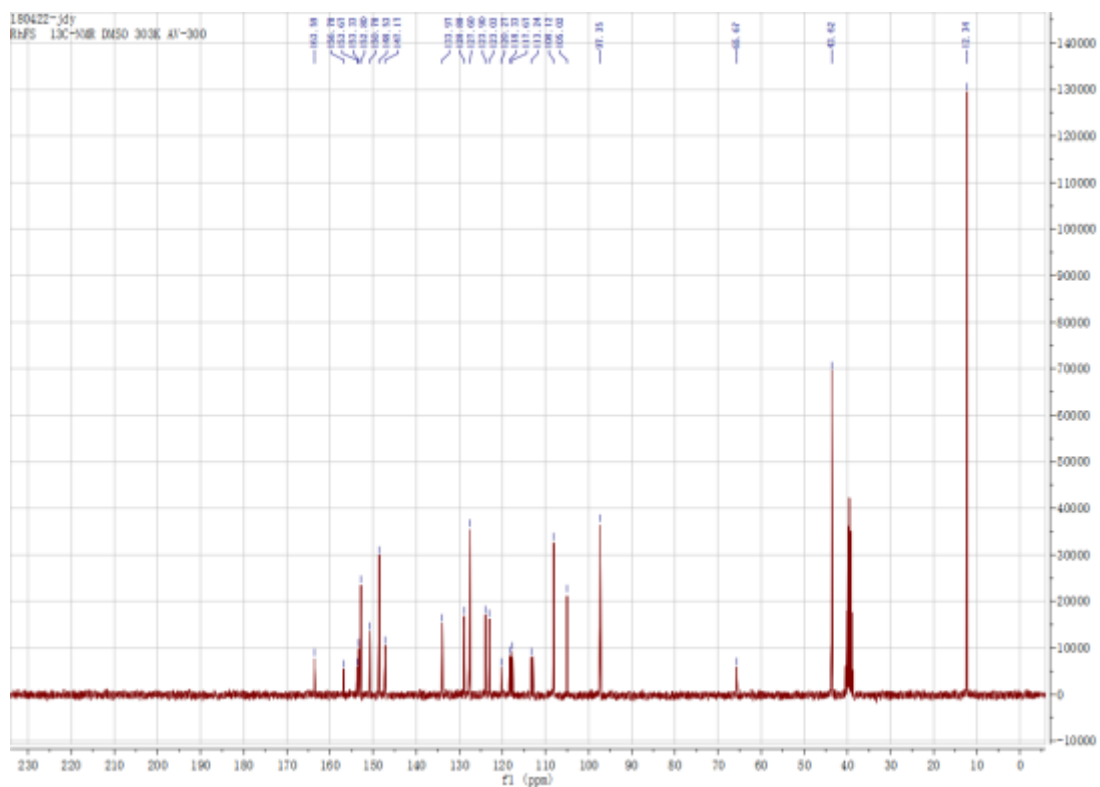
Fig. S84. ^{13}C NMR of **RhFS** in DMSO-d_6.
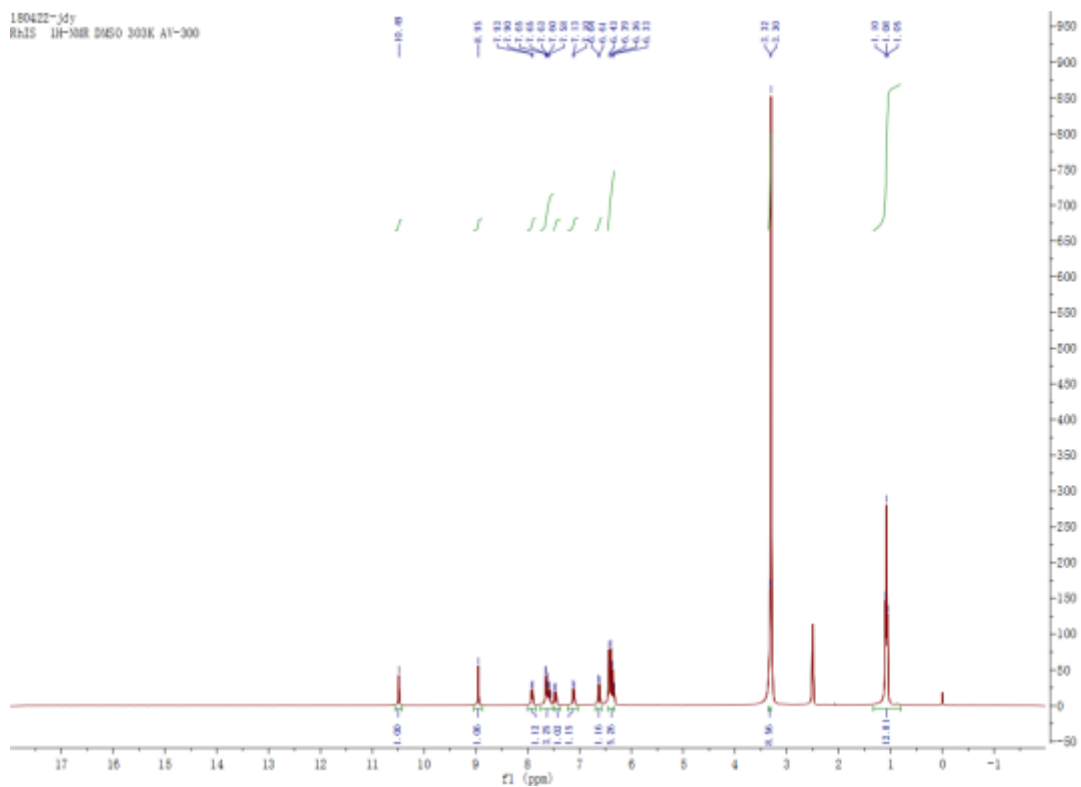
Fig. S85. ^{1}H NMR of **RhIS** in DMSO-d_6.
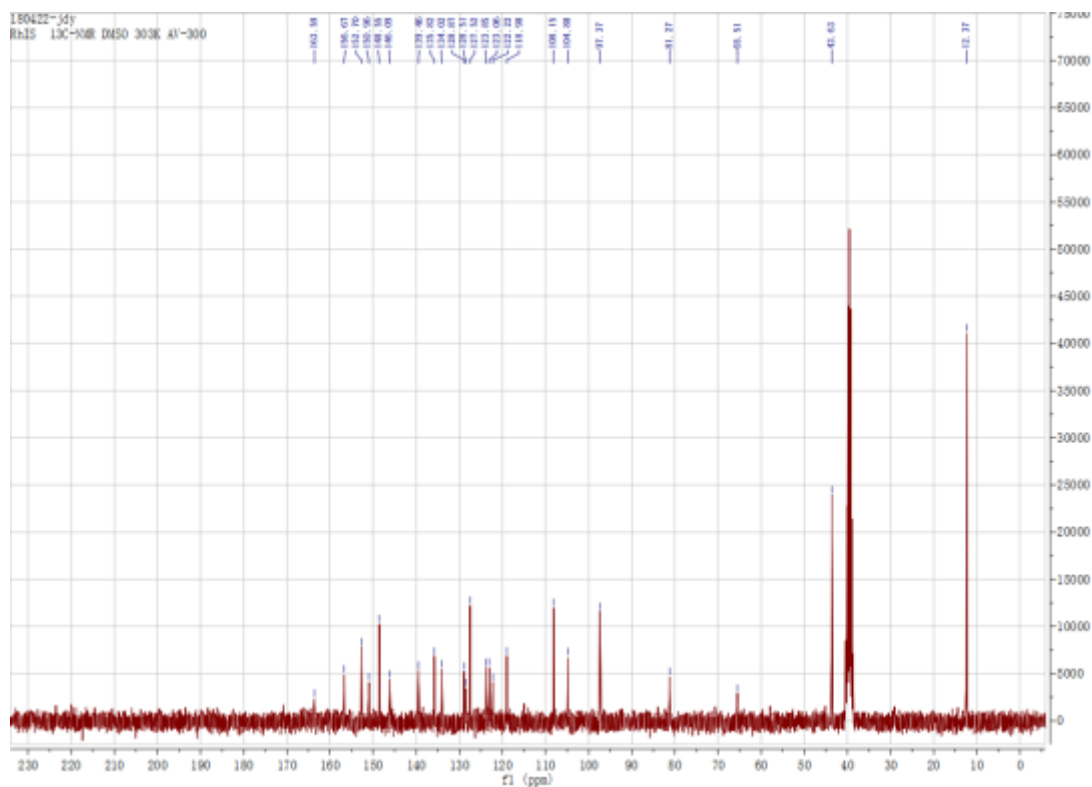
Fig. S86. ^{13}C NMR of **RhIS** in DMSO-d_6.
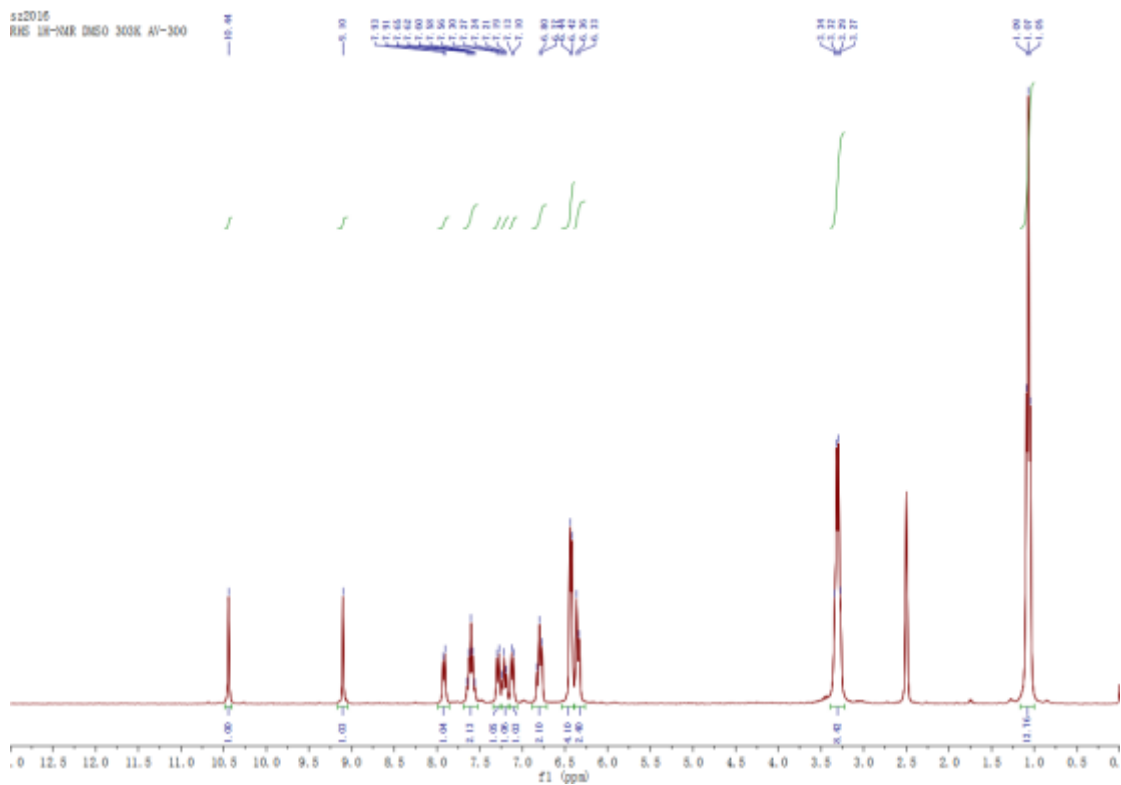
Fig. S87. ^{1}H NMR spectrum of **RhS** in DMSO-d_6.
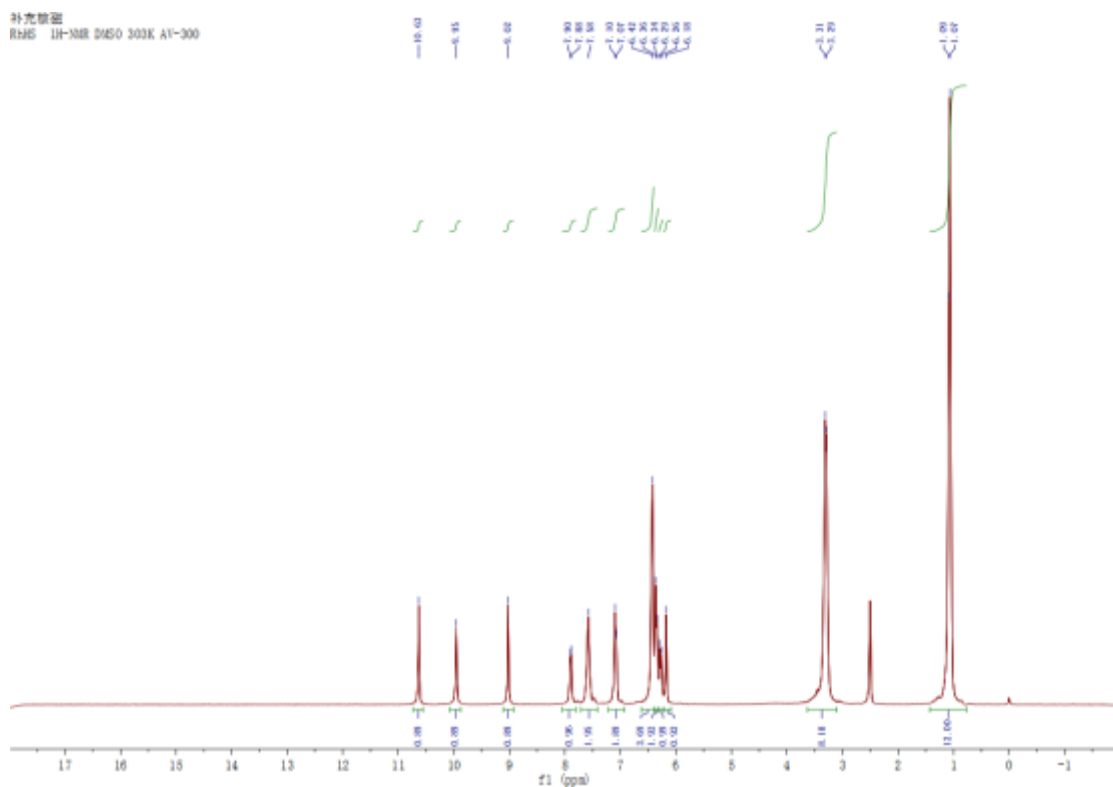
Fig. S88. ^{1}H NMR spectrum of **RhHS** in DMSO-d_6.

Fig. S89. ¹H NMR spectrum of **ReDBS** in DMSO-d_6.

Fig. S90. ¹³C NMR spectrum of **ReDBS** in DMSO-d_6.
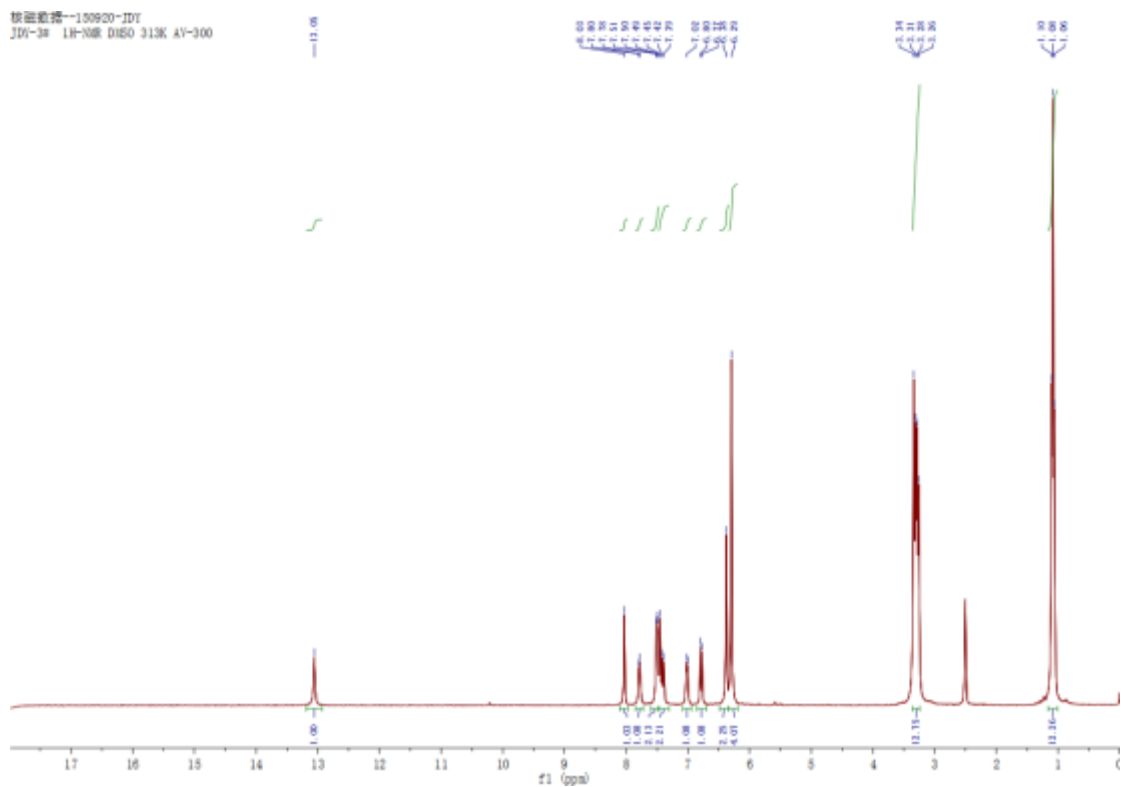
Fig. S91. ^{1}H NMR spectrum of **ReBS** in DMSO-d_6.
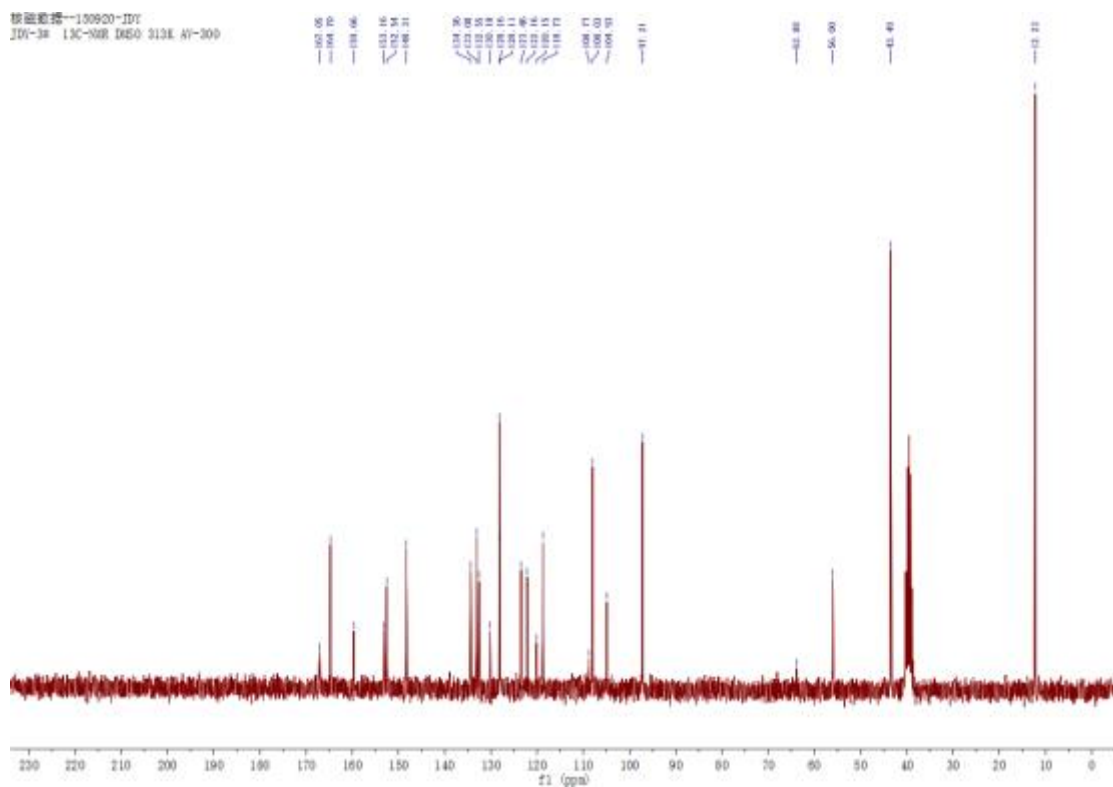
Fig. S92. ^{13}C NMR spectrum of **ReBS** in DMSO-d_6.
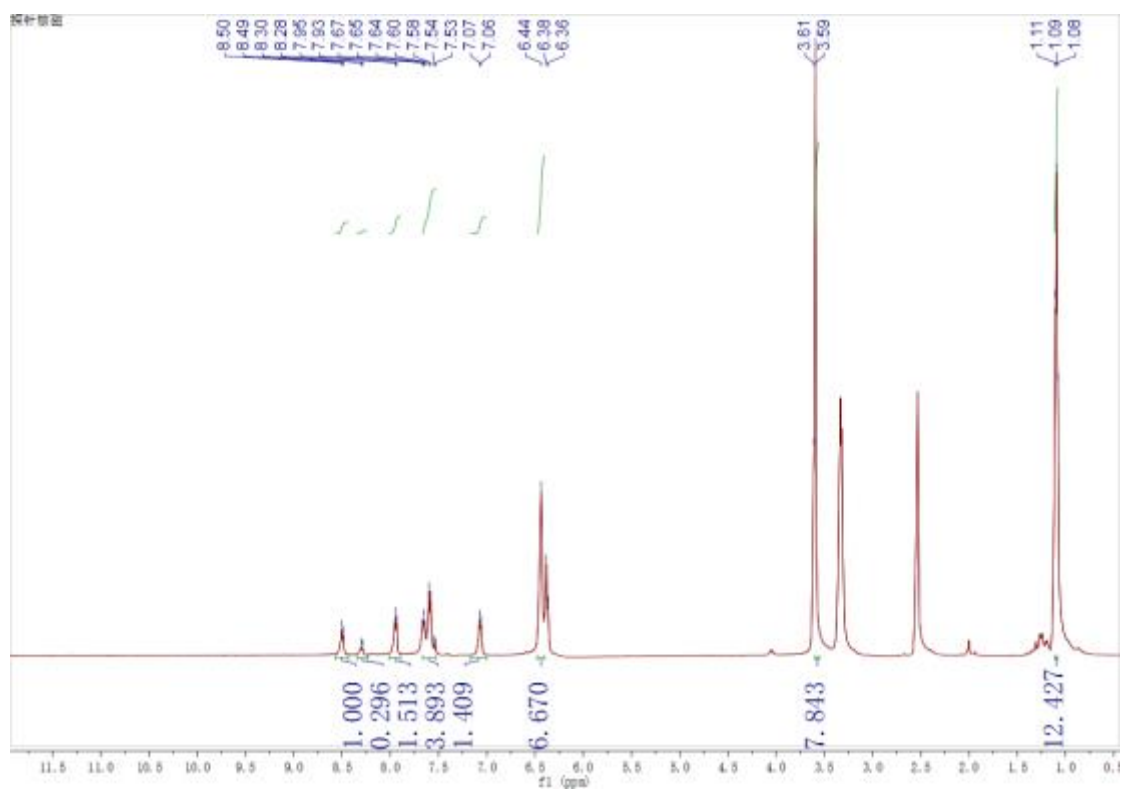
Fig. S93. ^{1}H NMR of **RhDGM** in DMSO-d_6.

Fig. S94. ^{13}C NMR of **RhDGM** in DMSO-d_6.

References
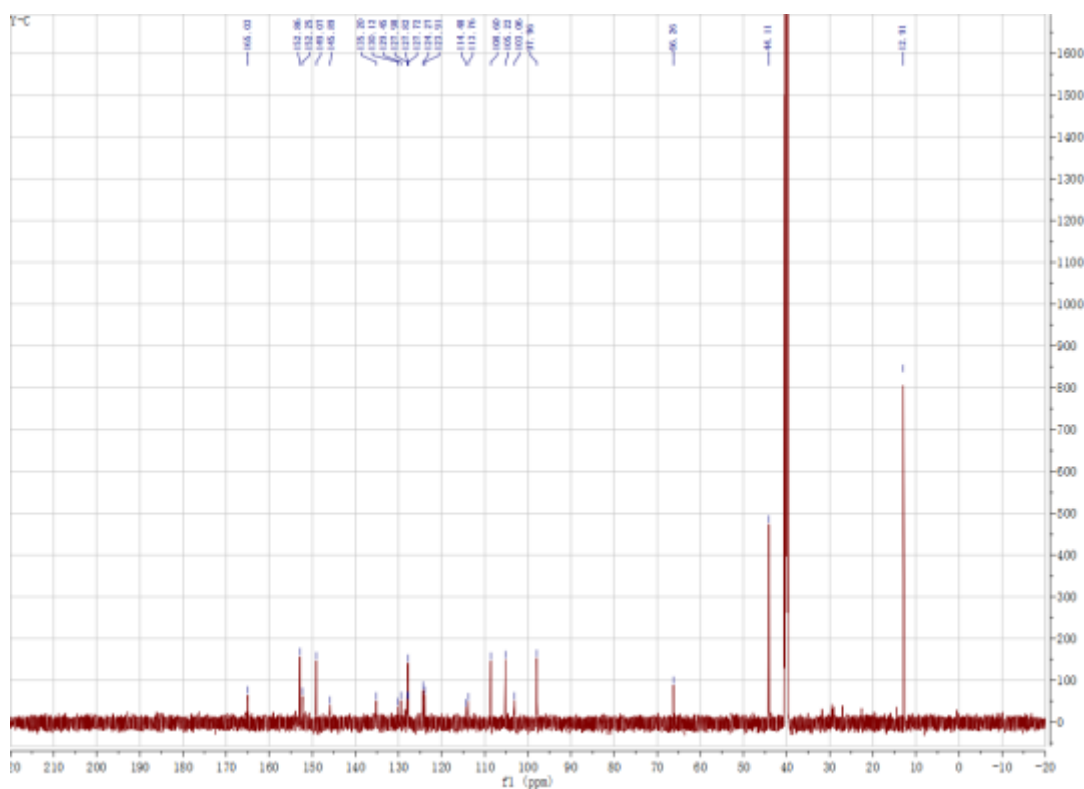
[1] G.M. Sheldrick, SHELXS-97, in: Program for Solution of Crystal Structures, University of Göttingen, Germany, 1997.

[2] G.M. Sheldrick, SHELXL-97, in: Program for Refinement of Crystal Structures, University of Göttingen, Germany, 1997.

[3] E.D. Carpio, L. Hernández, C. Ciangherotti, V.V. Coa, L. Jiménez, V. Lubes, G. Lubes, Coord. Chem. Rev. 372 (2018) 117–140.

[4] T. Mistri, R. Bhowmick, A. Katarkar, K. Chaudhuri, M. Ali, A novel three-input monomolecular logic circuit on a rhodamine inspired bio-compatible bi-compartmental molecular platform, J. Lumin. 185 (2017) 228–235.

[5] M. Sohrabi, M. Amirnasr, H. Farrokhpour, S. Meghdadi, A single chemosensor with combined ionophore/fluorophore moieties acting as a fluorescent "Off-On" Zn^{2+} sensor and a colorimetric sensor for Cu^{2+}: Experimental, logic gate behavior and TD-DFT calculations, Sens. Actuators B 250 (2017) 647–658.

[6] N.V. Ghule, R.S. Bhosale, A.L. Puyad, S.V. Bhosale, S.V. Bhosale, Naphthalenediimide amphiphile based colorimetric probe forrecognition of Cu^{2+} and Fe^{3+} ions, Sens. Actuators B 227 (2016) 17–23.

[7] R. Rani, K. Paul, V. Luxami, An NBD-based two-in-one Cu^{2+}/Ni^{2+} chemosensor with differential charge transfer processes, New J. Chem. 40 (2016) 2418-2422.

[8] Y.R. Bhorge, T.L. Chou, Y.Z. Chen, Y.P. Yen, New coumarin-based dual chromogenic probe: Naked eye detectionof copper and silver ions, Sens. Actuators B 220 (2015) 1139–1144.

[9] M. Li, X.J. Jiang, H.H. Wu, H.L. Lu, H.Y. Li, H. Xu, S.Q. Zang, T.C.W. Mak, A dual functional probe for "turn-on" fluorescence response of Pb^{2+} and colorimetric detection of Cu^{2+} based on a rhodamine derivative in aqueous media, Dalton Trans. 44 (2015) 17326–17334.

[10] S.G. Dogaheh, H. Khanmohammadi, E. C. Sañudo, Selective detection of Cu^{2+} and Co^{2+} in aqueous media: Asymmetric chemosensors, crystal structure and spectroscopic studies, Spectrochim. Acta Part A 179 (2017) 32–41.

[11] S.Z. Pu, H.C. Ding, G. Liu, C.H. Zheng, H.Y. Xu, Multiaddressing fluorescence switch based on a new photochromic diarylethene with a triazole-linked rhodamine B unit, J. Phys. Chem. C 118 (2014) 7010-7017.

[12] S.Z. Qu, C.H. Zheng, G.M. Liao, C.B. Fan, G. Liu, S.Z. Pu, A fluorescent chemosensor for Sn^{2+} and Cu^{2+} based on a carbazole-containing diarylethene, RSC Adv. 7 (2017) 9833–9839.

[13] S.Y. Lee, K.H. Bok, J. A. Kim, S. Y. Kim, C. Kim, Simultaneous detection of Cu^{2+} and Cr^{3+} by a simple Schiff-base colorimetric chemosensor bearing NBD (7-nitrobenzo-2-oxa-1,3-diazolyl) and julolidine moieties, Tetrahedron 72 (2016) 5563-5570.

[14] J. Jeong, B. A. Rao, Y.A. Son, Dual sensing performance of a rhodamine-derived scaffold for thedetermination of Cu^{2+} and Ce^{4+} in aqueous media, Sens. Actuators B 220 (2015) 1254–1265.

[15] F.J. Huo, J. Su, Y.Q. Sun, C.X. Yin, H.B. Tong, Z.X. Nie, A rhodamine-based dual chemosensor for the visual detection of copper and the ratiometric fluorescent detection of vanadium, Dyes Pigm. 86 (2010) 50-55.

[16] G. T. Selvan, S. Poomalai, S. Ramasamy, P. M. Selvakumar, I. V. M. V. Enoch, S. G. Lanas and A. Melchior, Differential metal ion sensing by an antipyrine derivative in aqueous and β-cyclodextrin media: Selectivity tuning by β-cyclodextrin, Anal. Chem. 2018, 90, 13607-13615.

[17] C. Varadaraju, G. Tamilselvan, I. V. M. V. Enoch, V. Srinivasadesikan, S.-L. Lee and P. M. Selvakumar, The first highly selective turn ''ON'' fluorescent sensor for vanadyl (VO^{2+}) ions: DFT studies and molecular logic gate behavior, *New J. Chem.,* 2018, 42, 3833-3839.

[18] M.M. Bordbar, H. Khajehsharifi, A. Solhjoo, PC-ANN assisted to the determination of Vanadium (IV) ion using an optical sensor based on immobilization of Eriochorome Cyanine R on a triacetylcellulose film, Spectrochim. Acta Part A 151 (2015) 225–231.

[19] M.S. Qureshi, A.R.b.M. Yusoff, A. Shah, A. Nafady, Sirajuddin, A new sensitive electrochemical method for the determination of vanadium(IV) and vanadium(V) in Benfield sample, Talanta 132 (2015) 541-547.

[20] N.J. Turro, Modern molecular photochemistry, Benjamin/Cummings Publishing Co., Inc., Menlo Park, CA, 1978.

[21] R. Debashis, C. Arijit, G. Rina, Perimidine based selective colorimetric andfluorescent turn-off chemosensor of aqueous Cu^{2+}: studies on its antioxidant property along with its interaction with calf thymus-DNA, RSC Adv. 7 (2017) 40563-40570.

[22] A.A.M. Belal, M.A. Zayed, M. El-Desawy, Sh.M.A.H. Rakha, Structure investigation of three hydrazones Schiff's bases by spectroscopic, thermal and molecular orbital calculations and
their biological activities, Spectrochim. Acta Part A 138 (2015) 49–57.

[23] Y. Xiang, A.J. Tong, P.Y. Jin, Y. Ju, New fluorescent rhodamine hydrazone chemosensor for Cu(II) with high selectivity and sensitivity, Org. Lett. 8 (2006) 2863–2866.

[24] H.L. Chen, B.J. Zhou, R.L. Ye, J. Zhu, X.F. Bao, Synthesis and evaluation of a new fluorescein and rhodamine B-based chemosensor for highly sensitive and selective detection of cysteine over other amino acids and its application in living cell imaging, Sens. Actuators B 251 (2017) 481–489.

[25] X.F. Yang, M.L. Zhao, G. Wang, A rhodamine-based fluorescent probe selective for bisulfite anion in aqueous ethanol media, Sens. Actuators B 152 (2011) 8–13.